# Studies on epidemiology and control of H5 high pathogenicity avian influenza virus in Japan

（日本における
H5 高病原性鳥インフルエンザウイルス
の疫学および制御に関する研究）

**Hew Yik Lim**

## Contents

## List of figures and tables

## Abbreviations

| | |
|---|---|
| AAALAC | Association for Assessment and Accreditation of Laboratory Animal Care |
| AIV(s) | avian influenza virus(es) |
| BLAST | Basic Local Alignment Search Tool |
| BSL-3 | biosafety level 3 |
| cDNA | complimentary deoxyribonucleic acid |
| $ClO_2$ | chlorine dioxide |
| $CLD_{50}$ | 50% chicken lethal dose |
| cm | centimeter |
| COI | cytochrome c oxidase |
| CPE | cytopathic effect |
| dpc | days post-challenge |
| $EID_{50}$ | 50% egg infectious dose |
| EMPRES-i | EMPRES Global Animal Disease Information System |
| G2 | group 2 |
| GISAID | Global Initiative on Sharing All Influenza Data |
| h | hour(s) |
| HA | hemagglutinin or hemagglutination |
| HI | hemagglutination inhibition |
| HPAI | high pathogenicity avian influenza |
| HPAIV(s) | high pathogenicity avian influenza virus(es) |
| HPD | highest posterior density |
| IAV(s) | influenza A virus(es) |
| L | liter(s) |
| LPAIV(s) | low pathogenicity avian influenza virus(es) |

| | |
|---|---|
| m | meter |
| M | matrix protein |
| MCC | maximum clade credibility |
| MDCK cells | Madin-Darby canine kidney cells |
| MEM | minimum essential medium |
| mg | milligram |
| min | minute(s) |
| mL | milliliter |
| ML | maximum likehood |
| MTBD | Multi-Type Birth Death |
| NA | neuraminidase |
| NaOCI | sodium hypochlorite |
| NGS | next-generation sequencing |
| NP | nucleoprotein |
| NS | non-structural protein |
| PA | polymerase acidic protein |
| PB1 | polymerase basic protein 1 |
| PB2 | polymerase basic protein 2 |
| PCR | polymerase chain reaction |
| ppmv | parts per million by volume |
| QAC | quaternary ammonium compounds |
| $R_e$ | effective reproductive number |
| RNA | ribonucleic acid |
| SARS-CoV-2 | severe acute respiratory syndrome coronavirus 2 |
| $TCID_{50}$ | 50% tissue culture infectious dose |
| WHO | World Health Organization |

| | |
|---|---|
| μL | microliter |

## Notes

Contents of the present thesis were published in the following articles:

**1.** Hew, L. Y.; Isoda, N.; Takaya, F.; Ogasawara, K.; Kobayashi, D.; Huynh, L.T.; Morita, T.; Harada, R.; Zinyakov, N.G.; Andreychuk, D.B.; Chvala, I.A.; Irza, V.N.; Watanabe, Y.; Fujita, H.; Saito, K.; Hiono, T.; Sakoda, Y. Continuous introduction of H5 high pathogenicity avian influenza viruses in Hokkaido, Japan: Characterization of viruses isolated in winter 2022–2023 and early winter 2023–2024. *Transbound Emerg Dis.* **2024**, 1199876. DOI: 10.1155/2024/1199876



**2.** Hew, Y. L.; Hiono, T.; Monne, I.; Nabeshima, K.; Sakuma, S.; Kumagai, A.; Okamura, S.; Soda, K.; Ito, H.; Esaki, M.; Okuya, K.; Ozawa, M.; Yabuta, T.; Takakuwa, H.; Nguyen, L.B.; Isoda, N.; Miyazawa, K.; Onuma, M.; Sakoda, Y. Cocirculation of genetically distinct highly pathogenic avian influenza H5N5 and H5N1 viruses in crows, Hokkaido, Japan. *Emerg Infect Dis.* **2024**, *30*(9), 1912–1917. DOI:10.3201/eid3009.240356



**3.** Hew, Y. L.; Guinat, C.; Couty, M.; Fornasiero, D.; Hiono, T.; Isoda, N.; Sakoda, Y. Introduction and inter-species transmission dynamics of high pathogenicity avian influenza H5N1 viruses in Japan 2021–2025. *Under submission*

**4.** Hew, Y. L.; Isoda, N.; Miura, T.; Hiono, T.; Sakoda, Y. Evaluation of the efficacy of low-concentration gaseous chlorine dioxide in inactivating airborne H5 high pathogenicity avian influenza virus *in vivo* model. *Food Environ Virol*. **2026**. *In press*

## Preface

Avian influenza is a highly contagious viral disease affecting a wide range of avian species, with domestic poultry being particularly vulnerable. The disease is caused by influenza A viruses (IAVs), which belong to the genus *Alphainfluenzavirus* in the family *Orthomyxoviridae*. These viruses have eight segmented, single-stranded, negative-sense RNA genomes [1]. Classification of IAVs is based on the antigenic properties of their two surface glycoproteins, hemagglutinin (HA) and neuraminidase (NA), which define 19 HA (H1–H19) and 11 NA (N1–11) subtypes [2–4]. Wild aquatic birds, especially migratory waterfowl, serve as the natural reservoir for avian influenza viruses (AIVs) and play a central role in maintaining and spreading these viruses across the globe [5]. AIVs are further categorized according to their pathogenicity in chickens as either low pathogenicity (LPAIVs) or high-pathogenicity avian influenza viruses (HPAIVs). HPAIVs emerge when certain LPAIVs, restricted to H5 and H7 subtypes, acquired multiple basic amino acid residues at the HA cleavage site during the amplification among the chickens. This change enables cleavage by ubiquitous host proteases, allowing the virus to cause systemic infection [6–8]. While LPAIVs usually cause mild or subclinical infections, HPAIVs can lead to severe disease and high mortality in poultry, often resulting in substantial economic and ecological losses.

A H5N1 HPAIV was first confirmed in 1996 when A/goose/Guangdong/1/1996 (Gs/Gd; H5N1) was isolated from poultry in Guangdong, China. Descendants of this virus lineage, collectively referred to as the Gs/Gd lineage, have spread globally via migratory birds, causing recurrent outbreaks in avian species and occasional spillover into mammalian hosts [9]. Following widespread outbreaks in poultry in East Asia during 2003–2004 and a mass die-off of migratory birds at Qinghai Lake in 2005 [10, 11], the virus expanded into Europe, Africa, and later North America [12, 13]. Viruses in the Gs/Gd lineage show significant genetic diversity, frequently reassorting with co-circulating LPAIVs since the emergence of clade 2.3.3.4 and evolving into eight subgroups (a–h), as defined by the World Health Organization (WHO) in 2022 [14]. Clade 2.3.4.4 has predominated globally since 2014, giving rise to multiple HA–NA combinations collectively known as H5Nx viruses, including H5N1, H5N2, H5N6, and H5N8 [15]. Viruses in clade 2.3.4.4b have driven the largest epidemic waves since 2016,

particularly in Europe and Asia [16]. H5N8 was the predominant subtype during the 2020–2021 epidemic, but H5N1 became dominant in subsequent years as a result of genetic reassortment between clade 2.3.4.4b H5N8 HPAIVs and locally circulating LPAIVs [17]. Such reassortment has produced diverse genotypes with differing pathogenicity and host adaptation. Between 2020 and 2023, HPAI outbreaks continued across Europe, impacting both wild birds and poultry, and also caused an increase in spillover into mammals [18].

Since early 2021, H5N1 HPAIVs circulating in Europe during the 2020–2021 season have spread beyond Europe to West Africa and later to countries in southern Africa [19, 20]. By late 2021, H5N1 HPAIVs belonging to clade 2.3.4.4b were also detected in South and East Asia [21–23]. In December 2021, a strain closely related to the northern European 2020–2021 viruses was introduced into North America [24], and in early 2022, another incursion occurred via the Pacific flyway involving viruses circulating in Japan [25]. Since then, the virus has spread extensively across North America, undergoing reassortment with LPAIVs of American lineages [25]. The global dissemination of clade 2.3.4.4b H5N1 HPAIVs from 2021 to 2025 marks a previously unprecedent event, characterized by ongoing circulation in wild bird populations and continued geographic expansion into North and South America, and even Antarctica [26–28]. Phylogenetic and phylodynamic analyses show that these viruses have developed greater adaptability in wild birds, along with increased ability to persist in the environment, helping their continued intercontinental spread [29]. In Japan, H5 HPAIVs had emerged in 2004, with outbreaks caused by the H5N1, H5N8, and H5N6 subtypes [30]. Located at the center of the East Asian–Australasian flyway, both the Republic of Korea and Japan are highly susceptible to HPAIV introduction because of the large influx of migratory birds [31]. Over the past decade, both countries have reported numerous high pathogenicity avian influenza (HPAI) outbreaks, enabling analyses of the spatiotemporal dynamics of HPAIV occurrence. Recent studies have also identified East Asia as a potential source of HPAI outbreaks in Central Asia and Alaska. In addition, these regions remain vulnerable to viral incursions from continental Europe, and the Black Sea–Mediterranean region, forming an interconnected network that facilitates the intercontinental spread of HPAIVs [32].

The ongoing global circulation of H5N1 HPAIV has led to increased poultry outbreaks and substantial economic losses. Thus, effective control measures, including culling infected flocks, enforcing movement restrictions, improving farm biosecurity, conducting thorough disinfection, and implementing an appropriate vaccination program where permitted, play an important role in preventing HPAIV outbreaks in poultry. Among these, strict biosecurity and disinfection are crucial for preventing the introduction and spread of viruses via contaminated equipment, vehicles, or clothing. Therefore, alternative approaches can be considered, such as using disinfectants that are safe for humans and animals, compatible with equipment, and demonstrate virucidal efficacy even at low concentrations, thereby further improving biosecurity measures. Lastly, continuous monitoring, epidemiological modelling, and molecular surveillance are essential for predicting outbreaks and guiding timely interventions.

This study aims to clarify the epidemiological and pathogenic characteristics (Chapters I and II) and phylodynamic features (Chapter III) of H5 HPAIVs in Japan, with a particular focus on their evolution and transmission dynamics. Additional research in Chapter IV assesses the use of gaseous chlorine dioxide ($ClO_2$) as a biosecurity measure to control H5 HPAIV. By integrating molecular and field data, this research seeks to improve understanding of HPAIV ecology and support the development of effective strategies to minimize its impact on poultry production and public health.

# Chapter I

# Continuous introduction of H5 high pathogenicity avian influenza viruses in Hokkaido, Japan: Characterization of viruses isolated in winter 2022–2023 and early winter 2023–2024

## Introduction

The worldwide circulation of H5 HPAIVs has contributed to a significant global economic loss due to outbreaks in the poultry industry across Asia, Europe, Africa, and, most recently, North and South America [28, 33–35]. Most H5 HPAIVs are derived from an isolate of the Gs/Gd lineage that has been circulating in wild birds for >25 years and has branched into numerous clades and subclades due to selective genetic mutations and reassortment with multiple influenza subtypes [36]. Among those clades, H5 HPAIVs in clade 2.3.4.4 have rapidly spread and constantly caused outbreaks worldwide since 2014 [37]. In particular, H5 HPAIVs in clade 2.3.4.4b have been consistently isolated in Europe and Asia since 2016 [16]. In late spring 2021, a new epidemiologic trend of H5N1 HPAIV was confirmed in Europe by reassortant viruses between clade 2.3.4.4b H5N8 HPAIVs and LPAIVs locally circulated and led to a large number of infections in wild birds and poultry in many European countries [17]. It was further introduced into the Far East, such as Japan, the Republic of Korea, Russia, and China, possibly by bird migrations [21, 38, 39].

In Japan, in winter 2021–2022, 25 HPAI outbreaks in poultry and 107 cases in wild birds were reported [40]. Four HPAI outbreaks in poultry, 70 cases in wild birds, and two cases in wild mammals from an Ezo red fox (*Vulpes vulpes schrencki*) and a raccoon dog (*Nyctereutes procyonoides*) were confirmed in Hokkaido Prefecture, located in the northernmost part of Japan and facing the Far East parts of Russia which usually have the nesting site of migratory birds [21, 41]. Based on the genetic analysis of HPAIVs isolated in Hokkaido in winter 2021–2022, most H5N1 HPAIVs were genetically close to H5 HPAIVs circulating in Europe and North America in the same winter, demonstrating that the wider dispersion of HPAIVs to both edges of the Eurasian continent in the same season could be originated from the lakes in Siberia, where migratory birds nest in summer [21].

In summer 2022, no H5 HPAIV cases were reported in Japan, differing from the situation in Europe, where H5 HPAIVs were sustained throughout summer 2022. However, HPAIVs were reintroduced back to Japan at the beginning of the new winter 2022–2023. Subsequently, 242 HPAI cases and 84 outbreaks were reported in wild birds and poultry, respectively [42], implying that Japan should still be at high risk of HPAIV

introduction. The continual introduction of H5N1 HPAIVs with various genetic features may display a different level of pathogenicity in chickens, with slight antigenic differences even within clade 2.3.4.4b H5 HPAIVs [35]. Thus, in this study, H5 HPAIVs isolated from wild birds, mammals such as foxes, and poultry in Hokkaido in winter 2022–2023 were genetically analyzed to obtain epidemiologic findings relating to HPAIV incursion to Hokkaido. Furthermore, the antigenic difference of isolates was analyzed to determine whether the antigenicity of H5 HPAIVs had changed during maintenance in birds, and the pathogenicity of four representative HPAIV strains was experimentally assessed in chickens.

## Materials and Methods

### Fecal and swab sample collection, virus isolation, and identification

Two hundred fourteen fecal samples of wild waterfowls were collected during the active survey at Lake Komuke (latitude: 44°25′47″N; longitude: 143°50′25″E) and Notsuke Peninsula (latitude: 43°36′12″N; longitude: 145°17′35″E) in eastern Hokkaido in October 2022. The collected fecal samples were mixed with a virus transport medium consisting of minimum essential medium (MEM, Shimadzu Diagnostics Corporation, Tokyo, Japan) containing 10 mg/mL streptomycin (Meiji Seika Pharma, Tokyo, Japan), 10,000U/mL penicillin G (Meiji Seika Pharma), 250 U/mL nystatin (Sigma–Aldrich, St. Louis, MO, USA), 0.3mg/mL gentamicin (MSD, Tokyo, Japan), and 0.5% bovine serum albumin fraction V (Roche, Basel, Switzerland) and inoculated into 10-day-old embryonated eggs for virus isolation [43]. To identify the host species, DNA was extracted from the fecal sample using NucleoSpin DNA Stool (Takara bio, Shiga, Japan) and 749 base pairs near the 5′-terminus of the cytochrome c oxidase (COI) gene of a host bird were amplified using the primers described previously [44]. The polymerase chain reaction (PCR) product was sequenced and compared to the sequence data of the COI gene obtained from Barcode of Life Data Systems. For the passive survey of HPAIV infections in dead animals in Hokkaido, tracheal swabs collected from dead birds, organ homogenates from dead foxes, and lung homogenates of dead chickens in poultry farms with HPAI outbreaks were inoculated into 10-day-old embryonated eggs for virus isolation. Lung samples from the deceased wild fox (Ezo red fox) were homogenized using a Multi-Beads Shocker (Yasui Kikai, Osaka, Japan) to prepare 10% suspension in a virus transport medium. Lung homogenates of dead chickens from HPAI-affected poultry farms were kindly provided by the Ishikari livestock hygiene services in Hokkaido.

Virus propagation in the collected allantoic fluid was confirmed by the hemagglutination (HA) assay. The isolated viruses were subtyped by an hemagglutination inhibition (HI) test using chicken hyperimmune sera against the referenced influenza virus strain for subtyping [45]. Two H5N1 HPAIVs, A/crow/Khabarovsk/776-56/2022 (H5N1) and A/goose/Magadan/2272-5/2022 (H5N1), were isolated from crow in April 2022 and wild goose in October 2022, respectively, in eastern Russia. To determine the

pathogenicity of isolates, viral RNA was extracted from the allantoic fluid using TRIzol LS Reagent (Thermo Fisher Scientific, Waltham, MA, USA) or QIAamp viral RNA mini kit (Qiagen, Hilden, Germany) and sequenced by direct sequencing after PCR using a region-specific primer set to confirm multiple basic amino acid residues at the HA gene, the molecular marker of HPAIV [46]. The full length of the viral genome was amplified by reverse transcription-PCR using gene-specific primers to each of the eight viral gene segments for Sanger sequencing [47]. Each gene was directly sequenced using BigDye Terminator v3.1, Cycle Sequencing Kit (Thermo Fisher Scientific), and 3500 Genetic Analyzer (Thermo Fisher Scientific). For next-generation sequencing (NGS) of isolates in Japan, the primer sets described by Ip et al [48], were used to amplify the whole genome of AIV for NGS analysis together with three primer sets that specifically improve the yield of polymerase basic protein 2 (PB2), polymerase basic protein 1 (PB1), and polymerase acidic (PA) segments (Table 1). Oxford Nanopore libraries were prepared using the NEB Ultra II End Repair/dA-Tailing Module (New England Biolabs, Ipswich, MA, USA) and sequenced on Flongle using the Nanopore Direct cDNA sequencing kit or Ligation Sequencing kit V14 (Oxford Nanopore Technologies, Oxford, England). The obtained reads were mapped and assembled using FluGAS version 2 (World Fusion, Tokyo, Japan). For whole-genome sequencing of isolates in Russia, cDNA synthesis was performed using the cDNA Synthesis Kit (Roche). The libraries of genome-wide sequencing were prepared by using the commercial Nextera XT Library Prep Kit (Illumina, Hayward, CA, USA) and Nextera XT Index Kits (Illumina) and sequenced on MiSeq genetic analyzer (Illumina) following the manufacturer's instructions for the resequencing of small genomes. The obtained reads were mapped in GS Reference Mapper v2.7 (Roche) and de novo assembled in GS De Novo Assembler v2.7 (Roche).

**Genetic analysis**

All whole genomes of 30 HPAIVs isolated in Hokkaido and two HPAIVs from Russia were used in the genetic analysis (Table 2). The nucleotide sequences of the 32 isolates were phylogenetically analyzed based on the maximum likelihood (ML) method using the best-fit general time-reversible model of the nucleotide substitution with gamma-distribution rate variation among sites (with four rate categories, Γ) according to

**Table 1. Primer sets for AIV genome amplification of polymerase gene segments**

| Primer name | Nucleotide sequence |
|---|---|
| MitchellBUni12 PB2 | 5’-TTTCTGTTGGTGCTGATATTGTTACGCGCCAGCAAAAGCAGGTC-3’ |
| MitchellBUni12 PB1 | 5’-TTTCTGTTGGTGCTGATATTGTTACGCGCCAGCAAAAGCAGGCA-3’ |
| MitchellBUni12 PA | 5’-TTTCTGTTGGTGCTGATATTGTTACGCGCCAGCAAAAGCAGGTAC-3’ |
| MitchellBUni13 PB2 | 5’-ACTTGCCTGTCGCTCTATCTTCGTTACGCGCCAGTAGAAACAAGGTC-3’ |
| MitchellBUni13 PB1 | 5’-ACTTGCCTGTCGCTCTATCTTCGTTACGCGCCAGTAGAAACAAGGCAT-3’ |
| MitchellBUni13 PA | 5’-ACTTGCCTGTCGCTCTATCTTCGTTACGCGCCAGTAGAAACAAGGTAC-3’ |

**Table 2. List of H5 HPAIVs isolated in Hokkaido and eastern part of Russia in winter 2022–2023 and early winter 2023–2024**

| ID | Virus | Subgroup | Genotype | Sample collection date | City/town | Latitude | Longitude | Accession number of strain[1] |
|---|---|---|---|---|---|---|---|---|
| 1 | A/Eurasian wigeon/Hokkaido/Q71/2022 (H5N1) | G2b | V | 11/11/2022 | Betsukai | 43°36′12″N | 145°17′35″E | EPI_ISL_15576617 |
| 2 | A/Eurasian wigeon/Hokkaido/M184/2022 (H5N1) | G2b | V | 27/11/2022 | Monbetsu | 44°25′47″N | 143°50′25″E | EPI_ISL_15732766 |
| 3 | A/large-billed crow/Hokkaido/B003/2022 (H5N2) | G2d | III | 28/10/2022 | Sapporo | 43°03′50″N | 141°20′35″E | EPI_ISL_15732741 |
| 4 | A/slaty-backed gull /Hokkaido/011M111/2022 (H5N1) | G2d | I | 06/11/2022 | Shari | 43°56′17″N | 144°42′43″E | EPI_ISL_16698579 |
| 5 | A/slaty-backed gull /Hokkaido/011M114/2022 (H5N1) | G2d | I | 16/11/2022 | Abashiri | 44°01′15″N | 144°16′24″E | EPI_ISL_16955798 |
| 6 | A/red-crowned crane/Hokkaido /20221120001/2022 (H5N1) | G2d | I | 20/11/2022 | Tobetsu | 43°13′47″N | 141°31′32″E | EPI_ISL_16698576 |
| 7 | A/white-tailed eagle/Hokkaido /20221123001/2022 (H5N1) | G2d | I | 23/11/2022 | Urahoro | 42°48′33″N | 143°39′30″E | EPI_ISL_16955829 |
| 8 | A/large-billed crow /Hokkaido/011E084/2022 (H5N1) | G2d | I | 24/11/2022 | Mukawa | 42°37′31″N | 142°00′32″E | EPI_ISL_16955748 |
| 9 | A/large-billed crow/Hokkaido /0112P083−2/2022 (H5N1) | G2d | I | 05/12/2022 | Kushiro | 42°57′14″N | 144°31′56″E | EPI_ISL_16955765 |
| 10 | A/large-billed crow/Hokkaido/B004/2022 (H5N1) | G2d | IV | 12/12/2022 | Sapporo | 43°03′50″N | 141°20′35″E | EPI_ISL_17267427 |
| 11 | A/large-billed crow/Hokkaido/B00B/2022 (H5N1) | G2d | IV | 18/12/2022 | Sapporo | 43°03′50″N | 141°20′35″E | EPI_ISL_17317372 |
| 12 | A/large-billed crow/Hokkaido/B00C/2022 (H5N1) | G2d | IV | 19/12/2022 | Sapporo | 43°03′50″N | 141°20′35″E | EPI_ISL_17317373 |

**Table 2** (*cont*)**. List of H5 HPAIVs isolated in Hokkaido and eastern part of Russia in winter 2022–2023 and early winter 2023–2024**

| ID | Virus | Subgroup | Genotype | Sample collection date | City/town | Latitude | Longitude | Accession number of strain[1] |
|---|---|---|---|---|---|---|---|---|
| 13 | A/large-billed crow/Hokkaido/B005/2022 (H5N1) | G2d | I | 21/12/2022 | Sapporo | 43°04′50″N | 141°20′26″E | EPI_ISL_17267428 |
| 14 | A/large-billed crow/Hokkaido/B006/2023 (H5N1) | G2d | IV | 04/02/2023 | Sapporo | 43°03′50″N | 141°20′35″E | EPI_ISL_17316075 |
| 15 | A/large-billed crow/Hokkaido/B007/2023 (H5N1) | G2d | IV | 13/03/2023 | Sapporo | 43°03′50″N | 141°20′35″E | EPI_ISL_17316489 |
| 16 | A/large-billed crow/Hokkaido/B008/2023 (H5N1) | G2d | IV | 13/03/2023 | Sapporo | 43°03′50″N | 141°20′35″E | EPI_ISL_17316965 |
| 17 | A/large-billed crow /Hokkaido/0103E088/2023 (H5N1) | G2d | I | 24/03/2023 | Mukawa | 42°37′31″N | 142°00′32″E | EPI_ISL_17950087 |
| 18 | A/large-billed crow /Hokkaido/0103E089/2023 (H5N1) | G2d | I | 29/03/2023 | Mukawa | 42°37′31″N | 142°00′32″E | EPI_ISL_17950253 |
| 19 | A/large-billed crow/Hokkaido/B049/2023 (H5N1) | G2d | IV | 11/04/2023 | Sapporo | 43°03′50″N | 141°20′35″E | EPI_ISL_17950254 |
| 20 | A/large-billed crow/Hokkaido/B052/2023 (H5N1) | G2d | I | 13/04/2023 | Sapporo | 43°03′50″N | 141°20′35″E | EPI_ISL_18007229 |
| 21 | A/large-billed crow/Hokkaido/B053/2023 (H5N1) | G2d | IV | 18/04/2023 | Sapporo | 43°03′50″N | 141°20′35″E | EPI_ISL_18007230 |
| 22 | A/large-billed crow/Hokkaido/B067/2023 (H5N1) | G2d | I | 23/11/2023 | Sapporo | 43°03′50″N | 141°20′35″E | EPI_ISL_18591747 |
| 23 | A/chicken/Hokkaido/HU-E001/2022 (H5N1) | G2d | II | 07/11/2022 | Atsuma | 42°43′26″N | 141°52′42″E | EPI_ISL_16698060 |

**Table 2** (*cont*)**. List of H5 HPAIVs isolated in Hokkaido and eastern part of Russia in winter 2022–2023 and early winter 2023–2024**

| ID | Virus | Subgroup | Genotype | Sample collection date | City/town | Latitude | Longitude | Accession number of strain[1] |
|---|---|---|---|---|---|---|---|---|
| 24 | A/chicken/Hokkaido/HU-E008/2022 (H5N1) | G2d | I | 11/11/2022 | Date | 42°30′44″N | 140°52′03″E | EPI_ISL_16698477 |
| 25 | A/chicken/Hokkaido/HU-E010/2022 (H5N1) | G2d | I | 11/11/2022 | Date | 42°30′44″N | 140°52′03″E | EPI_ISL_17267420 |
| 26 | A/chicken/Hokkaido/HU-B102/2023 (H5N1) | G2c | VI | 27/03/2023 | Chitose | 42°49′15″N | 141°39′05″E | EPI_ISL_17638141 |
| 27 | A/chicken/Hokkaido/HU-B202/2023 (H5N1) | G2c | VI | 02/04/2023 | Chitose | 42°49′15″N | 141°39′05″E | EPI_ISL_17638143 |
| 28 | A/chicken/Hokkaido/HU-B301/2023 (H5N1) | G2c | VI | 06/04/2023 | Chitose | 42°49′15″N | 141°39′05″E | EPI_ISL_17638448 |
| 29 | A/Ezo red fox/Hokkaido/3/2023 (H5N1) | G2d | IV | 20/02/2023 | Sapporo | 43°03′50″N | 141°20′35″E | EPI_ISL_17857959 |
| 30 | A/Ezo red fox/Hokkaido/2/2023 (H5N1) | G2d | IV | 12/04/2023 | Sapporo | 43°03′50″N | 141°20′35″E | EPI_ISL_17766057 |
| 31 | A/crow/Khabarovsk/776-56/2022 (H5N1) | G2d | I | 15/04/2022 | Khabarovsk | 50°39′12″N | 136°57′16″E | EPI_ISL_18074199 |
| 32 | A/goose/Magadan/2272-5/2022 (H5N1) | G2d | I | 10/09/2022 | Magadan | 59°32′41″N | 150°53′08″E | EPI_ISL_18071580 |

[1]The GISAID accession number.

the Tamura and Nei model [49]. Bootstrap analysis under 1,000 replications was applied to construct the phylogenetic tree in MEGA 7 with default parameters [50]. Sequence data of the gene were compared to the reference nucleotide sequence of the representative H5Nx (with different NA subtypes) in clade 2.3.4.4 strains downloaded from the Global Initiative on Sharing All Influenza Data (GISAID) and GenBank. Basic Local Alignment Search Tool (BLAST) in the GISAID database was used to identify the most homologous nucleotide sequences of HPAIVs isolated in this study.

**Antigenic analysis**

The antigenicity of HPAIVs isolated in winter 2022–2023 and an isolate in early winter 2023–2024 was compared to each other and to that in the past season in Japan using a cross-HI test. Three representative HPAIV strains isolated in winter 2022–2023, A/chicken/Hokkaido/HU-E001/2022 (Ck/Hok/E001/22; H5N1) isolated from a dead chicken of an HPAI outbreak in a poultry farm in Hokkaido in October 2022, A/large-billed crow/Hokkaido/B003/2022 (Cr/Hok/B003/22; H5N2) isolated from a dead crow in an urban garden in the capital of Hokkaido Prefecture, and A/Eurasian wigeon/Hokkaido/Q71/2022 (Ew/Hok/Q71/22; H5N1) isolated from a fecal sample of wild waterfowl were selected according to the potential antigenic difference based on phylogenetic analysis. Hyperimmune serum against each of these three strains was prepared, as described by Kida and Yanagawa [45]. For antiserum production, 500 μg antigen was mixed with Freund's complete or incomplete adjuvant at the first and second injections, respectively, and injected intramuscularly into the thigh muscle of a naïve chicken twice at 14-day intervals. Fourteen days after the second injection, whole blood was collected from the chickens to obtain the serum. Other antigens in the representative strains in clade 2.3.4.4, such as A/white-tailed eagle/Hokkaido/22-RU-WTE-2/2022 (WTE/Hok/R22/22; H5N1), A/northern pintail/Hokkaido/M13/2020 (NP/Hok/M13/20; H5N8) [51], A/Ezo red fox/Hokkaido/2/2023 (H5N1), A/large-billed crow/Hokkaido/B049/2023 (H5N1), A/chicken/Hokkaido/HU-B102/2023 (Ck/Hok/B102/23; H5N1), A/large-billed crow/Hokkaido/B067/2023 (Cr/Hok/B067/23; H5N1), A/chicken/Kumamoto/1-7/2014 (Ck/Kum/1-7/14; H5N8) [52], A/black swan/Akita/1/2016 (Bs/Aki/1/16; H5N6) [53], and A/Muscovy duck/DR Congo/KAF1/2017 (Mdk/DRC/KAF1/17; H5N8) [54], were analyzed between and

within clade 2.3.4.4 using antiserum; WTE/Hok/R22/22 (H5N1), Ck/Kum/1-7/14 (H5N8), Bs/Aki/1/16 (H5N6), and Mdk/DRC/KAF1/17 (H5N8) for cross-reactivity of hyperimmune antisera and their corresponding antigens. The Japanese stockpile vaccine strain for H5 HPAIV infection in Japan, A/duck/Hokkaido/Vac-1/2004 (Dk/Hok/Vac-1/04; H5N1), was also used for the cross-HI test [55]. Antigenic cartography was generated based on the HI test estimated using web-based software [56]. The x–y coordinates of each antiserum and antigen were obtained by loading the data of the titers of the cross-HI test.

**Animal experiments**

Three chicken breeds free from the antibodies against H5 AIV were prepared to assess the pathogenicity of H5 HPAIVs. White Leghorn chickens were hatched from embryonated eggs and fed at Hokkaido University. Thirty-one-week-old Rhode Island Red chickens were kindly provided by the Field Science Center for Northern Biosphere, Hokkaido University (Hokkaido, Japan). Four-week-old Chunky chickens were kindly provided by Nippon White Farm (Hokkaido, Japan) and Prifoods (Aomori, Japan). Each of the four viruses, Ck/Hok/E001/22 (H5N1), Cr/Hok/B003/22 (H5N2), Ew/Hok/Q71/22 (H5N1), and Ck/Hok/B102/23 (H5N1), was challenged to four White Leghorn or Chunky chickens. Only three viruses, Ck/Hok/E001/22 (H5N1), Cr/Hok/B003/22 (H5N2), and Ew/Hok/Q71/22 (H5N1), were challenged to three Rhode Island Red chickens. All chickens were intranasally challenged with representative HPAIVs at $10^{6.0}$ times of 50% egg infectious dose ($EID_{50}$) and monitored daily for clinical manifestation for 14 days post-challenge (dpc). Tracheal and cloacal swabs were collected from each bird daily until 7 dpc or its death, and the swabs were suspended in a 2 mL of virus transport medium. The infectious titers of the swabs were expressed in 50% tissue culture infectious dose ($TCID_{50}$), which was determined using Madin-Darby canine kidney (MDCK) cells by observing the cytopathic effect (CPE) of virus-infected cells.

**Mutational analysis**

Mutational analysis was conducted using ClustalW in GENETYX version 16 (Nihon Server, Tokyo, Japan) for sequence alignment of Hokkaido isolates for single nucleotide polymorphisms analysis and referring to other previously published mutation

of concerns [57].

**Ethic statements**

All chicken experiments were conducted at the Animal Biosafety Level 3 (BSL-3) Facility, Faculty of Veterinary Medicine, Hokkaido University, which has been accredited by the Association for Assessment and Accreditation of Laboratory Animal Care (AAALAC) International since 2007 and were approved by the Institutional Animal Care and Use Committee of the Faculty of Veterinary Medicine, Hokkaido University with the approval numbers 18-0037, 23-0050, and 23-0053. Additionally, the study was approved by the Biosafety Management Committee on Pathogens and Other Hazardous Agents at the Faculty of Veterinary Medicine, Hokkaido University (approval no. 2022-1-78).

## Results

### Genetic analysis

In winter 2022–2023, nine of 214 fecal samples of wild waterfowls, 56 swab samples of migratory or resident birds, 15 and 2 lung homogenate samples of dead chickens and wild foxes, respectively, in Hokkaido, were diagnosed as positive for H5 AIV infections by detection of H5 HA of AIVs. No other HA subtypes of AIV were isolated from any other samples. All H5 viruses were subtyped as H5N1, except for one H5N2 strain isolated from a dead crow in the capital city of Hokkaido (Cr/Hok/B003/22; H5N2). The pathogenicity of all isolates in chickens was deduced as highly pathogenic by confirming the multiple basic amino acid motif at the HA1/HA2 proteolytic cleavage site on the HA gene. Twenty-nine selected isolates from 82 H5 HPAIVs were composed of six from poultry samples, two from fecal samples of migratory birds, two from fox carcasses, and the remaining 19 isolates from resident birds selected for genetic analysis. Two additional H5N1 HPAIVs isolated in eastern Russia in spring and autumn 2022 were included for genetic analysis. During the early winter 2023–2024, an HPAIV was additionally isolated from a resident crow in Hokkaido in November; the virus was also included in the genetic analysis. The whole sequences of all eight gene segments of these 32 HPAIVs were registered in the GISAID database (Table 2). In the COI gene database, the sequence of mitochondrial DNA extracted from fecal samples of two migratory birds showed 100% homology to the COI gene of *Mareca penelope* (Eurasian wigeon).

In the phylogenetic analysis of the H5 HA gene, all 32 isolates were categorized in clade 2.3.4.4b and classified into the Group 2 (G2) genotype, which is closely related to clade 2.3.4.4b H5N8 HPAIVs that shared the common ancestor with viruses detected in Europe in late 2020 (Figure 1A) [58]. Based on the structure of the phylogenetic tree, the G2 genotype was further classified into multiple subgroups (G2a–e). Most isolates in 2022–2023 were entered into the same subgroup, which was tentatively designated as G2d, which contains HPAIVs isolated in Hokkaido in winter 2021–2022 and remarkably also clustered with A/crow/Khabarovsk/776-56/2022 (H5N1) and A/goose/Magadan/2272-5/2022 (H5N1) isolated in eastern Russia in spring and autumn 2022, respectively. Interestingly, the isolate in Hokkaido in November 2023 was also grouped into subgroup of G2d. Ew/Hok/Q71/22 (H5N1) and A/Eurasian wigeon/Hokkaido/M184/2022

(Ew/Hok/M184/22; H5N1) isolated from fecal samples of wild waterfowls were categorized into a different subgroup of G2 clade (G2b), which was clustered with HPAIVs isolated in southern Japan in winter 2021–2022 [59]. Interestingly, one HPAIV A/chicken/Hokkaido/TU25-3/2022 (Ck/Hok/TU25-3/22; H5N1), which was isolated in the HPAI outbreak in a poultry farm in Hokkaido in May 2022, was also included in the G2b subgroup. At the end of March 2023, three H5 HPAI outbreaks were confirmed in poultry farms in Hokkaido. The causal agents of these outbreaks, Ck/Hok/B102/23 (H5N1), A/chicken/Hokkaido/HU-B202/2023 (H5N1), and A/chicken/Hokkaido/HU-B301/2023 (H5N1), were clustered into another new subgroup, which was tentatively designated as G2c. In this G2c subgroup, Hokkaido isolates were closely clustered with isolates predominantly prevalent in southern Japan in 2022–2023.

Based on the nucleotide sequence of the HA gene, HPAIVs isolated in Hokkaido were divided into three groups. Similar trends were also confirmed in phylogenetic trees of the N1 NA gene, except for one virus with H5N2 subtype, and other internal genes, such as PB1, nucleoprotein (NP), matrix (M), and non-structural (NS) gene segments (Figure 1B–H). However, there were different trends in the phylogenetic trees of PB2 and PA genes. In phylogenetic trees of PB2 and PA genes, some isolates, such as Ck/Hok/E001/22 (H5N1), Cr/Hok/B003/22 (H5N2), and A/large-billed crow/Hokkaido/B004/2022 (H5N1), deviated from the major group of Hokkaido isolates in G2d subgroup, indicating that these isolates have undergone reassortment and acquired other wild bird lineages of PB2 and PA genes of LPAIVs (Table 3). Based on BLAST analysis, PB2 and PA genes were highly homologous to the corresponding gene segments of LPAIVs isolated in Far East Asia, including China, Mongolia, and Russia (Table 3). Phylogenetic analysis in all eight gene segments has identified six types of gene constellations of H5 HPAIVs in Hokkaido in 2022–2023 (Figure 2). The subgroup of G2d includes four different gene constellations; a major genotype among isolates in Hokkaido in 2022–2023 (genotype I) has the same gene constellation as the dominant genotype in 2021–2022 in Hokkaido and an isolate in the early winter 2023–2024 in Hokkaido, and two genotypes of two different gene constellations in PB2 and PA gene (genotypes II and IV) and one genotype of three different gene constellations in PB2, PA, and NA (genotype III) were identified as descendants of the dominant genotype in 2021–2022. Ew/Hok/Q71/22 (H5N1) and Ew/Hok/M184/22 (H5N1) in the subgroup of

G2b formulated single gene constellation and were designated as genotype V, which also includes Ck/Hok/TU25-3/22 (H5N1). Meanwhile, all the H5 HPAIV isolates in subgroup G2c in Hokkaido also formed a unique gene constellation designated genotype VI.

**Antigenic analysis**

Three viruses, Ck/Hok/E001/22 (H5N1) in subgroup G2d, Cr/Hok/B003/22 (H5N2) in subgroup G2d, and Ew/Hok/Q71/22 (H5N1) in subgroup G2b, were selected for antigenic analysis using the cross-HI test (Table 4). The antiserum against Ck/Hok/E001/22 (H5N1) showed homologous reaction (same HI titers) with Cr/Hok/B003/22 (H5N2) and Ew/Hok/Q71/22 (H5N1) antigens. Meanwhile, the antiserum against Cr/Hok/B003/22 (H5N2) was closely reacted (twofold HI titer differences) with Ck/Hok/E001/22 (H5N1) antigens and Ew/Hok/Q71/22 (H5N1) antigens. The same applies to the antiserum against Ew/Hok/Q71/22 (H5N1), which also displayed close reactivity to the Ck/Hok/E001/22 (H5N1) (twofold HI titer differences) and Cr/Hok/B003/22 (H5N2) (fourfold HI titer differences). Antigenic cartography demonstrated that antigenicity among groups of HPAIVs isolated in winter 2022–2023 and an isolate in November 2023 was almost identical and similar to those of the previously isolated clade 2.3.4.4b (Figure 3). The antigenicity of clade 2.3.4.4b viruses was slightly different from Ck/Kum/1-7/14 (H5N8) in clade 2.3.4.4c. Viruses in clade 2.3.4.4b exhibited more than two antigenic units distant from the vaccine strain: Dk/Hok/Vac-1/04 (H5N1) in the classical clade and Bs/Aki/1/16 (H5N6) in clade 2.3.4.4e.

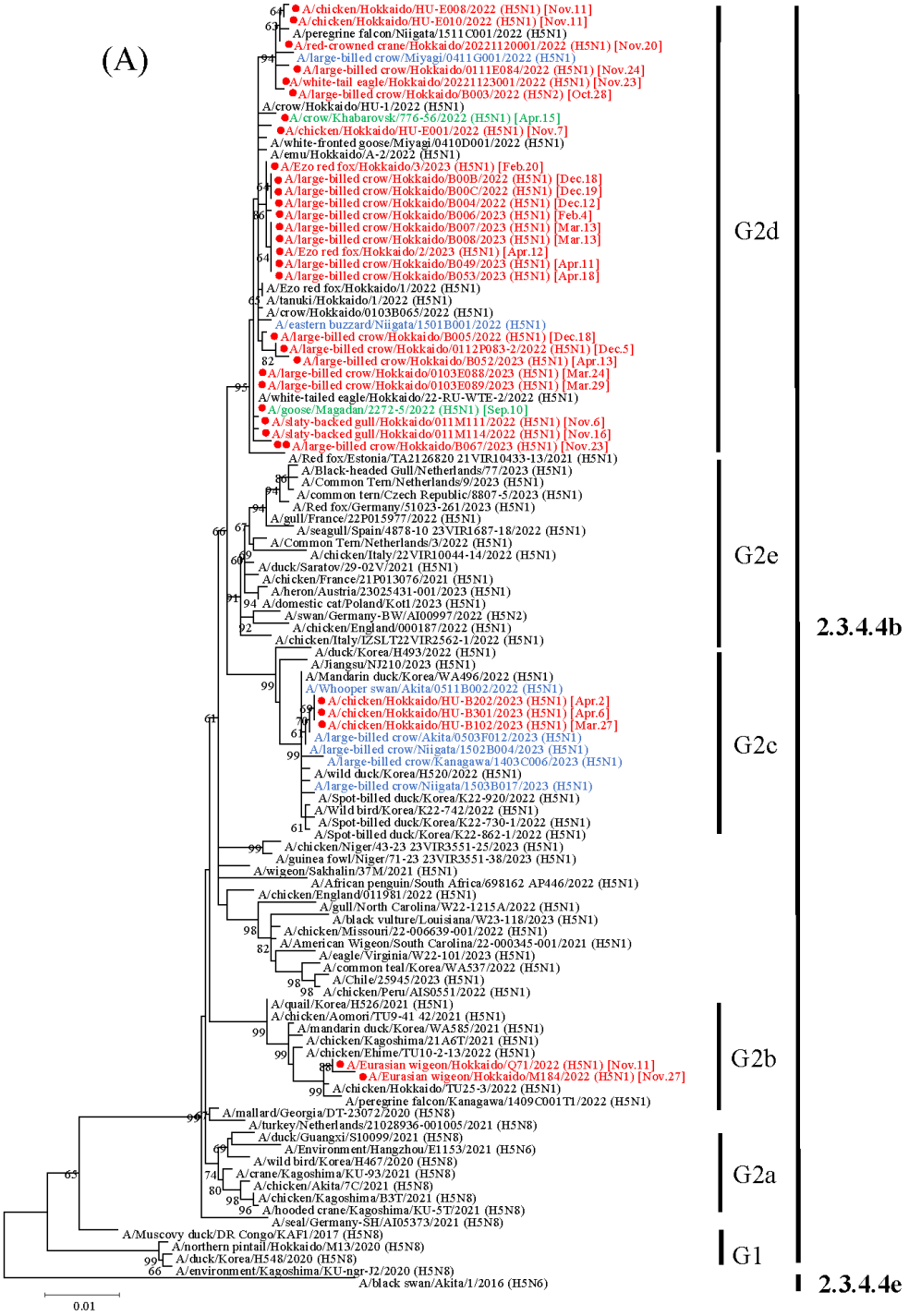


**Figure 1. Phylogenetic analysis of H5 HPAIVs isolated in the Far East in winter 2022–2023 and early winter 2023–2024**. The H5 HA **(A)**, N1 NA **(B)**, PB2 **(C)**, PB1 **(D)**, PA **(E)**, NP **(F)**, M **(G)**, and NS **(H)** gene segments of 29 H5 HPAIV isolates, including those from Hokkaido (winter 2022–2023 and early winter 2023–2024). Isolates from Hokkaido, eastern Russia, and Honshu are shown in red, green, and blue, respectively. For the HA and NA gene segments, the collection dates are listed after the strain names. All isolates are represented by circles, with early winter 2023–2024 isolates indicated by double circles.

(B)


**Figure 1** (*cont*)**. Phylogenetic analysis of H5 HPAIVs isolated in the Far East in winter 2022–2023 and early winter 2023–2024**

(C)


**Figure 1** (*cont*)**. Phylogenetic analysis of H5 HPAIVs isolated in the Far East in winter 2022–2023 and early winter 2023–2024**

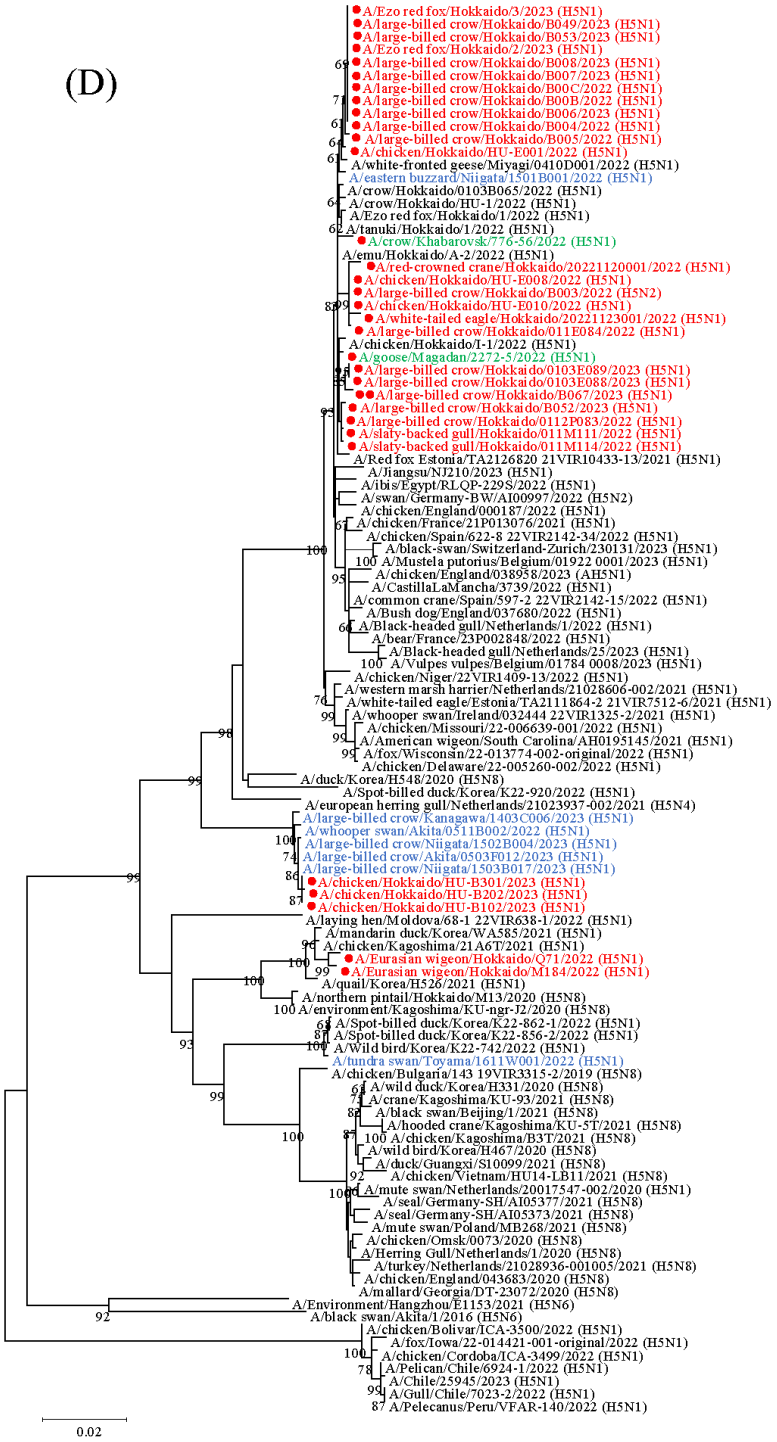


**Figure 1** (*cont*). **Phylogenetic analysis of H5 HPAIVs isolated in the Far East in winter 2022–2023 and early winter 2023–2024**

(E)

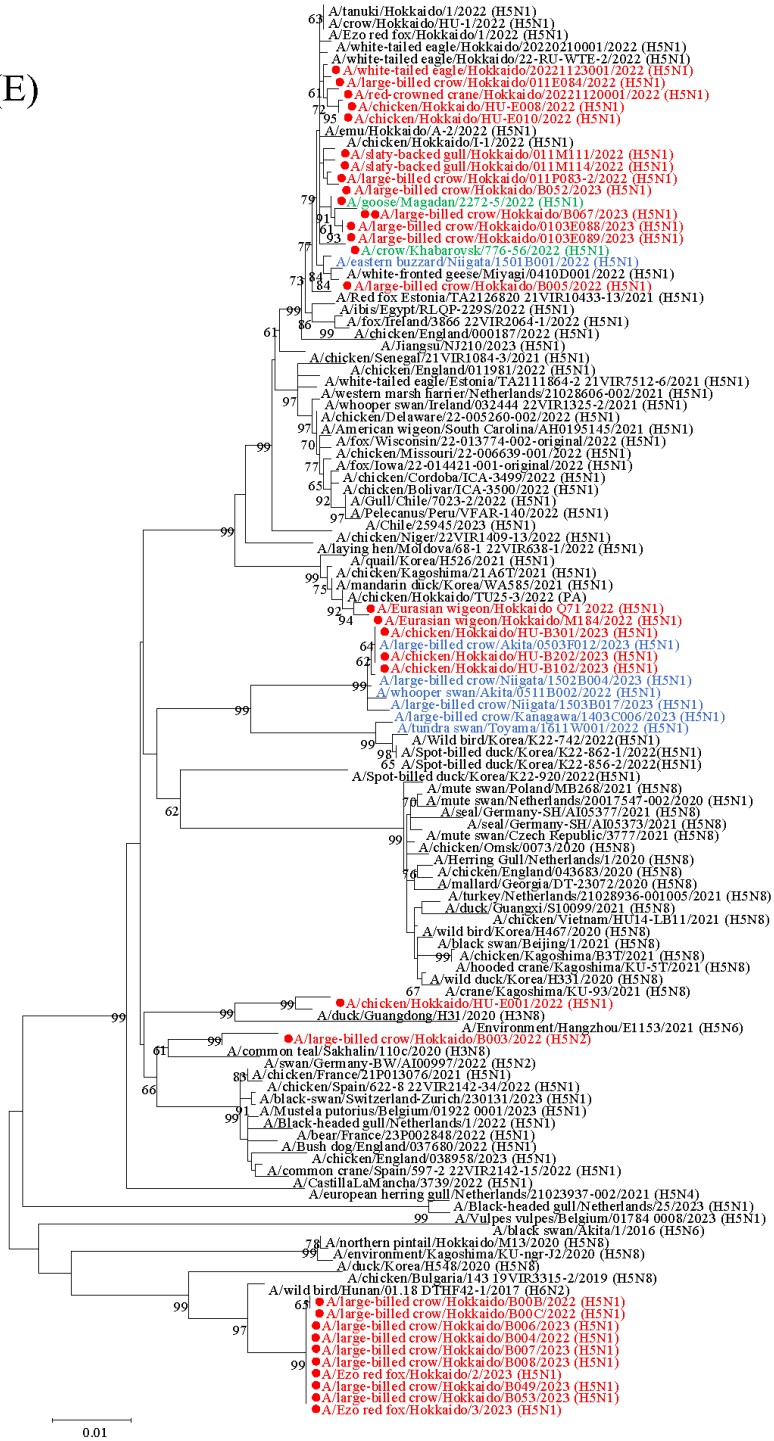


**Figure 1** (*cont*)**. Phylogenetic analysis of H5 HPAIVs isolated in the Far East in winter 2022–2023 and early winter 2023–2024**

(F)

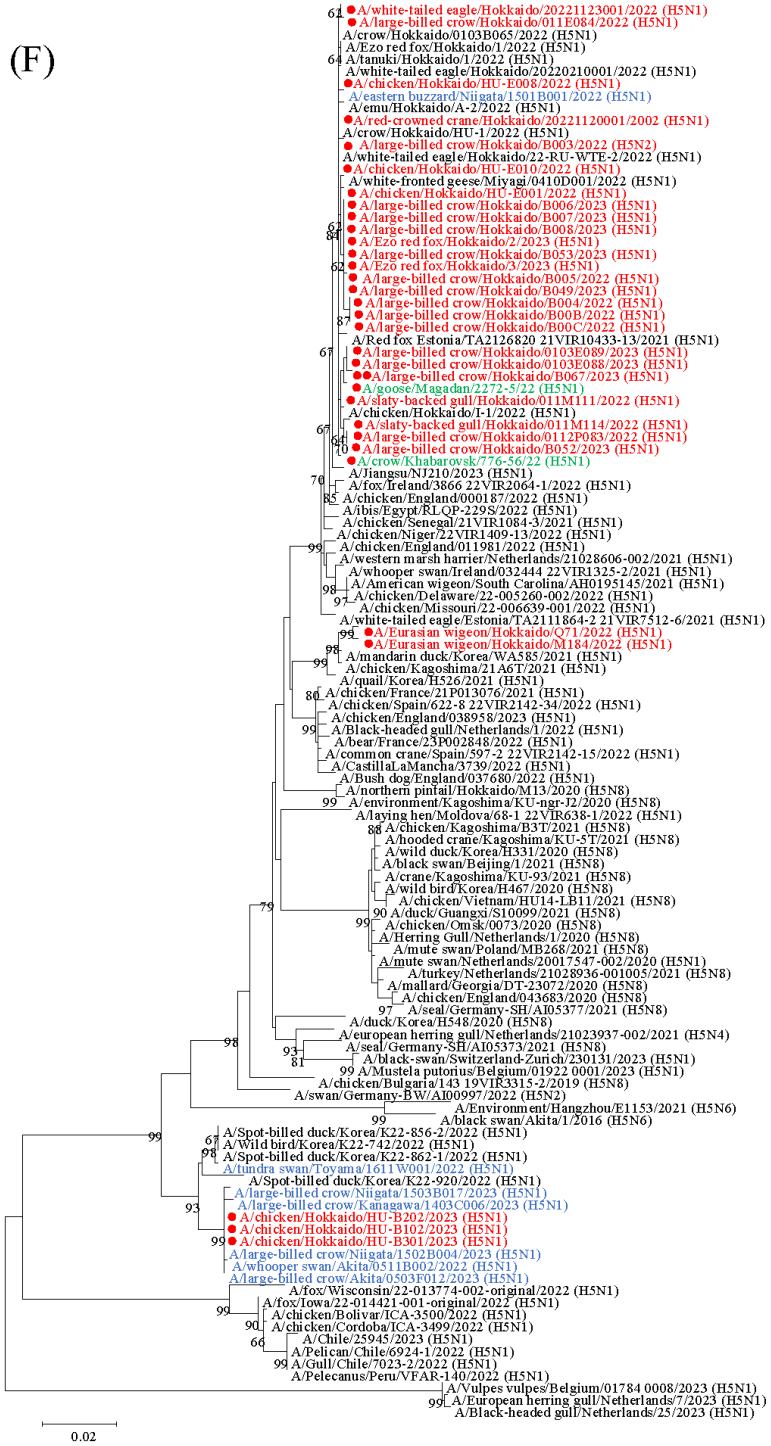


**Figure 1** (*cont*)**. Phylogenetic analysis of H5 HPAIVs isolated in the Far East in winter 2022–2023 and early winter 2023–2024**


**Figure 1** (*cont*)**. Phylogenetic analysis of H5 HPAIVs isolated in the Far East in winter 2022–2023 and early winter 2023–2024**

(H)


**Figure 1** (*cont*)**. Phylogenetic analysis of H5 HPAIVs isolated in the Far East in winter 2022–2023 and early winter 2023–2024**

**Table 3. BLAST search results of H5 HPAIVs in Hokkaido in 2022–2023 in the GISAID database**

| Virus | Gene | Most homologous strain | Homology | Accession number |
|---|---|---|---|---|
| A/chicken/ Hokkaido/ HU-E001/2022 (H5N1) | PB2 | A/common teal/ Sakhalin/66c/2020 (H3N8) | 99.5% | EPI1847524 |
| | PB1 | A/large-billed crow/ Hokkaido/B004/2022 (H5N1) | 99.9% | EPI2475271 |
| | PA | A/duck/Guangdong/H31/ 2020 (H3N8) | 99.3% | EPI1838459 |
| | HA | A/crow/Hokkaido/HU-1 /2022 (H5N1) | 99.8% | EPI2181811 |
| | NP | A/red-crowned crane/ Hokkaido/20221120001/ 2022 (H5N1) | 99.8% | EPI2318018 |
| | NA | A/crow/Hokkaido/HU-1 /2022 (H5N1) | 99.6% | EPI2181813 |
| | M | A/chicken/Hokkaido/ HU-E010/2022 (H5N1) | 99.7% | EPI2475262 |
| | NS | A/large-billed crow/ Hokkaido/B004/2022 (H5N1) | 99.8% | EPI2475277 |
| A/large-billed crow/ Hokkaido/ B003/2022 (H5N2) | PB2 | A/common teal/ Sakhalin/110c/2020 (H3N8) | 99.6% | EPI1847516 |
| | PB1 | A/chicken/Hokkaido/ HU-E010/2022 (H5N1) | 100.0% | EPI2475257 |
| | PA | A/common teal/ Sakhalin/110c/2020 (H3N8) | 99.3% | EPI1847515 |
| | HA | A/white-tailed eagle/ Hokkaido/20221123001/ 2022 (H5N1) | 99.9% | EPI2412813 |
| | NP | A/red-crowned crane/ Hokkaido/20221120001/ 2022 (H5N1) | 99.9% | EPI2318018 |
| | NA | A/duck/Vietnam/HN6038/ 2019 (H11N2) | 98.9% | EPI1974765 |
| | M | A/chicken/Hokkaido/ HU-E010/2022 (H5N1) | 100.0% | EPI2475262 |
| | NS | A/chicken/Hokkaido/ HU-E010/2022 (H5N1) | 99.8% | EPI2475263 |

**Table 3** (*cont*)**. BLAST search results of H5 HPAIVs in Hokkaido in 2022–2023 in the GISAID database**

| Virus | Gene | Most homologous strain | Homology | Accession number |
|---|---|---|---|---|
| A/large-billed crow/ Hokkaido/B004/ 2022 (H5N1) | PB2 | A/duck/Mongolia/ MN18-14/2018 (H3N8) | 98.7% | EPI1903620 |
| | PB1 | A/chicken/Hokkaido/ HU-E001/2022 (H5N1) | 99.9% | EPI2317990 |
| | PA | A/wild bird/Hunan/ 01.18 DTHF42-1/2017 (H6N2) | 99.1% | EPI1485602 |
| | HA | A/crow/Hokkaido/ HU-1/2022 (H5N1) | 99.8% | EPI2181811 |
| | NP | A/red-crowned crane/ Hokkaido/20221120001/ 2022 (H5N1) | 99.7% | EPI2318018 |
| | NA | A/crow/Hokkaido/ HU-1/2022 (H5N1) | 99.6% | EPI2181813 |
| | M | A/chicken/Hokkaido/ HU-E010/2022 (H5N1) | 99.9% | EPI2475262 |
| | NS | A/chicken/Hokkaido/ HU-E001/2022 (H5N1) | 99.8% | EPI2317996 |

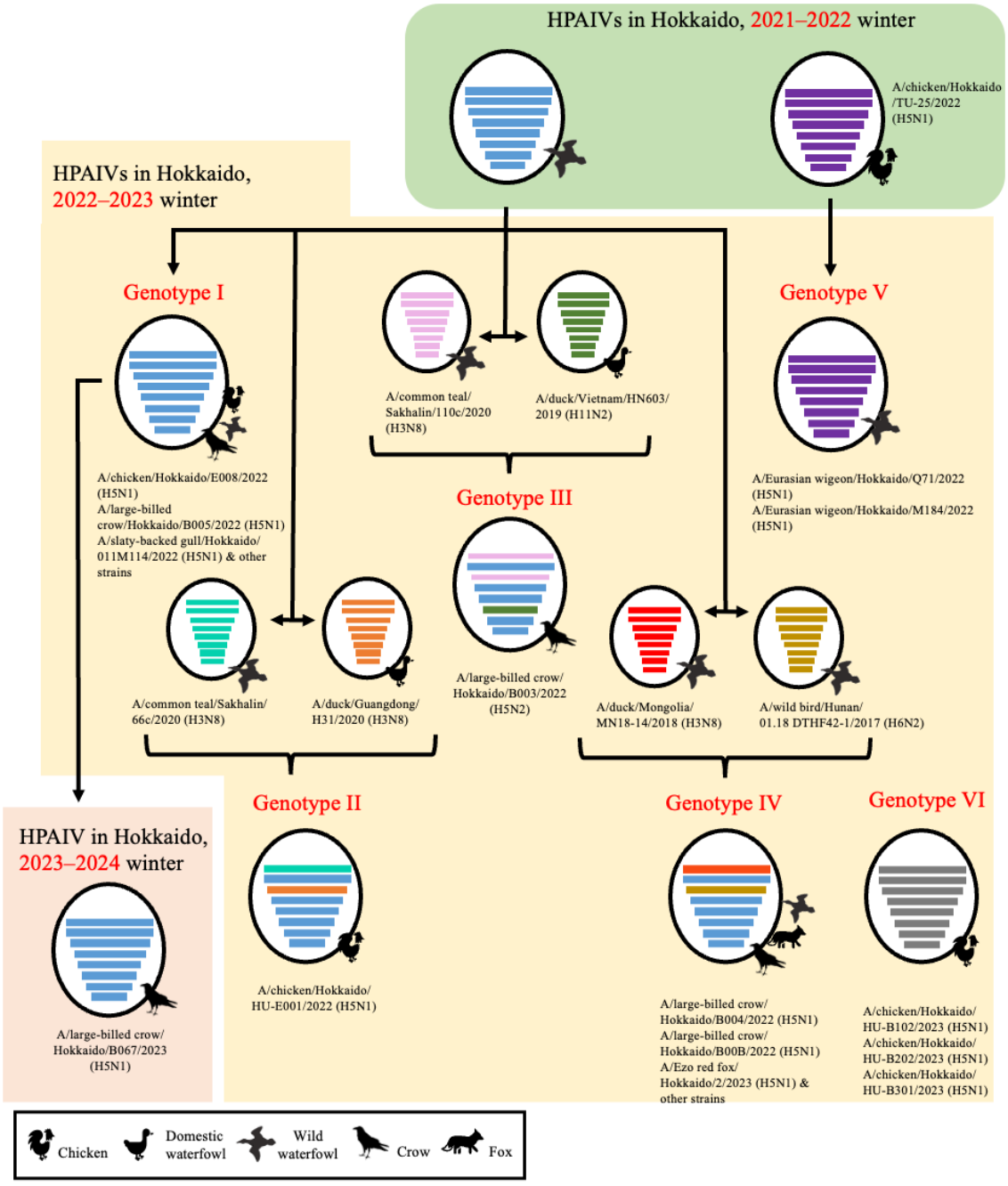


**Figure 2. Genome constellation of clade 2.3.4.4b H5 HPAIVs in Hokkaido in winter 2022–2023 and early winter 2023–2024**. Oval lines represent avian influenza virus; horizontal bars indicate the eight gene segments (from top to bottom): PB2, PB1, PA, HA, NP, NA, M, and NS. Each color represents a different viral origin.

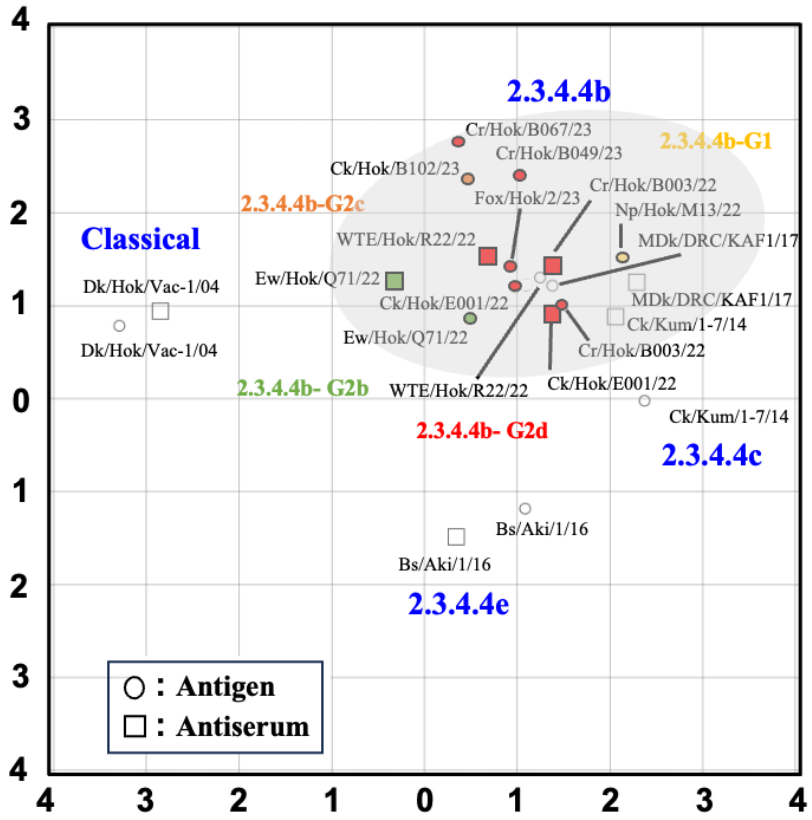


**Figure 3. Antigenic map based on cross-HI test on clade 2.3.4.4 H5 viruses and the sera**. The antigenic relationship among clade 2.3.4.4 H5 viruses, including six viruses in Hokkaido in winter 2022–2023 and a virus in early winter 2023–2024 in a different subclade of 2.3.4.4b, was visualized using antigenic cartography based on cross-HI test results, as indicated in Table 4. In the antigenic map, horizontal and vertical axes indicate the antigenic distance of spacing between the grid lines, representing one antigenic unit corresponding to a two-fold dilution in the HI assay. Antigen and antiserum in the subgroup of G2d in red, the subgroup of G1 in yellow, the subgroup of G2c in orange, and the subgroup of G2b in green. The highlighted gray area indicates H5 viruses and the sera in clade 2.3.4.4b.

**Table 4. Cross-HI assay of H5 HPAIVs in Hokkaido in winter 2022–2023 and early winter 2023–2024**

| Virus[1] | Subtype | Clade | Subclade | Hemagglutination inhibition titer[2] | | | | | | | |
|---|---|---|---|---|---|---|---|---|---|---|---|
| | | | | Cr/Hok/ B003/22 | Ck/Hok/ E001/22 | Ew/Hok/ Q71/22 | WTE/Hok/ R22/22 | Mdk/DRC/ KAF1/17 | Ck/Ku/ 1-7/14 | Bs/Aki/ 1/16 | Dk/Hok/ Vac-1/ 04 |
| Cr/Hok/B003/22 | H5N2 | 2.3.4.4b | G2d | 640[3] | 640 | 80 | 320 | 1280 | 640 | 160 | 20 |
| Ck/Hok/E001/22 | H5N1 | 2.3.4.4b | G2d | 320 | 640 | 160 | 320 | 1280 | 640 | 80 | 40 |
| Ew/Hok/Q71/22 | H5N1 | 2.3.4.4b | G2b | 320 | 640 | 320 | 160 | 1280 | 320 | 160 | 80 |
| WTE/Hok/R22/22 | H5N1 | 2.3.4.4b | G2d | 640 | 640 | 160 | 320 | 2560 | 640 | 80 | 40 |
| Np/Hok/M13/20 | H5N8 | 2.3.4.4b | G1 | 640 | 640 | 20 | 160 | 2560 | 640 | 40 | 20 |
| Mdk/DRC/KAF1/17 | H5N8 | 2.3.4.4b | N/A[4] | 640 | 640 | 80 | 160 | 1280 | 640 | 80 | 40 |
| Fox/Hok/2/23 | H5N1 | 2.3.4.4b | G2d | 640 | 640 | 160 | 320 | 1280 | 640 | 80 | 80 |
| Cr/Hok/B049/23 | H5N1 | 2.3.4.4b | G2d | 640 | 160 | 80 | 160 | 640 | 320 | 40 | 40 |
| Ck/Hok/B102/23 | H5N1 | 2.3.4.4b | G2c | 640 | 320 | 80 | 320 | 160 | 160 | 40 | 40 |
| Cr/Hok/B067/23 | H5N1 | 2.3.4.4b | G2d | 160 | 160 | 80 | 320 | 320 | 80 | 40 | 40 |
| Ck/Kum/1-7/14 | H5N8 | 2.3.4.4c | N/A | 320 | 640 | 40 | 20 | 640 | 640 | 80 | 20 |
| Bs/Akita/1/16 | H5N6 | 2.3.4.4e | N/A | 160 | 320 | 20 | 80 | 320 | 160 | 640 | 20 |
| Dk/Hok/Vac-1/04 | H5N1 | Classic | N/A | < 20 | 20 | 20 | 40 | 40 | < 20 | 40 | 640 |

[1]Each of abbreviated name is as following; Cr/Hok/B003/22: A/large-billed crow/Hokkaido/B003/2022 (H5N2), Ck/Hok/E001/22: A/chicken/Hokkaido/HU-E001/2022 (H5N1), Ew/Hok/Q71/22: A/Eurasian wigeon/Hokkaido/Q71/2022 (H5N1), WTE/Hok/R22/22: A/white-tailed eagle/Hokkaido/22-RU-WTE-2/2022 (H5N1), Np/Hok/M13/20: A/northern pintail/Hokkaido/M13/2020 (H5N1), Mdk/DRC/KAF1/17: A/Muscovy duck/DR Congo/KAF1/2017 (H5N8), Fox/Hok/2/23: A/Ezo red fox/Hokkaido/2/2023 (H5N1), Cr/Hok/49/2023: A/large-billed crow/Hokkaido/49/2023 (H5N1), Ck/Hok/B102/23: A/chicken/Hokkaido/HU-B102/2023 (H5N1), Cr/Hok/B067/23: A/large-billed crow/Hokkaido/B067/2023 (H5N1), Ck/Kum/1-7/14: A/chicken/Kumamoto/1-7/2014 (H5N8), Bs/Akita/1/16: A/black swan/Akita/1/2016 (H5N6), Dk/Hok/Vac-1/04: A/duck/Hokkaido/Vac-1/2004 (H5N1). [2]Antiserum against H5 virus isolates was used to test antigenicity of different H5Nx HPAIVs. [3]Underline values indicate homologous titers. [4]N/A: not applicable.

**Pathogenicity analysis of four representative HPAIV strains in chickens**

All 4-week-old White Leghorn and Chunky chickens were intranasally challenged with $10^{6.0}$ $EID_{50}$ of each of the four viruses, and all 31-week-old Rhode Island Red chickens were intranasally challenged with same titer of three viruses. All chickens challenged with Ck/Hok/E001/22 (H5N1) died at 2 dpc, whereas chickens challenged with Cr/Hok/B003/22 (H5N2) died between 2 and 4 dpc (Figure 4). Chickens challenged with Ew/Hok/Q71/22 (H5N1) died between 3 and 5 dpc. Meanwhile, chickens challenged with Ck/Hok/B102/23 (H5N1) started to die between 2 and 4 dpc. Remarkably, one of the chickens inoculated with Ck/Hok/B102/23 (H5N1) survived until 14 dpc, but with no detectable antiserum collected on the last day of the experiment against the virus (Figure 4). Furthermore, no viruses were recovered from the swab samples of the survived chicken throughout 7 days after challenge.

Virus titers in tracheal swabs collected from chickens challenged with Ck/Hok/E001/22 (H5N1) rapidly peaked at 1–2 dpc (Tables 5–7). In contrast, virus titers in tracheal swabs of chickens challenged with Cr/Hok/B003/22 (H5N2) at 1 dpc were low (< 2.5 $\log_{10}$ $TCID_{50}$/mL) but rapidly increased at 2–3 dpc (> 4.0 $\log_{10}$ $TCID_{50}$/mL) (Tables 5–7). Virus recovery was not confirmed from tracheal swabs of chickens challenged with Ew/Hok/Q71/22 (H5N1) on 1 dpc but confirmed with a steady increase in virus titer from 2 to 5 dpc and the virus titers recovered at the peak of infection was much lower (< 4.0 $\log_{10}$ $TCID_{50}$/mL) when compared to ones after challenge of Ck/Hok/E001/22 (H5N1) and Cr/Hok/B003/22 (H5N2) (Tables 5–7). For the virus recovery from the tracheal swabs of chicken challenged with Ck/Hok/B102/23 (H5N1), virus growth was not recognized at 1 dpc (< 0.5 $\log_{10}$ $TCID_{50}$/mL) but rapidly peaked at 2 and 3 dpc (> 3.5 $\log_{10}$ $TCID_{50}$/mL). Interestingly, the virus recovery from the tracheal swabs of chunky chickens challenged with Ck/Hok/B102/23 (H5N1) showed a steady increase in the virus titers from 2 to 4 dpc (Tables 5 and 6). Virus recoveries from cloacal swabs also demonstrated a similar viral load observed in tracheal swabs in all three chicken breeds. Pathogenicity and viral titers in swab samples varied among challenged strains. While viral loads in tracheal and cloacal swabs differed among the three chicken breeds based on the strains, the growth ability of each virus remained consistent across breeds, regardless of species or age.

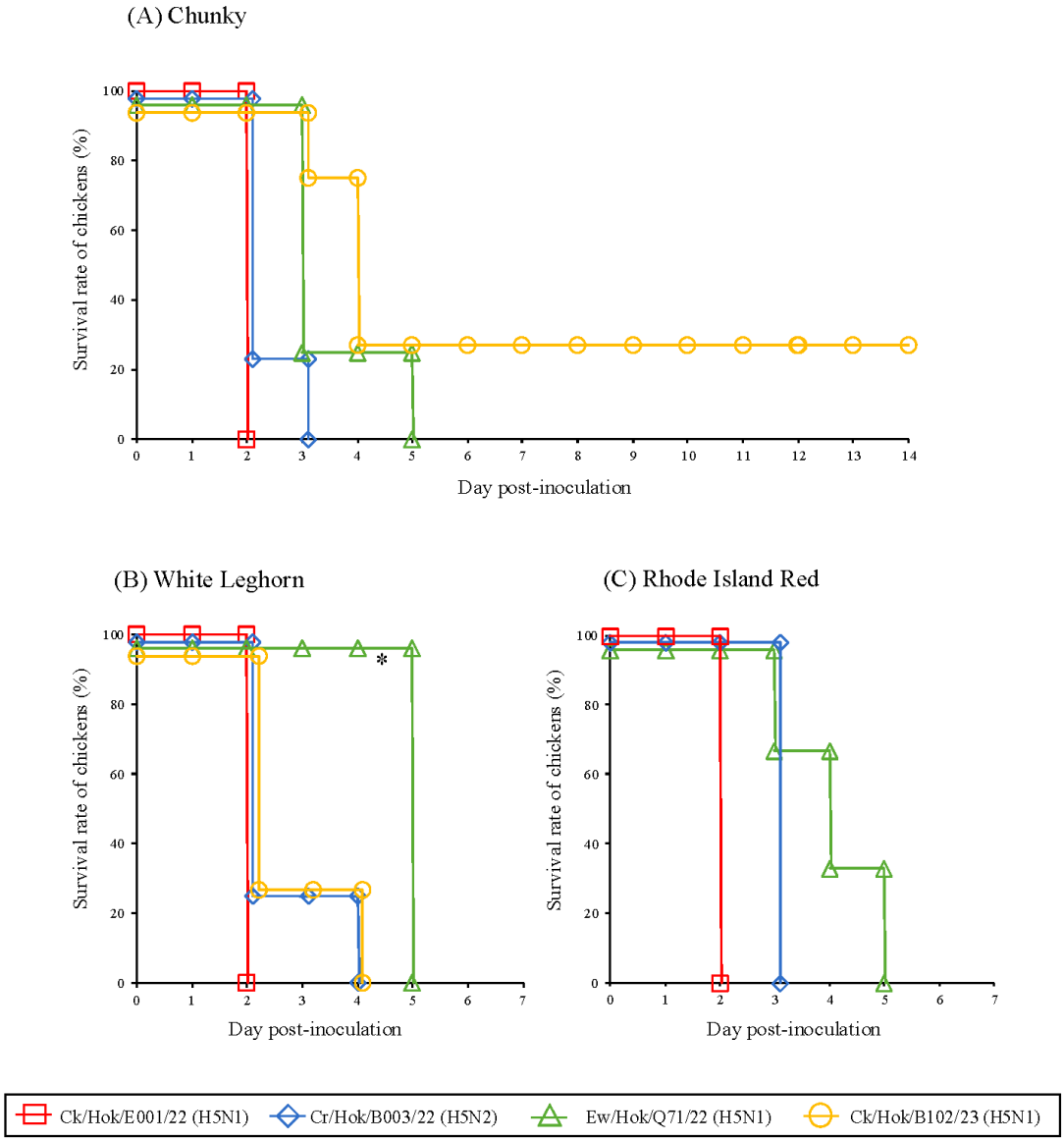


**Figure 4. Survival curve of three chicken breeds inoculated with four H5 HPAIVs**. Three groups of four 4-week-old Chunky **(A)** and White Leghorn **(B)** and three 31-week-old of Rhode Island red **(C)** chickens were intranasally inoculated with $10^{6.0}$ $EID_{50}$/0.1 mL Ck/Hok/E001/22 (H5N1), Cr/Hok/B003/22 (H5N2), Ew/Hok/Q71/22 (H5N1), and Ck/Hok/B102/23, except for Rhode Island Red chickens only challenged with Ck/Hok/E001/22 (H5N1), Cr/Hok/B003/22 (H5N2), and Ew/Hok/Q71/22 (H5N1), respectively, and monitored for 14 days after virus challenge. Clinical manifestation of each chicken was observed, and their survival was recorded daily to calculate the survival rate of each group per day. The survival curve in this figure shows only 14 dpc for chunky chickens and 7 dpc for White Leghorn and Rhode Island Red chickens, and the *P*-values for survival rate were calculated using the Kaplan–Meier survival curve log-rank test ($^{*}p < 0.05$).

**Table 5. Virus recovery from swabs collected in Chunky chickens after post-inoculation with four representative viruses**

| Virus | Days on dead | Virus titers in swab sample ($log_{10}$ $TCID_{50}$/mL) | | | | | | | | | | | | | |
|---|---|---|---|---|---|---|---|---|---|---|---|---|---|---|---|
| | | Day 1 | | Day 2 | | Day 3 | | Day 4 | | Day 5 | | Day 6 | | Day 7 | |
| | | Trac[1] | Cloa[2] | Trac | Cloa | Trac | Cloa | Trac | Cloa | Trac | Cloa | Trac | Cloa | Trac | Cloa |
| Ck/Hok/ | 2 | 1.4 | 2.7 | 5.5 | 3.7 | –[3] | – | – | – | – | – | – | – | – | – |
| E001/22 | 2 | 2.5 | 3.5 | 4.7 | 5.0 | – | – | – | – | – | – | – | – | – | – |
| (H5N1) | 2 | < 0.5[4] | < 0.5 | 5.0 | 3.7 | – | – | – | – | – | – | – | – | – | – |
| | 2 | 2.0 | 2.2 | 4.7 | 4.3 | – | – | – | – | – | – | – | – | – | – |
| Cr/Hok/ | 2 | < 0.5 | < 0.5 | 5.5 | 4.7 | – | – | – | – | – | – | – | – | – | – |
| B003/22 | 2 | < 0.5 | < 0.5 | 6.0 | 5.0 | – | – | – | – | – | – | – | – | – | – |
| (H5N2) | 2 | < 0.5 | < 0.5 | 5.5 | 3.5 | – | – | – | – | – | – | – | – | – | – |
| | 3 | < 0.5 | < 0.5 | 1.5 | < 0.5 | 5.7 | 3.5 | – | – | – | – | – | – | – | – |
| Ew/Hok/ | 5 | < 0.5 | < 0.5 | < 0.5 | < 0.5 | 2.5 | < 0.5 | 3.7 | 2.3 | 2.7 | 1.7 | – | – | – | – |
| Q71/22 | 3 | < 0.5 | < 0.5 | 3.5 | 1.5 | 3.3 | 3.5 | – | – | – | – | – | – | – | – |
| (H5N1) | 3 | < 0.5 | < 0.5 | 3.5 | 2.0 | 3.5 | 2.5 | – | – | – | – | – | – | – | – |
| | 3 | < 0.5 | < 0.5 | 4.3 | 2.0 | 4.0 | 2.0 | – | – | – | – | – | – | – | – |
| Ck/Hok/ | 4 | < 0.5 | < 0.5 | 1.8 | < 0.5 | 3.0 | 2.7 | 4.5 | 2.3 | – | – | – | – | – | – |
| B102/23 | 4 | < 0.5 | < 0.5 | < 0.5 | < 0.5 | < 0.5 | < 0.5 | 4.5 | 4.7 | – | – | – | – | – | – |
| (H5N1) | 3 | < 0.5 | < 0.5 | 4.3 | 4.3 | 4.3 | 4.0 | – | – | – | – | – | – | – | – |
| | 14[5] | < 0.5 | < 0.5 | < 0.5 | < 0.5 | < 0.5 | < 0.5 | < 0.5 | < 0.5 | < 0.5 | < 0.5 | < 0.5 | < 0.5 | < 0.5 | < 0.5 |

[1]Trac: Tracheal. [2]Cloa: Cloacal. [3]No samples were collected. [4]< 0.5 $log_{10}$ $TCID_{50}$/mL is the lowest detection limit of the virus titers. [5]Euthanized on 14 dpc.

**Table 6. Virus recovery from swabs collected in White Leghorn chickens after post-inoculation with four representative viruses**

| Virus | Days on dead | Virus titers in swab sample ($log_{10}$ $TCID_{50}$/mL) | | | | | | | | | |
|---|---|---|---|---|---|---|---|---|---|---|---|
| | | Day 1 | | Day 2 | | Day 3 | | Day 4 | | Day 5 | |
| | | Tracheal | Cloacal | Tracheal | Cloacal | Tracheal | Cloacal | Tracheal | Cloacal | Tracheal | Cloacal |
| Ck/Hok/E001/22 (H5N1) | 2 | 1.5 | 2.0 | 3.7 | 2.3 | –[1] | – | – | – | – | – |
| | 2 | 2.0 | 2.7 | 3.7 | 1.7 | – | – | – | – | – | – |
| | 2 | 4.0 | 1.3 | 4.7 | 3.0 | – | – | – | – | – | – |
| | 2 | 2.5 | < 0.5[2] | 4.3 | 3.7 | – | – | – | – | – | – |
| Cr/Hok/B003/22 (H5N2) | 2 | 2.5 | < 0.5 | 6.0 | 3.5 | – | – | – | – | – | – |
| | 2 | < 0.5 | < 0.5 | 4.0 | 3.0 | – | – | – | – | – | – |
| | 2 | 2.3 | 2.3 | 4.0 | 3.5 | – | – | – | – | – | – |
| | 4 | < 0.5 | < 0.5 | 1.7 | < 0.5 | 3.7 | 2.7 | – | – | – | – |
| Ew/Hok/Q71/22 (H5N1) | 5 | < 0.5 | < 0.5 | < 0.5 | < 0.5 | 1.0 | < 0.5 | 2.7 | < 0.5 | 2.7 | 1.5 |
| | 5 | < 0.5 | < 0.5 | 1.0 | < 0.5 | 1.7 | < 0.5 | 2.0 | < 0.5 | 2.7 | 1.8 |
| | 5 | < 0.5 | < 0.5 | < 0.5 | < 0.5 | < 0.5 | < 0.5 | 3.5 | 1.7 | 2.7 | 2.0 |
| | 5 | < 0.5 | < 0.5 | < 0.5 | 1.0 | 1.3 | 1.5 | 3.5 | 2.0 | 3.5 | 1.7 |
| Ck/Hok/B102/23 (H5N1) | 2 | < 0.5 | < 0.5 | 3.7 | 3.0 | – | – | – | – | – | – |
| | 2 | < 0.5 | < 0.5 | 4.0 | 2.7 | – | – | – | – | – | – |
| | 2 | < 0.5 | < 0.5 | 4.5 | 2.7 | – | – | – | – | – | – |
| | 4 | < 0.5 | < 0.5 | < 0.5 | < 0.5 | 2.7 | 2.7 | 2.3 | 2.3 | – | – |

[1]No samples were collected. [2]< 0.5 $log_{10}$ $TCID_{50}$/mL is the lowest detection limit of the virus titers.

**Table 7. Virus recovery from swabs collected in Rhode Island Red chickens after post-inoculation with three representative viruses**

| Virus | Days on dead | Virus titers in swab sample ($log_{10}$ $TCID_{50}$/mL) | | | | | | | | | |
|---|---|---|---|---|---|---|---|---|---|---|---|
| | | Day 1 | | Day 2 | | Day 3 | | Day 4 | | Day 5 | |
| | | Tracheal | Cloacal | Tracheal | Cloacal | Tracheal | Cloacal | Tracheal | Cloacal | Tracheal | Cloacal |
| Ck/Hok/E001/22 (H5N1) | 2 | 1.5 | 2.0 | 4.7 | 5.7 | –[1] | – | – | – | – | – |
| | 2 | 1.0 | 2.0 | 6.0 | 4.0 | – | – | – | – | – | – |
| | 2 | 1.3 | 1.5 | 4.0 | 4.5 | – | – | – | – | – | – |
| Cr/Hok/B003/22 (H5N2) | 3 | < 0.5[2] | < 0.5 | 2.0 | 1.5 | 4.7 | 4.7 | – | – | – | – |
| | 3 | < 0.5 | < 0.5 | 4.0 | 3.7 | 4.7 | 4.7 | – | – | – | – |
| | 3 | 1.0 | 1.5 | 6.0 | 5.5 | 6.3 | 5.3 | – | – | – | – |
| Ew/Hok/Q71/22 (H5N1) | 3 | < 0.5 | < 0.5 | < 0.5 | < 0.5 | 2.0 | 2.5 | – | – | – | – |
| | 4 | < 0.5 | < 0.5 | 1.0 | < 0.5 | 2.0 | 3.7 | 1.0 | 3.0 | – | – |
| | 5 | < 0.5 | < 0.5 | 2.0 | < 0.5 | 3.3 | < 0.5 | 2.0 | < 0.5 | 2.5 | 1.5 |

[1]Indicate no samples were collected.

[2]< 0.5 $log_{10}$ $TCID_{50}$/mL is the lowest detection limit of the virus titers.

**Mutational analysis**

Detailed mutational analysis was performed with 30 isolates in Hokkaido with whole-genome sequences to identify amino acid substitutions that could contribute to virulence, transmissibility, or host adaptation. Thirty-eight variable sites were identified and specifically linked to phenotypes, such as virulence, transmission, or host adaptation, as reported previously [57]. Of these 38 variable sites, eight were identified in PB2, three in PB1, one in PB1-F2 [60], five in PA, eight in HA based on H5 numbering, three in NP, three in M1, and seven in NS1 (Table 8). Due to the introduction of multiple HPAIV genotypes in Hokkaido in 2022–2023, different variables have been found across some genotypes, such as L292V in PB2, S224P in PA, and N319K in NP, previously reported to have contributed to enhancing polymerase activity and virulence in mice [61–63]. Some mutations, such as K207R in PB1 and Q400P in PA, known to decrease polymerase activity in mice, have also been identified in some genotypes [64, 65]. Interestingly, one mutation, such as M105V in NP, was exclusively found in all isolates, except for Ew/Hok/Q71/22 (H5N1) and Ew/Hok/M184/22 (H5N1), as this mutation is known to increase pathogenicity in chickens [66]. In addition, the signature of mammalian adaptation gene markers, such as lysine and asparagine at positions 627 and 701 in PB2, was not found in all isolates investigated and deceased Ezo red foxes.

**Table 8. Mutational analysis on all the reported amino acid positions of H5 HPAIVs isolated in Hokkaido in winter 2022–2023 and early winter 2023–2024**

| Segment | Mutation | Amino acid in the following number of virus[1] | | | | | | | | | | | | | | | | | | | | | | | | | | | | | | Associated phenotypes |
|---|---|---|---|---|---|---|---|---|---|---|---|---|---|---|---|---|---|---|---|---|---|---|---|---|---|---|---|---|---|---|---|---|
| | | 1 | 2 | 3 | 4 | 5 | 6 | 7 | 8 | 9 | 10 | 11 | 12 | 13 | 14 | 15 | 16 | 17 | 18 | 19 | 20 | 21 | 22 | 23 | 24 | 25 | 26 | 27 | 28 | 29 | 30 | |
| PB2 | L89V | V | •[2] | • | • | • | • | • | • | • | • | • | • | • | • | • | • | • | • | • | • | • | • | • | • | • | • | • | • | • | • | Enhanced polymerase activity, increased virulence in mice |
| | I292V | I | • | • | • | V | V | V | • | V | V | V | • | • | V | • | V | • | • | V | • | V | • | • | • | • | • | • | • | V | V | Enhanced polymerase activity, increased virulence in mice |
| | G309D | D | • | • | • | • | • | • | • | • | • | • | • | • | • | • | • | • | • | • | • | • | • | • | • | • | • | • | • | • | • | Enhanced polymerase activity, increased virulence in mice |
| | T339K | K | • | • | • | • | • | • | • | • | • | • | • | • | • | • | • | • | • | • | • | • | • | • | • | • | • | • | • | • | • | Enhanced polymerase activity, increased virulence in mice |
| | R477G | G | • | • | • | • | • | • | • | • | • | • | • | • | • | • | • | • | • | • | • | • | • | • | • | • | • | • | • | • | • | Enhanced polymerase activity, increased virulence in mice |
| | I495V | V | • | • | • | • | • | • | • | • | • | • | • | • | • | • | • | • | • | • | • | • | • | • | • | • | • | • | • | • | • | Enhanced polymerase activity, increased virulence |
| | A676T | T | • | I | • | • | • | • | • | • | • | • | • | • | • | • | • | • | • | • | • | • | • | • | • | • | • | • | • | • | • | Enhanced polymerase activity, increased virulence in mice |
| | S715N | N | • | • | • | • | • | • | • | • | • | • | • | • | • | • | • | • | • | • | • | • | • | • | • | • | • | • | • | • | • | Decreased virulence in mice |
| PB1 | D3V | V | • | • | • | • | • | • | • | • | • | • | • | • | • | • | • | • | • | • | • | • | • | • | • | • | • | • | • | • | • | Enhanced polymerase activity and replication in mammalian cell line |
| | K207R | K | • | R | • | • | R | R | R | • | • | • | • | • | • | • | • | • | • | • | • | • | • | • | R | R | • | • | • | • | • | Decreased polymerase activity in mammalian cell line |
| | D622G | G | • | • | • | • | • | • | • | • | • | • | • | • | • | • | • | • | • | • | • | • | • | • | • | • | • | • | • | • | • | Enhanced polymerase activity, increased virulence in mice |

**Table 8** (*cont*)**. Mutational analysis on all the reported amino acid positions of H5 HPAIVs isolated in Hokkaido in winter 2022–2023 and early winter 2023–2024**

| Segment | Mutation | Amino acid in the following number of virus[1] | | | | | | | | | | | | | | | | | | | | | | | | | | | | | | Associated phenotypes |
|---|---|---|---|---|---|---|---|---|---|---|---|---|---|---|---|---|---|---|---|---|---|---|---|---|---|---|---|---|---|---|---|---|
| | | 1 | 2 | 3 | 4 | 5 | 6 | 7 | 8 | 9 | 10 | 11 | 12 | 13 | 14 | 15 | 16 | 17 | 18 | 19 | 20 | 21 | 22 | 23 | 24 | 25 | 26 | 27 | 28 | 29 | 30 | |
| PB1-F2 | N66S | N | •[2] | S | S | S | S | S | S | S | S | S | S | S | S | S | S | S | S | S | S | S | S | S | S | S | S | S | S | S | S | Enhanced polymerase activity, virulence and antiviral response in mice |
| | S224P | S | • | • | P | P | • | • | P | • | • | • | • | • | • | • | • | • | • | • | P | • | • | • | • | • | • | • | • | • | • | Enhanced polymerase activity, increased virulence in mice and duck |
| PA | S224P | S | • | • | P | P | • | • | P | • | • | • | • | • | • | • | • | • | • | • | P | • | • | • | • | • | • | • | • | • | • | Enhanced polymerase activity and virulence in mice and duck |
| | H266R | R | • | • | • | • | • | • | • | • | • | • | • | • | • | • | • | • | • | • | • | • | • | • | • | • | • | • | • | • | • | Enhanced polymerase activity and replication in mammalian cell line |
| | N383D | N | • | • | • | • | • | • | • | • | D | D | D | • | D | D | D | • | • | D | • | D | • | • | • | • | D | D | D | D | D | Enhanced polymerase activity and replication in mammalian cell line |
| | Q400P | Q | • | • | P | P | P | P | P | P | • | • | • | P | • | • | • | P | P | • | P | • | P | P | P | P | P | P | P | • | • | Decreased virulence in mice |
| | A515T | T | • | • | • | • | • | • | • | • | • | • | • | • | • | • | • | • | • | • | • | • | • | • | • | • | • | • | • | • | • | Enhanced polymerase activity, increased virulence in mammals and birds |
| | S107R | R | • | • | • | • | • | • | • | • | • | • | • | • | • | • | • | • | • | • | • | • | • | • | • | • | • | • | • | • | • | Increased virulence in chicken and mice, increased PH fusion |
| HA[3] | T108I | I | • | • | • | • | • | • | • | • | • | • | • | • | • | • | • | • | • | • | • | • | • | • | • | • | • | • | • | • | • | Increased virulence in chicken and mice, increased PH fusion |
| | S123P | P | • | • | • | • | • | • | • | • | • | • | • | • | • | • | • | • | • | • | • | • | • | • | • | • | • | • | • | • | • | Increased virus binding to α2-6 |

**Table 8** (*cont*)**. Mutational analysis on all the reported amino acid positions of H5 HPAIVs isolated in Hokkaido in winter 2022–2023 and early winter 2023–2024**

| Segment | Mutation | Amino acid in the following number of virus[1] | | | | | | | | | | | | | | | | | | | | | | | | | | | | | | Associated phenotypes |
|---|---|---|---|---|---|---|---|---|---|---|---|---|---|---|---|---|---|---|---|---|---|---|---|---|---|---|---|---|---|---|---|---|
| | | 1 | 2 | 3 | 4 | 5 | 6 | 7 | 8 | 9 | 10 | 11 | 12 | 13 | 14 | 15 | 16 | 17 | 18 | 19 | 20 | 21 | 22 | 23 | 24 | 25 | 26 | 27 | 28 | 29 | 30 | |
| HA[3] | S133A | A | •[2] | • | • | • | • | • | • | • | • | • | • | • | • | • | • | • | • | • | • | • | • | • | • | • | • | • | • | • | • | Increased pseudovirus binding to α2-6 |
| | T156A | A | • | • | • | • | • | • | • | • | • | • | • | • | • | • | • | • | • | • | • | • | • | • | • | • | • | • | • | • | • | Increased virus binding to α2-6, increased transmission in guinea pigs |
| | K218Q | Q | • | • | • | • | • | • | • | • | • | • | • | • | • | • | • | • | • | • | • | • | • | • | • | • | • | • | • | • | • | Increased virus binding to α2-6 and α2-3 |
| | S223R | R | • | • | • | • | • | • | • | • | • | • | • | • | • | • | • | • | • | • | • | • | • | • | • | • | • | • | • | • | • | Increased virus binding to α2-6 and α2-4 |
| | P235S | P | • | • | • | • | • | • | • | • | • | • | S | • | • | • | • | • | • | • | • | • | • | • | • | • | • | • | • | • | • | Increased virus binding to α2-6 |
| NP | M105V | M | • | V | V | V | V | V | V | V | V | V | V | V | V | V | V | V | V | V | V | V | V | V | V | V | V | V | V | V | V | Increased virulence in chickens |
| | A184K | K | • | • | • | • | • | • | • | • | • | • | • | • | • | • | • | • | • | • | • | • | • | • | • | • | • | • | • | • | • | Increased replication in avian cells and virulence in chickens |
| | N319K | N | • | K | K | K | K | K | K | K | K | K | K | K | K | K | K | K | K | K | K | K | K | K | K | K | • | • | • | K | K | Increased polymerase activity and replication in mammalian cell line |
| | M105V | M | • | V | V | V | V | V | V | V | V | V | V | V | V | V | V | V | V | V | V | V | V | V | V | V | V | V | V | V | V | Increased virulence in chickens |
| | A184K | K | • | • | • | • | • | • | • | • | • | • | • | • | • | • | • | • | • | • | • | • | • | • | • | • | • | • | • | • | • | Increased replication in avian cells and virulence in chickens |
| | N319K | N | • | K | K | K | K | K | K | K | K | K | K | K | K | K | K | K | K | K | K | K | K | K | K | K | • | • | • | K | K | Increased polymerase activity and replication in mammalian cell line |

**Table 8** (*cont*)**. Mutational analysis on all the reported amino acid positions of H5 HPAIVs isolated in Hokkaido in winter 2022–2023 and early winter 2023–2024**

| Segment | Mutation | Amino acid in the following number of virus[1] | | | | | | | | | | | | | | | | | | | | | | | | | | | | | | Associated phenotypes |
|---|---|---|---|---|---|---|---|---|---|---|---|---|---|---|---|---|---|---|---|---|---|---|---|---|---|---|---|---|---|---|---|---|
| | | 1 | 2 | 3 | 4 | 5 | 6 | 7 | 8 | 9 | 10 | 11 | 12 | 13 | 14 | 15 | 16 | 17 | 18 | 19 | 20 | 21 | 22 | 23 | 24 | 25 | 26 | 27 | 28 | 29 | 30 | |
| M1 | N30D | D | •[2] | • | • | • | • | • | • | • | • | • | • | • | • | • | • | • | • | • | • | • | • | • | • | • | • | • | • | • | • | Increased virulence in mice |
| | I43M | M | • | • | • | • | • | • | • | • | • | • | • | • | • | • | • | • | • | • | • | • | • | • | • | • | • | • | • | • | • | Increased virulence in chickens |
| | T215A | A | • | • | • | • | • | • | • | • | • | • | • | • | • | • | • | • | • | • | • | • | • | • | • | • | • | • | • | • | • | Increased virulence in mice |
| NS1 | P42S | S | • | • | • | • | • | • | • | • | • | • | • | • | • | • | • | • | • | • | • | • | • | • | • | • | • | • | • | • | • | Increased virulence and decreased antiviral response in mice |
| | K55E | E | • | • | • | • | • | • | • | • | • | • | • | • | • | • | • | • | • | • | • | • | • | • | • | • | • | • | • | • | • | Increased replication in mammalian cells and decreased interferon response |
| | K66E | E | • | • | • | • | • | • | • | • | • | • | • | • | • | • | • | • | • | • | • | • | • | • | • | • | • | • | • | • | • | Increased replication in mammalian cells and decreased interferon response |
| | L103F | F | • | • | • | • | • | • | • | • | • | • | • | • | • | • | • | • | • | • | • | • | • | • | • | • | • | • | • | • | • | Increased replication in mammalian cells and virulence in mice |
| | I106M | M | • | • | • | • | • | • | • | • | • | • | • | • | • | • | • | • | • | • | • | • | • | • | • | • | • | • | • | • | • | Increased replication in mammalian cells and virulence in mice |
| | C138F | F | • | • | • | • | • | • | • | • | • | • | • | • | • | • | • | • | • | • | • | • | • | • | • | • | • | • | • | • | • | Increased replication in mammalian cells and decreased interferon response |
| | V149A | A | • | • | • | • | • | • | • | • | • | • | • | • | • | • | • | • | • | • | • | • | • | • | • | • | • | • | • | • | • | Increased virulence and decreased interferon responded in chickens |

[1]The number of the virus is corresponding to ID in Table 2. [2]Dot indicates same amino acid in virus number 1. [3]H5 numbering relative to A/Vietnam/1203/2004 (H5N1).

## Discussion

The global spread of clade 2.3.4.4b H5 HPAIVs has caused a large-scale outbreak, significantly impacting the poultry industry and wildlife. The Far East, such as Japan and other countries, has been recognized as a hotspot due to the continuous introduction of HPAIVs. In winter 2021–2022, high numbers of dead wild birds and outbreaks in the poultry farm were affected in Hokkaido due to the introduction of 2.3.4.4b H5N1 HPAIVs [21]. The continuous circulation of H5 HPAIVs in 2023 by migratory birds has disseminated viruses into rarely affected countries in the South American region, such as Peru, Ecuador, and Venezuela [28]. Hokkaido was no exception to the continual invasion of clade 2.3.4.4b H5 HPAIVs in winter 2022–2023. In this study, 30 HPAIVs isolated in Hokkaido were genetically analyzed in all eight gene segments. Based on the phylogenetic analysis of the HA gene segment, all Hokkaido isolates still belonged to clade 2.3.4.4b and further formed three phylogenetic clusters of G2b, G2c, and G2d (Figure 1A). HPAIVs in the G2d subgroup share common ancestors closely related to Hokkaido isolates in winter 2021–2022, together with A/crow/Khabarovsk/776-56/2022 (H5N1) and A/goose/Magadan/2272-5/2022 (H5N1) isolated in eastern Russia in spring and autumn 2022. This might indicate that Hokkaido isolates in winter 2021–2022 in the G2d subgroup had been carried over outside of Hokkaido, including eastern Russia, by spring migration and could have been maintained in the nested lake in northern Russia during summer 2022. An isolate in Hokkaido in November 2023 was also grouped into the subgroup G2d. The continuous introduction of HPAIVs in the subgroup G2d during the three consecutive seasons could reveal that the viruses in this subgroup should be sustained in the Russian Far East and carried back and forth from Hokkaido, even with three different subgroups (G2b, G2c, and G2d) of H5 HPAIVs been introduced into Hokkaido in winter 2022–2023. This finding can also be supported by the results of gene constellation analysis that genotype I, which is a dominant genotype in Hokkaido in winter 2022–2023, had dominantly caused outbreaks for a certain period [21], was also a majority in winter 2021–2022 and isolated at the beginning of winter 2023–2024. A similar assumption was also proposed for HPAIV isolates in the G2b subgroup. Based on BLAST analysis, some Hokkaido isolates in winter 2022–2023, such as Ew/Hok/Q71/22 (H5N1) and Ew/Hok/M184/22 (H5N1) in the G2b subgroup, showed high sequence

identity to Ck/Hok/TU25-3/22 (H5N1) isolated in the poultry outbreak at the end of spring 2022 in Hokkaido. The nucleotide sequences of those isolates were highly homologous to H5 HPAIVs isolated in southern Japan in winter 2021–2022. These observations also suggested that HPAIV isolates in the G2b subgroup were likely to be brought to Hokkaido by bird migration in spring 2022 and maintained in northern and eastern Russia during summer 2022. These HPAIVs were reintroduced into the Far East in the following autumn migration [21]. Multiple HPAI outbreaks caused by H5 HPAIVs in Hokkaido poultry were also reported in early April 2023. One of the isolates from the poultry outbreak, Ck/Hok/B102/23 (H5N1), clustered in G2c subgroup, showed high genetic similarity to isolates from southern Japan in winter 2022–2023. Those isolates were also genetically close to those circulating in the Republic of Korea and China [39], and invasion of HPAIVs in southern Japan to Hokkaido was speculated once again in winter 2022–2023 following the spring migration.

During the winter 2022–2023, multiple genotypes of HPAIVs could have been sporadically introduced into Hokkaido. Extensive reassortment events in 2.3.4.4b H5N1 HPAIVs have been frequently reported, such as the recent cases in the Republic of Korea and China, where genetic reassortment was observed between clade 2.3.4.4b H5 HPAIVs with Eurasian LPAIVs [38, 39, 58]. Based on phylogenetic trees of other internal gene segments in this study, it was confirmed that multiple genotypes, genotypes II and III, were reassorted (Figure 2). Reassorted HPAIVs were produced between clade 2.3.4.4b H5 HPAIVs, genotype I, circulating predominantly in Hokkaido in winter 2021–2022, and LPAIVs originated from wild birds in the Far East. It was speculated that dominant H5N1 HPAIVs in European or Asian countries could undergo genetic reassortment with other LPAIVs during migration or at the breeding sites of migratory birds. Thus, further genetic analysis should provide the role of wild birds in contributing to the reshuffle of genetic properties of AIVs, which allows the formation of a temporary genome constellation of viruses that might enhance the transmission and pathogenicity in wild birds [67]. However, there were limitations in this study, as many HPAIV cases in wild birds were reported through the passive survey for H5 HPAIV in Japan from the suspected dead birds. This may not represent the true ecology of the geographical distribution of three H5 HPAIV subgroups (G2b, G2c, and G2d) in Japan.

The unusually high number of dead crows positive for H5 HPAIVs in Hokkaido was also reported in winter 2022–2023, similar to winter 2021–2022 [21]. Interestingly, multiple H5 HPAIV genotypes, genotypes I, III, and IV (Figure 2), were identified among dead crows discovered in the city center of Hokkaido, in winter 2022–2023, indicating that crows could play a role in virus transmission by introducing various genotypes of HPAIVs from the outside to inside of the poultry farm. Many HPAI cases in crows may have led to virus spillover to foxes, as HPAIVs isolated from crows and foxes were genetically highly homologous to another. The increase in spillover of HPAIVs from birds to mammals has also caused great concern for public health regarding the adaptation of HPAIVs in mammals.

The antigenicity of isolates in winter 2022–2023 and an isolate in November 2023 was close to those of clade 2.3.4.4b H5 HPAIVs isolated in Japan or the Democratic Republic of the Congo of Africa in the past few years and still close with H5 HPAIVs in clade 2.3.4.4c (Figure 3). In contrast, moderate differences in antigenicity between clades 2.3.4.4b and 2.3.4.4e H5 HPAIVs were observed, as supported by the previous study investigating clade 2.3.4.4b H5 HPAIVs in Japan and Africa [51, 54]. In addition, slight differences in antigenicity among isolates of three subgroups, G2b, G2c, and G2d, were observed, corresponding to an observation in a study among subgroups G2b and G2d of 2.3.4.4b H5 HPAIV isolates in Japan in winter 2021–2022 [35]. Since autumn 2021, the Eurasian lineage of H5 HPAIVs in clade 2.3.4.4b has been spreading globally and eventually introduced into countries such as the South American region, which are rarely affected by H5 HPAIVs in this lineage. The constant widespread of H5 HPAIV might generate HPAIVs with different characteristics, including antigenicity. However, the antigenicity of the isolates in Hokkaido has demonstrated minor antigenicity changes in the past several seasons, indicating preservation of H5 HPAIVs in clade 2.3.4.4b under less selective pressure for major antigenicity changes.

A low morbidity rate but a sudden increase in lethality rates in broiler flocks has been described during an outbreak of clade 2.3.4.4b H5N1 HPAIV in Italy in winter 2021–2022 [68]. Thus, to understand the pathogenicity of H5 HPAIVs in different chicken breeds, four representative HPAIVs with different gene constellations were selected for pathogenicity study in three chicken breeds. In this study, it was highlighted that Chunky

(broiler) chickens also demonstrated similar mortality rates and clinical signs to the ones found in White Leghorn (layer) and Rhode Island Red (layer) chickens except for one strain. The pathogenicity of Ck/Hok/B102/23 (H5N1) in Chunky chicken was significantly lower than in White Leghorn chicken, corresponding to the observation reported in Italy broiler flocks even though the virus load recovered from the swab samples among Chunky and White Leghorn chickens were similar (Tables 5 and 6). The difference in the pathogenicity displayed in different chicken breeds can be due to the existence of some avian genes such as plasminogen activator urokinase, vascular cell adhesion molecule 1 protein, tumor necrosis factor receptor superfamily member 1A, and placental growth factor gene, which were downregulated during inflammatory response in the lungs of the chicken breed, which can affect disease tolerance; the commercial broiler in Spain was reported to be resistant toward the clade 2.3.4.4b H5N8 HPAIV infection [69]. In this study, it is estimated that the 50% chicken lethal dose ($CLD_{50}$) of Ck/Hok/B102/23 (H5N1) in Chunky chicken should be $10^{5.7}$ $EID_{50}$, which is higher than the ones previously reported in White Leghorn chicken [35]. Furthermore, in the pathogenicity assessment of representative HPAIVs in all three chicken breeds, the pathogenicity of Ck/Hok/E001/22 (H5N1) was generally highest, followed by Cr/Hok/B003/22 (H5N2), lastly Ew/Hok/Q71/22 (H5N1) and Ck/Hok/B102/22 (H5N1). A significant difference was observed in the mean death time between Ck/Hok/E001/22 (H5N1) and Ew/Hok/Q71/22 (H5N1), corresponding to a slower virus growth kinetics in swab samples of Ew/Hok/Q71/22 (H5N1) (Tables 5–7). The slower growth kinetics of Ew/Hok/Q71/22 (H5N1) indicated the inability of the virus to replicate well in respiratory and intestinal organs compared to Ck/Hok/E001/22 (H5N1) and Cr/Hok/B003/22 (H5N2). This demonstrated that different genotypes of HPAIVs can contribute to different characteristics in pathogenicity even within the same clade 2.3.4.4b H5 HPAIVs, as lower pathogenicity was observed in chickens challenged with H5N8 HPAIV compared to H5N1 HPAIV that was circulating at the same time [35]. As different pathogenicity characteristics were observed among the representative viruses, the difference in the amino acid in each of the representative HPAIV strains was compared according to pathogenicity markers in previously reported AIVs [57]. All identified polymorphic sites in isolates have been linked to several associated phenotypes, such as altering the activities of the polymerase, replication efficacy in mammalian cells, and virulence in mammalian or

avian hosts [57]. Interestingly, the relatively lower pathogenicity observed in chickens infected with Ew/Hok/Q71/22 (H5N1) might be due to the preservation of the amino acid (105M) in NP, as all isolates in this season, except for Ew/Hok/Q71/22 (H5N1) and Ew/Hok/M184/22 (H5N1) with the mutation (M105V) in NP, which could contribute to the increase in the pathogenicity of chickens [57, 66]. Though molecular determinants in contributing to different pathogenicity observed in four HPAIVs were unknown yet, it was speculated that viral segments originating from LPAIVs might play a role in contributing to switch virus pathogenicity, as some studies have demonstrated that reassortant viruses with PB2, PB1, PA, and NP genes could contribute to higher pathogenicity in ferrets [27]. As strain-specific mutations were observed across the substitution of polymerase units of the four representative viruses, the role of those unique amino acid residues observed across the investigated viruses might need to be clarified in future studies. Nevertheless, as a potential public health concern, the receptor binding sites of viral HA of all 30 isolates still indicate the preference to bind to $\alpha$2,3-sialic acid linkage (237G, 238Q, and 240G; H5 numbering). Any associated markers contributing to high virulence in mammals were not found in Hokkaido isolates, demonstrating that threat of these viruses on public health should be very low [57]. However, cases among mink-to-mink transmission in Spain should heighten the concern about HPAIV adaptation in mammals if viruses continue circulating among wild birds and mammals globally [70].

Overall, H5 HPAIVs isolated in Hokkaido in winter 2022–2023 were phylogenetically, antigenically, and pathogenetically characterized. These were genetically close to Eurasian viruses isolated in winter 2021–2022 and consisted of multiple genotypes identified across wild birds and poultry, indicating the possibility of introducing HPAIVs with different genotypes by migratory birds to Japan. Furthermore, the same genotype of H5 HPAIV was also reintroduced to Hokkaido in early winter 2023–2024. Thus, the invasion of multiple viruses with distinct characteristics, especially transmissibility, host range, and pathogenicity in multiple animals, may perplex the understanding of the epidemiology and ecology of pathogens in the field to reduce their risk. Therefore, continuous monitoring and information sharing of the latest HPAIVs must be essential at the global level to understand dominant or critical HPAIV strains to establish effective control actions.

## Brief summary

HPAI has impacted poultry and wild birds globally. The number of H5 HPAIV infection cases in wild birds in Hokkaido (northern Japan) was high in the last two seasons, contributing to virus spillover to resident birds and poultry. Therefore, H5 HPAIVs in birds and mammals in Hokkaido in winter 2022–2023 and 2023–2024 were monitored and viruses were phylogenetically, antigenically, and pathogenetically characterized. Thirty HPAIV isolates were subtyped and pathotyped by sequencing the HA gene of viruses. Phylogenetic analysis of the HA gene revealed that all isolated HPAIVs were categorized into clade 2.3.4.4b and divided into three groups (G2b, G2c, and G2d). Most isolates belonging to subgroup G2d clustered with isolates in winter 2021–2022 in Hokkaido. The other isolates were categorized into two subgroups, G2b and G2c, mainly composed of isolates in Honshu Island in winter 2021–2022 and 2022–2023, respectively. Two H5 HPAIVs isolated in eastern Russia in spring and autumn 2022 were genetically close to most Hokkaido isolates (G2d), and a virus isolated in Hokkaido in November 2023 was also grouped in subgroup G2d. Further analysis of all eight gene segments identified six types of gene constellations. Cross-HI test indicated that the antigenicity of H5 HPAIVs isolated in the last several seasons was similar within them but slightly different from that in the 2010s. Three chicken breeds were intranasally challenged with four representative isolates to assess their pathogenicity. All chickens except one broiler chicken were dead until 5 dpc with different pathogenicity of these viruses. The pathogenicity of one HPAIV strain was significantly lower in broiler chickens than in layer chickens. The mixture of multiple characteristics of HPAIVs in Hokkaido was confirmed by bird migration routes. Thus, many HPAIVs can be brought and scattered anywhere on Earth.

# Chapter II

# Cocirculation of genetically distinct high pathogenicity avian influenza H5N5 and H5N1 viruses in crows, Hokkaido, Japan

## Introduction

H5 HPAIVs of the Gs/Gd lineage have diversified into multiple clades, threatening wild birds and poultry worldwide. Clade 2.3.4.4b HPAIVs have been consistently isolated in Asia and Europe since 2016 [16, 36, 37], and expanded further to North America in late 2021 [27]. The global circulation of H5 HPAIVs over a relatively short time highlights the pivotal role of migratory birds in virus dissemination [9]. H5 HPAIVs in clade 2.3.4.4 frequently acquire the NA gene from locally circulating LPAIVs, which often infect waterfowl, leading to the generation of novel H5Nx reassortant viruses, such as H5N2, H5N6, and H5N8 [71].

During the winter seasons 2021–2022 and 2022–2023, Hokkaido, located in the northernmost part of Japan, experienced HPAIV outbreaks driven by bird migration that substantially affected poultry and other resident birds. Those viruses clustered in the G2 subgroup within clade 2.3.4.4.b, which has multiple subgroups, G2a–e, and shared a common ancestor with HPAIVs detected in Europe in late 2020 [58]. HPAIV subgroup G2d might have undergone intercontinental transmission from Europe to Japan [21, 72]. During winter 2023–2024, H5N5 HPAIVs were detected in a crow flock in Hokkaido, and further monitoring revealed cocirculation of 2 distinct viruses in the crow population. The genetic origin and antigenicity of H5N5 HPAIVs isolated in Hokkaido were investigated.

## Materials and Methods

### Sample collection and virus isolation

The passive surveillance of HPAIV infections in wild birds was conducted in the public garden of Sapporo City, Hokkaido. After dead crows were reported in the garden by garden staff, tracheal and cloacal swab samples were collected from the dead carcasses and immediately mixed with a virus transport medium consisting of MEM (Shimadzu Diagnostics Corporation) containing 10 mg/mL streptomycin (Meiji Seika Pharma), 10,000 U/mL penicillin G (Meiji Seika Pharma), 250 U/mL nystatin (Sigma-Aldrich), 0.3 mg/mL gentamicin (MSD), and 0.5% bovine serum albumin fraction V (Roche) and then inoculated into 10-day-old embryonated eggs for virus isolation [43]. The isolation of virus was confirmed in the collected allantoic fluid by using an HA assay. The isolated viruses were subtyped by using an HI test consisting of chicken hyperimmune serum against the referenced influenza virus subtyping strain [45]. The pathogenicity of the isolates was determined by using the viral RNA extracted from the allantoic fluid by using either TRIzol LS Reagent (Thermo Fisher Scientific), or the QIAamp Viral RNA Mini Kit (Qiagen), direct sequencing after PCR was conducted by using a region-specific primer set to confirm the presence of nucleotides in the HA gene encoding multiple basic amino acid residues, which is a molecular marker for HPAIV [46]. NGS was performed by using the Flongle adaptor (Oxford Nanopore Technologies) to determine the genetic background of the HPAIV isolates; the primers used to amplify all 8 gene segments of HPAIV isolates have been previously described [48]. Oxford nanopore libraries were prepared by using the NEB Ultra II End Repair/dA-Tailing Module (New England Biolabs) and sequenced on the Flongle adaptor by using the Ligation Sequencing Kit V14 (Oxford Nanopore Technologies). The sequencing reads were mapped and assembled by using FluGAS version 2 (World Fusion).

**Genetic analysis**

H5 HPAIVs isolated in Hokkaido and an H5N5 isolate from Kumamoto in winter 2023–2024 were used in the genetic analysis (Table 9). The nucleotide sequences of H5 HPAIVs were phylogenetically analyzed by using the ML method and the best-fit general time-reversible model of nucleotide substitution with gamma-distribution rate variation among sites (with 4 rate categories, Γ) according to the Tamura-Nei model [49]. Bootstrap analysis with 1,000 replications was applied to construct the phylogenetic tree in MEGA 7 by using default parameters. Sequence data of the genes were compared with reference nucleotide sequences of representative H5Nx viruses (with different NA subtypes) belonging to clade 2.3.4.4 strains downloaded from GISAID and GenBank. BLAST of the GISAID database was used to identify the most homologous HPAIV nucleotide sequences isolated in this study.

**Antigenic analysis**

Using a cross-HI test, the antigenicity of the representative H5N5 HPAIV from Hokkaido, A/large-billed crow/Hokkaido/B073/2024 (Cr/Hok/B073/24; H5N5), was compared with that of the past few seasons (2014–2023) in Japan. Other antigens were analyzed and compared in representative clade 2.3.4.4 strains, including Cr/Hok/B003/22 (H5N2), Ck/Hok/E001/22 (H5N1), Ew/Hok/Q71/22 (H5N1) [72], WTE/Hok/R22/22 (H5N1), A/duck/Vietnam/HU-16DD3/2023 (Dk/VN/HU16-DD3/23; H5N1), Mdk/DRC/KAF1/17 (H5N8) [54], Ck/Hok/B102/23 (H5N1), A/Ezo red fox/Hokkaido/1/2022 (H5N1), Cr/Hok/B067/23 (H5N1), NP/Hok/M13/20 (H5N8), Ck/Kum/1-7/14 (H5N8) [52], and Bs/Aki/1/16 (H5N6) [53], by using antiserum against Cr/Hok/B003/22 (H5N2), Ck/Hok/E001/22 (H5N1), Ew/Hok/Q71/22 (H5N1), WTE/Hok/R22/22 (H5N1), Dk/VN/HU16-DD3/23 (H5N1), Mdk/DRC/KAF1/17 (H5N8), Ck/Kum/1-7/14 (H5N8), and Bs/Aki/1/16 (H5N6) to determine cross-reactivity of hyperimmune antiserum and their corresponding antigens.

## Results

### Genetic analysis

During the winter 2023–2024, a total of 85 dead crows were identified in a garden in Sapporo through passive surveillance. By the end of April 2024, 80 of these were confirmed to be infected with H5 HPAIV. The complete genome sequences of all eight gene segments were successfully obtained from 15 representative HPAIV isolates, as well as from an additional isolate derived from a peregrine falcon (*Falco peregrinus*). All sequences were deposited in the GISAID database (Table 9). Phylogenetic analysis of the HA gene revealed that all 16 isolates belonged to clade 2.3.4.4b and were assigned to the G2 genotype, which shares a common ancestor with clade 2.3.4.4b H5N8 HPAIVs first detected in Europe in late 2020 (Figure 5A) [58]. The G2 genotype was further subdivided into multiple subgroups (G2a–e) based on phylogenetic clustering. Seven isolates from 2023–2024, including H5N1 and one H5N5 subtype, were classified into a subgroup tentatively designated G2d, which also includes HPAIVs previously detected in Hokkaido during winter 2022–2023.

In contrast, the remaining isolates from Hokkaido collected since December 2023 were grouped into the G2a subgroup, along with H5N5 viruses that clustered with H5 HPAIVs detected in southern Japan during winter 2020–2021. Notably, the H5N5 HPAIVs in the G2a subgroup formed a distinct cluster from those of 2020–2021, showing closer phylogenetic relationships to contemporary H5N5 isolates from North America and Europe. Similar clustering patterns were observed in phylogenetic trees of the internal gene segments (Figure 5B–H). BLAST analysis of all eight gene segments of the G2a subgroup H5N5 HPAIVs isolated in Hokkaido during winter 2023–2024 indicated high nucleotide identity (> 99.0%) with European isolates, suggesting recent intercontinental gene flow. Interestingly, the H5N5 isolate from the peregrine falcon found in southern Japan during the same season showed high homology with viruses in the G2d subgroup for all gene segments except NA (Table 10). The N5 NA gene of this isolate was closely related to LPAIVs circulating in East Asia, suggesting that this strain resulted from a reassortment event involving the NA gene.

**Table 9. List of H5 HPAIVs isolated in Hokkaido and an H5N5 HPAIV in Kumamoto, Japan in winter 2023–2024**

| Virus | Subgroup | Sample collection date | City/Town | Latitude | Longitude | Accession number of strain[1] |
|---|---|---|---|---|---|---|
| A/large-billed crow/Hokkaido/B067/2023 (H5N1) | G2d | 23/11/2023 | Sapporo | 43°03'50"N | 141°20'35"E | EPI_ISL_18591747 |
| A/large-billed crow/Hokkaido/B068/2023 (H5N1) | G2d | 24/11/2023 | Sapporo | 43°03'50"N | 141°20'35"E | EPI_ISL_18594618 |
| A/large-billed crow/Hokkaido/0112F066T/2023 (H5N5) | G2a | 19/12/2023 | Erimo | 42°00'59"N | 143°08'53"E | EPI_ISL_18837770 |
| A/large-billed crow/Hokkaido/0112F066C/2023 (H5N5) | G2a | 19/12/2023 | Erimo | 42°00'59"N | 143°08'53"E | EPI_ISL_18838019 |
| A/large-billed crow/Hokkaido/B073/2024 (H5N5) | G2a | 08/01/2024 | Sapporo | 43°03'50"N | 141°20'35"E | EPI_ISL_18792212 |
| A/large-billed crow/Hokkaido/B074/2024 (H5N5) | G2a | 09/01/2024 | Sapporo | 43°03'50"N | 141°20'35"E | EPI_ISL_18830859 |
| A/crow/Hokkaido/B075/2024 (H5N5) | G2a | 11/01/2024 | Sapporo | 43°03'50"N | 141°20'35"E | EPI_ISL_18830860 |
| A/large-billed crow/Hokkaido/B076/2024 (H5N1) | G2d | 12/01/2024 | Sapporo | 43°03'50"N | 141°20'35"E | EPI_ISL_18830861 |
| A/large-billed crow/Hokkaido/B078/2024 (H5N1) | G2d | 17/01/2024 | Sapporo | 43°03'50"N | 141°20'35"E | EPI_ISL_18876661 |
| A/carrion crow/Hokkaido/B079/2024 (H5N1) | G2d | 18/01/2024 | Sapporo | 43°03'50"N | 141°20'35"E | EPI_ISL_18876662 |
| A/large-billed crow/Hokkaido/B080/2024 (H5N1) | G2d | 22/01/2024 | Sapporo | 43°03'50"N | 141°20'35"E | EPI_ISL_18932042 |
| A/carrion crow/Hokkaido/B081/2024 (H5N1) | G2d | 26/01/2024 | Sapporo | 43°03'50"N | 141°20'35"E | EPI_ISL_18876663 |
| A/large-billed crow/Hokkaido/B104/2024 (H5N5) | G2a | 20/02/2024 | Sapporo | 43°03'50"N | 141°20'35"E | EPI_ISL_19033207 |
| A/large-billed crow/Hokkaido/B120/2024 (H5N5) | G2a | 16/03/2024 | Sapporo | 43°03'50"N | 141°20'35"E | EPI_ISL_19055087 |
| A/large-billed crow/Hokkaido/B157/2024 (H5N5) | G2a | 30/04/2024 | Sapporo | 43°03'50"N | 141°20'35"E | EPI_ISL_19174744 |
| A/peregrine falcon/Kumamoto/4301C001/2024 (H5N5) | G2d | 16/01/2024 | Kumamoto | 32°56'07"N | 130°33'45"E | EPI_ISL_18876660 |

[1]The GISAID accession numbers.

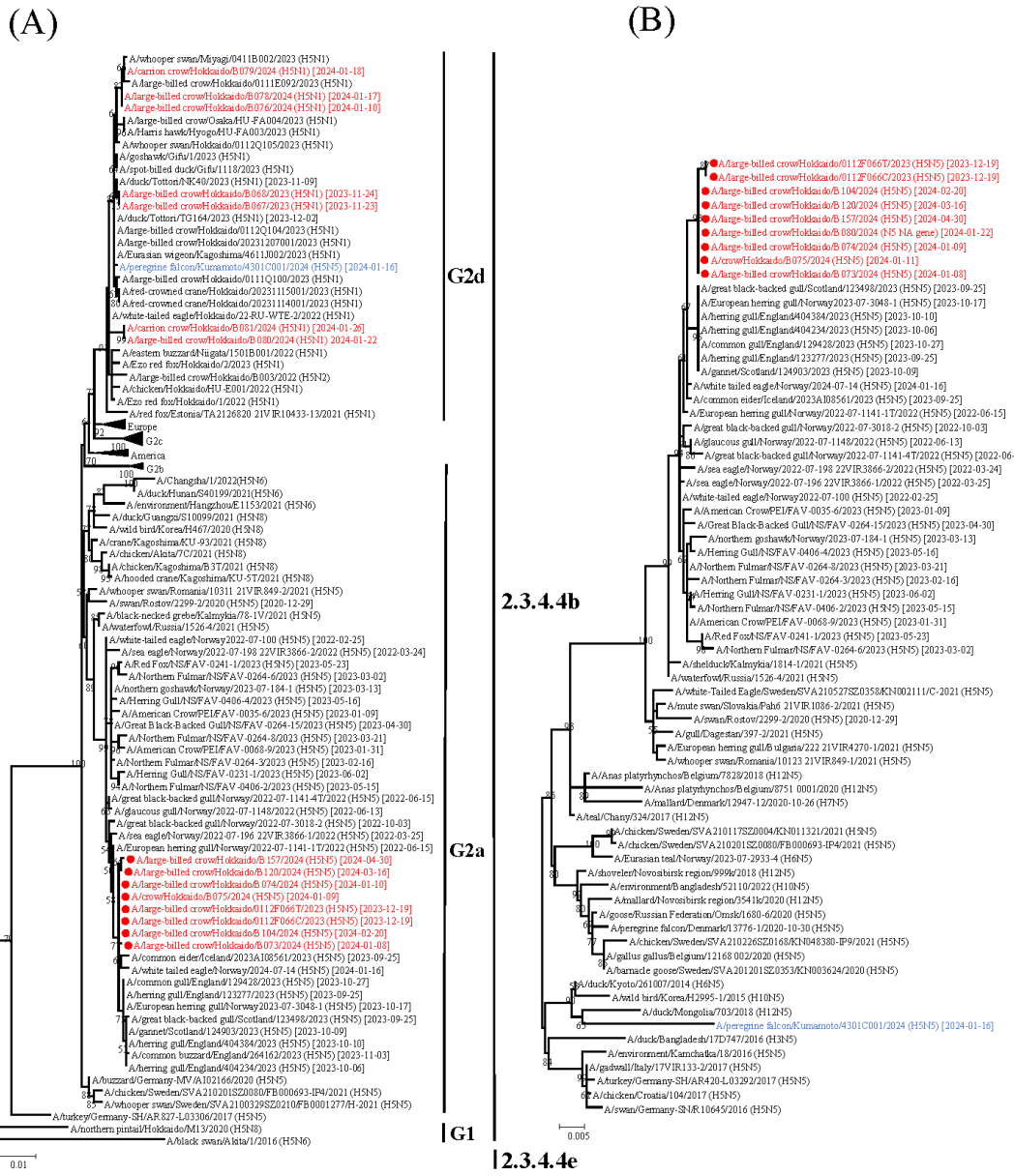


**Figure 5. Phylogenetic analysis of H5N5 and H5N1 HPAIVs isolated in Japan in winter 2023–2024**. The H5 HA **(A)**, N5 NA **(B),** PB2 **(C)**, PB1 **(D)**, PA **(E)**, NP **(F)**, M **(G)**, and NS **(H)** gene segments of H5N5 HPAIVs isolated in winter 2023–2024, together with reference strains from clade 2.3.4.4b and its subclades. The scale bar indicates nucleotide substitutions per site. Bootstrap support values (> 50%) were calculated from 1000 replicates. H5N5 HPAIVs from Hokkaido (2023–2024) are shown in red, and one isolate from southern Japan is shown in blue. Collection dates follow strain names, and Hokkaido isolates are marked with circles.

(C)

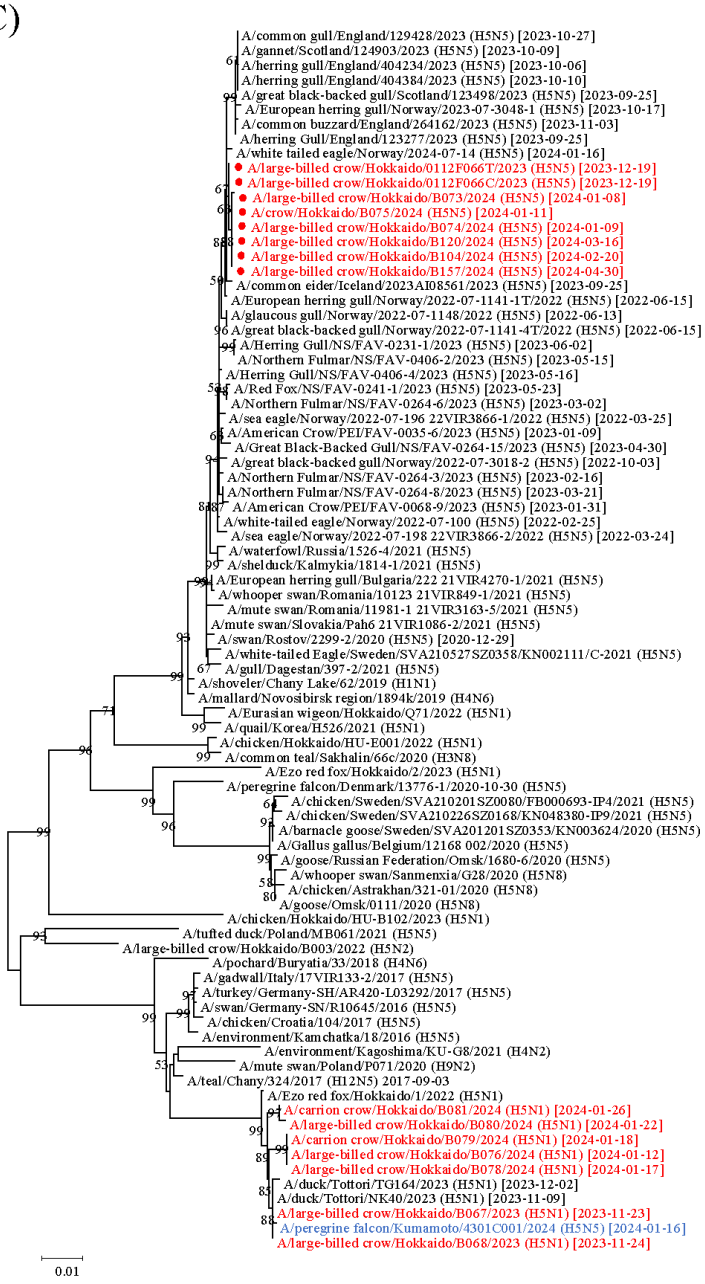


**Figure 5** (*cont*)**. Phylogenetic analysis of H5N5 and H5N1 HPAIVs isolated in Japan in winter 2023–2024**

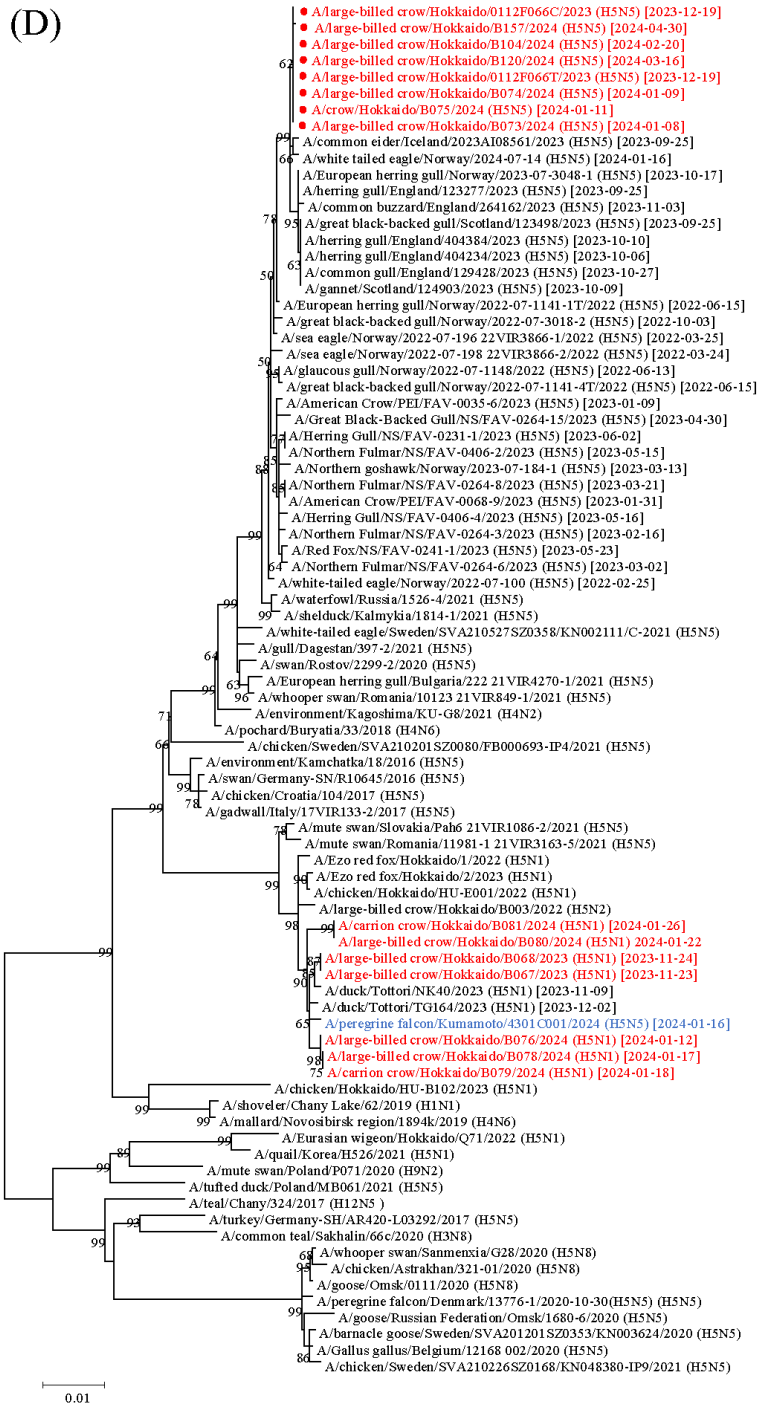


**Figure 5** (*cont*)**. Phylogenetic analysis of H5N5 and H5N1 HPAIVs isolated in Japan in winter 2023–2024**

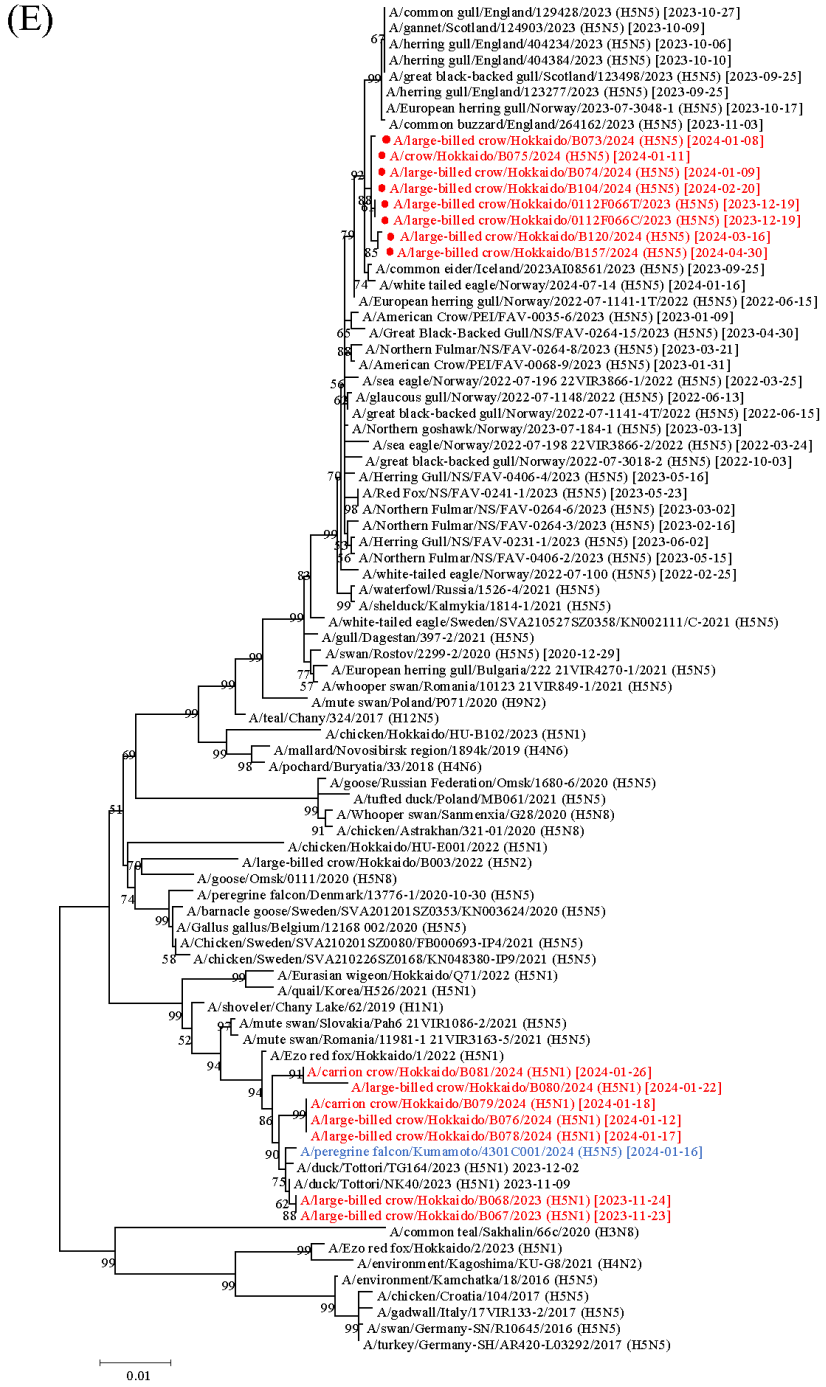


**Figure 5** (*cont*)**. Phylogenetic analysis of H5N5 and H5N1 HPAIVs isolated in Japan in winter 2023–2024**

(F)

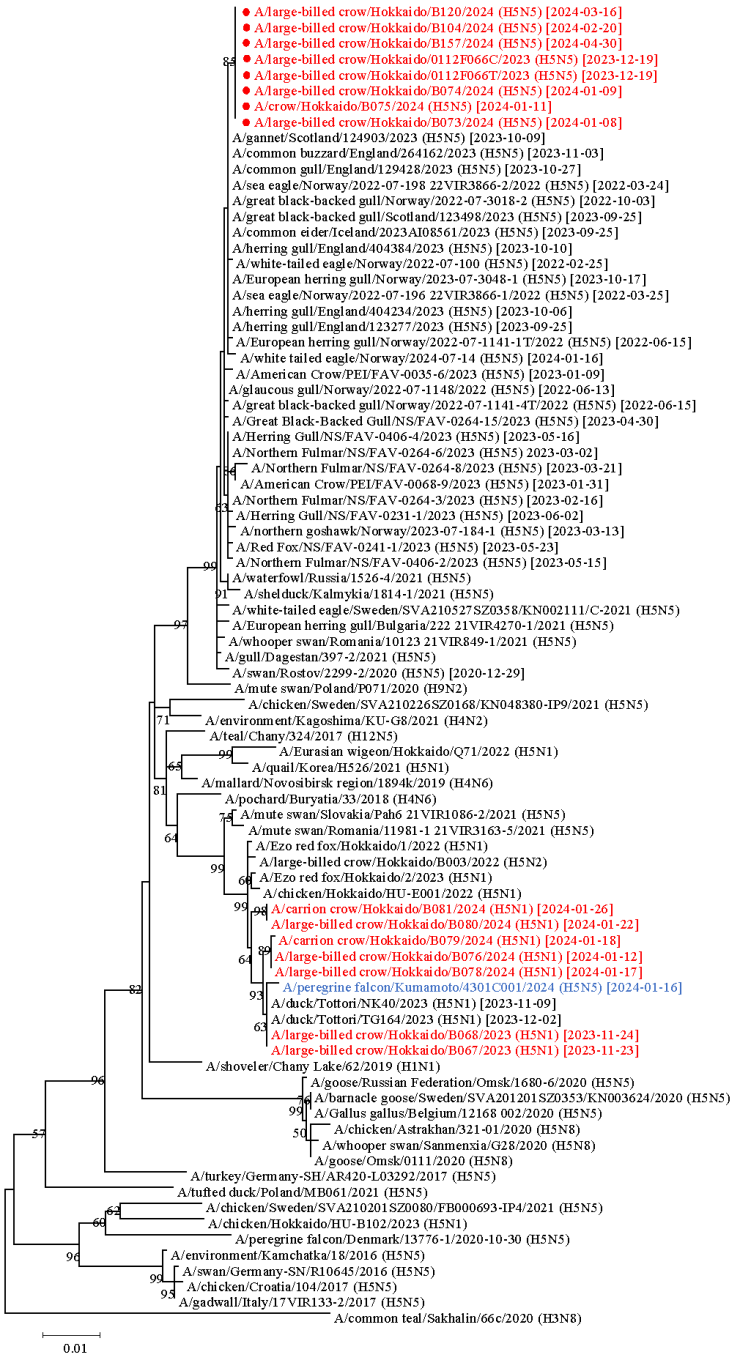


**Figure 5** (*cont*)**. Phylogenetic analysis of H5N5 and H5N1 HPAIVs isolated in Japan in winter 2023–2024**

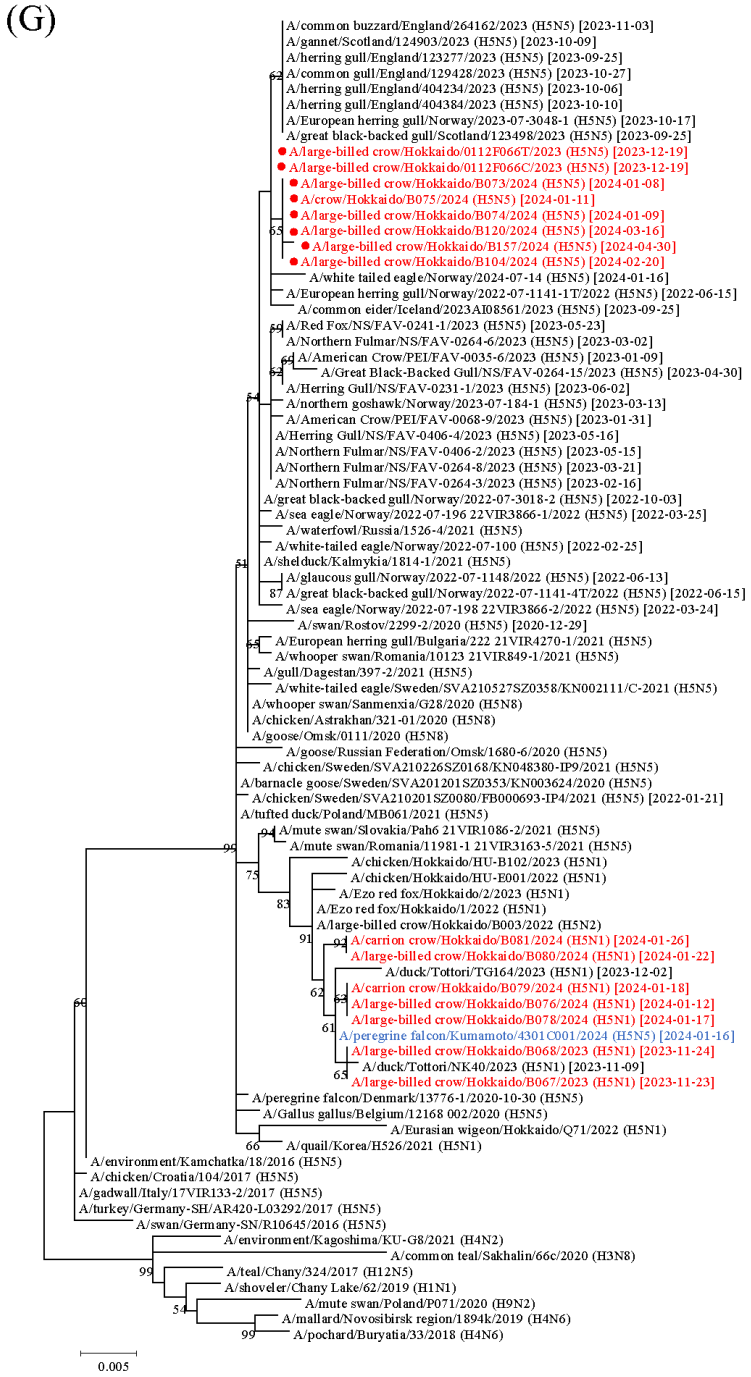


**Figure 5** (*cont*)**. Phylogenetic analysis of H5N5 and H5N1 HPAIVs isolated in Japan in winter 2023–2024**

(H)

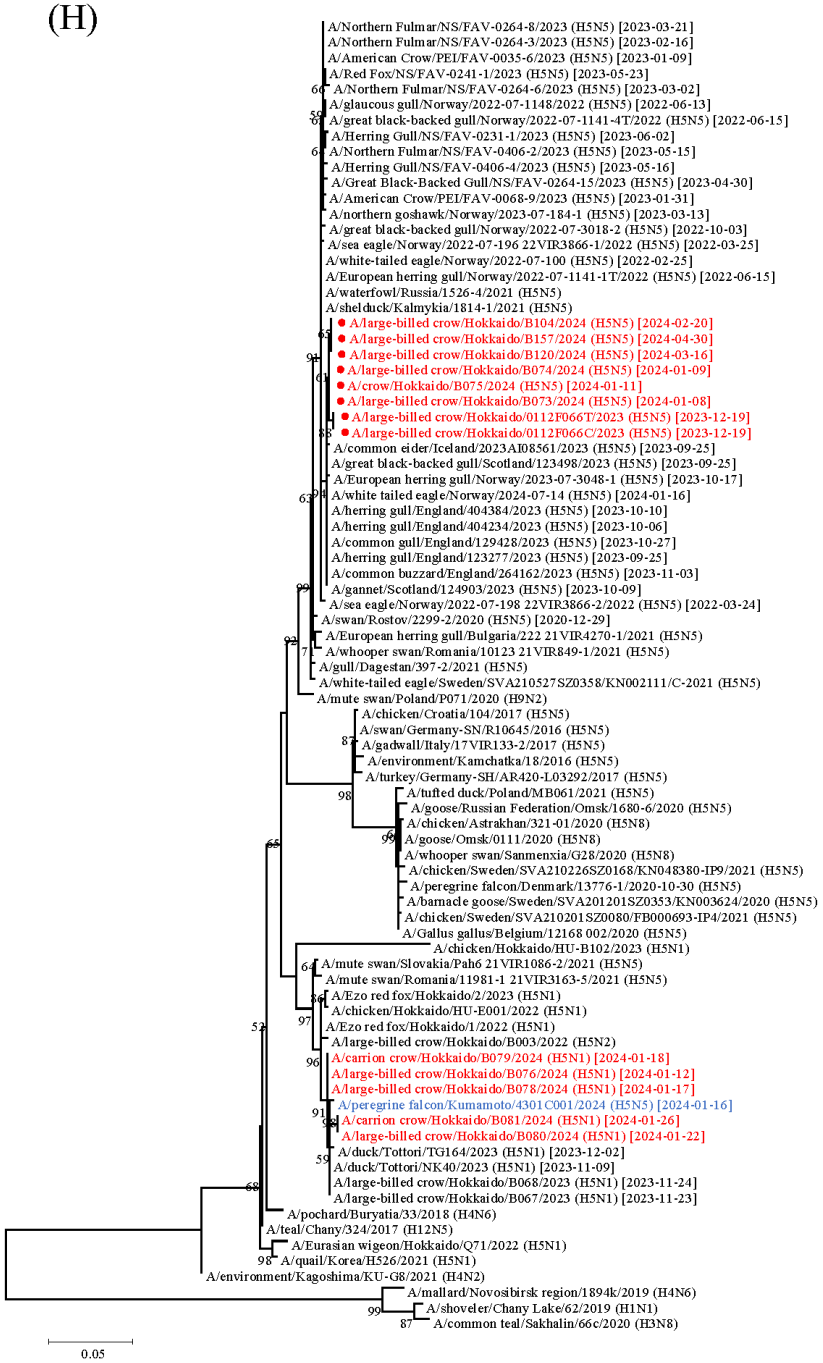


**Figure 5** (*cont*)**. Phylogenetic analysis of H5N5 and H5N1 HPAIVs isolated in Japan in winter 2023–2024**

**Table 10. BLAST search results of H5N5 HPAIVs isolated in Japan in winter 2023–2024 in study of cocirculation of genetically distinct H5N5 and H5N1 HPAIVs in crows, Hokkaido, Japan[1]**

| Virus name | Gene | Most homologous strain | Homology, % | Accession no. |
|---|---|---|---|---|
| A/large-billed crow/ Hokkaido/B073/ 2024 (H5N5)[2] | PB2 | A/Common eider/Iceland/ 2023AI08561/2023 (H5N5) | 99.7 | EPI2791002 |
| | PB1 | A/Common eider/Iceland/ 2023AI08561/2023 (H5N5) | 99.8 | EPI2791003 |
| | PA | A/Common eider/Iceland/ 2023AI08561/2023 (H5N5) | 99.7 | EPI2791001 |
| | HA | A/Common gull/ England/129428/2023 (H5N5) | 99.8 | EPI2815885 |
| | NP | A/Herring gull/England/404384/2023 (H5N5) | 99.9 | EPI2815894 |
| | NA | A/Herring gull/England/404384/2023 (H5N5) | 99.5 | EPI2815900 |
| | M | A/Herring gull/England/404384/2023 (H5N5) | 99.9 | EPI2815896 |
| | NS | A/Herring gull/England/404384/2023 (H5N5) | 99.9 | EPI2815895 |
| A/peregrine falcon/ Kumamoto/ 4301C001/2024 (H5N5)[3] | PB2 | A/large-billed crow/ Hokkaido/20231207001/2023 (H5N1) | 99.9 | EPI2898966 |
| | PB1 | A/large-billed crow/ Hokkaido/20231207001/2023 (H5N1) | 99.9 | EPI2898967 |
| | PA | A/large-billed crow/ Hokkaido/0111Q100/2023 (H5N1) | 99.8 | EPI2841124 |
| | HA | A/large-billed crow/ Hokkaido/20231207001/2023 (H5N1) | 99.9 | EPI2898969 |
| | NP | A/large-billed crow/ Hokkaido/0112Q104/2023 (H5N1) | 99.7 | EPI2815894 |
| | NA | A/Duck/Hokkaido/W24/2020 (H6N5) | 99.1 | EPI1896526 |
| | M | A/large-billed crow/ Hokkaido/20231207001/2023 (H5N1) | 100.0 | EPI2815896 |
| | NS | A/large-billed crow/ Hokkaido/20231207001/2023 (H5N1) | 99.9 | EPI2898973 |

[1]Gene segment sequences of 2 H5N5 HPAIVs were compared with those of other H5 virus sequences by using BLAST. Accession numbers are from GISAID.
[2]H5N5 HPAIV isolated in Hokkaido Prefecture in winter 2023–2024.
[3]H5N5 HPAIV isolated in Kumamoto Prefecture in winter 2023–2024.

**Antigenic analysis**

Cross-HI test was performed to assess the antigenic relationships among representative H5 HPAIVs from different genetic subgroups of clade 2.3.4.4 (Table 11). The H5N5 strain Cr/Hok/B073/24 (G2a subgroup) showed broadly comparable antigenic reactivity to recent H5 viruses. Antisera from subgroups G2b, G2c, and G2d reacted within a twofold range of HI titers against Cr/Hok/B073/24 (H5N5), indicating a high degree of antigenic similarity across these subgroups. The lowest reactivity was observed with the antiserum raised against Ew/Hok/Q71/22 (H5N1; G2b subgroup), although the reduction remained within the minor twofold variation threshold. Antisera derived from other clade 2.3.4.4 lineages, including 2.3.4.4c and 2.3.4.4e, also showed no substantial antigenic titer reductions compared with Cr/Hok/B073/24 (H5N5).

**Table 11. Cross-HI assay of H5 HPAIVs in Hokkaido in winter 2023–2024**

| Virus[1] | Subtype | Clade | Subgroup | Hemagglutination inhibition titer[2] | | | | | | | |
|---|---|---|---|---|---|---|---|---|---|---|---|
| | | | | Cr/Hok/ B003/22 | Ck/Hok/ E001/22 | Ew/Hok/ Q71/22 | WTE/Hok/ R22/22 | Dk/VN/ HU16-DD3 /23 | Mdk/DRC/ KAF1/17 | Ck/Ku/ 1-7/14 | Bs/Aki/ 1/16 |
| **Cr/Hok/B073/24[3]** | **H5N5** | **2.3.4.4b** | **G2a** | **640** | **160** | **40** | **640** | **320** | **640** | **320** | **320** |
| Cr/Hok/B003/22 | H5N2 | 2.3.4.4b | G2d | 640 | 640 | 80 | 320 | 640 | 1280 | 640 | 160 |
| Ck/Hok/E001/22 | H5N1 | 2.3.4.4b | G2d | 320 | 640 | 160 | 320 | 640 | 1280 | 640 | 80 |
| Ew/Hok/Q71/22 | H5N1 | 2.3.4.4b | G2b | 320 | 640 | 320 | 160 | 640 | 1280 | 320 | 160 |
| WTE/Hok/R22/22 | H5N1 | 2.3.4.4b | G2d | 640 | 640 | 160 | 320 | 640 | 2560 | 640 | 80 |
| Dk/VN/HU16-DD3 /23 | H5N1 | 2.3.4.4b | G2c | 640 | 320 | 80 | 640 | 640 | 320 | 320 | 80 |
| Ck/Hok/B102/23 | H5N1 | 2.3.4.4b | G2c | 640 | 320 | 80 | 320 | 1280 | 160 | 160 | 40 |
| Mdk/DRC/KAF1/17 | H5N8 | 2.3.4.4b | N/A[4] | 640 | 640 | 80 | 160 | 640 | 1280 | 640 | 80 |
| Fox/Hok/1/22 | H5N1 | 2.3.4.4b | G2d | 640 | 320 | 160 | 640 | 640 | 640 | 320 | 160 |
| Cr/Hok/B067/23 | H5N1 | 2.3.4.4b | G2d | 160 | 160 | 80 | 320 | 640 | 320 | 80 | 40 |
| Np/Hok/M13/20 | H5N8 | 2.3.4.4b | G1 | 640 | 640 | 20 | 160 | 640 | 2560 | 640 | 40 |
| Ck/Kum/1-7/14 | H5N8 | 2.3.4.4c | N/A | 320 | 640 | 40 | 20 | 160 | 640 | 640 | 80 |
| Bs/Akita/1/16 | H5N6 | 2.3.4.4e | N/A | 160 | 320 | 20 | 80 | 160 | 320 | 160 | 640 |
| Fox/Hok/1/22 | H5N1 | 2.3.4.4b | G2d | 640 | 320 | 160 | 640 | 640 | 640 | 320 | 160 |
| Cr/Hok/B067/23 | H5N1 | 2.3.4.4b | G2d | 160 | 160 | 80 | 320 | 640 | 320 | 80 | 40 |
| Np/Hok/M13/20 | H5N8 | 2.3.4.4b | G1 | 640 | 640 | 20 | 160 | 640 | 2560 | 640 | 40 |

[1]Each abbreviated name is defined as follows: Cr/Hok/B073/24 (H5N5), A/large-billed crow/Hokkaido/B073/2024 (H5N5); Cr/Hok/B003/22, A/large-billed crow/Hokkaido/B003/2022 (H5N2); Ck/Hok/E001/22, A/chicken/Hokkaido/HU-E001/2022 (H5N1); Ew/Hok/Q71/22, A/Eurasian wigeon/Hokkaido/Q71/2022 (H5N1); WTE/Hok/R22/22, A/white-tailed eagle/Hokkaido/22-RU-WTE-2/2022 (H5N1); Dk/VN/HU-16-DD3/23, A/duck/Vietnam/HU16-DD3/2023 (H5N1); Ck/Hok/B102/23, A/chicken/Hokkaido/HU-B102/2023 (H5N1); Mdk/DRC/KAF1/17, A/Muscovy duck/DR Congo/KAF1/2017 (H5N8); Fox/Hok/1/22, A/Ezo red fox/Hokkaido/1/2022 (H5N1); Cr/Hok/B067/23, A/large-billed crow/Hokkaido/B067/2023 (H5N1); Np/Hok/M13/20, A/northern pintail/Hokkaido/M13/2020 (H5N1); Ck/Kum/1-7/14, A/chicken/Kumamoto/1-7/2014 (H5N8); Bs/Akita/1/16, A/black swan/Akita/1/2016 (H5N6). [2]Antiserum against H5 virus isolates was used to test antigenicity of different H5Nx HPAIVs. Underline values indicate homologous titers. [3]H5N5 virus isolated in Hokkaido in winter 2023–2024. [4]N/A, not applicable.

## Discussion

Passive surveillance of HPAIV infections in wild birds was conducted in a public garden in Sapporo, the prefectural capital of Hokkaido, Japan, where approximately 2,000 crows congregate during winter and are routinely monitored by garden staff. Viruses were isolated from tracheal and cloacal swab samples collected from dead crows during winter 2023–2024. In contrast, HA genes of 3 H5 HPAIVs isolated from dead crows on January 8–11, 2024, were closely related to the G2a subgroup of H5N5 HPAIVs found in northern Europe and North America. Subsequent whole-genome sequencing analysis of the 3 G2a HPAIVs confirmed their subtype was H5N5; they were named Cr/Hok/B073/24 (H5N5), A/large-billed crow/Hokkaido/B074/2024 (H5N5), and A/crow/Hokkaido/B075/2024 (H5N5) (Table 9).

Phylogenetic analysis was performed on virus isolates together with reference sequences obtained from GISAID. The HA genes of H5N5 HPAIVs isolated in Hokkaido diverged considerably from those of HPAIVs detected in Japan during the winter 2020–2021 [73], forming a distinct branch within the G2a subgroup (Figure 5A). In addition, the other gene segments of H5N5 HPAIVs from Hokkaido were genetically distant from those in HPAIV strains isolated in Japan during winter 2021–2022 (Figures 5B–H). BLAST analysis of sequences from GISAID revealed that all 8 gene segments of H5N5 HPAIVs from Hokkaido were very close (genetic similarity > 99%) to H5N5 HPAIVs detected in northern Europe since 2022, in contrast to those from North America (Table 10), suggesting a low possibility of virus transmission from North America. H5N5 HPAIVs from Hokkaido shared a common ancestor with H5N5 HPAIV from Europe assigned the genotype EA-2021-I by the European Food Safety Authority [74]. Parent strains of H5N5 HPAIVs from Europe, represented by A/swan/Rostov/2299-2/2020 (H5N5), were proposed to originate in western Russia during autumn 2020. Those viruses underwent genetic evolution via reassortment events involving H5N8 HPAIVs circulating in Europe since 2018 [75], and the N5 NA gene derived from concurrently circulating LPAIVs [76]. H5N5 HPAIVs reported in northern Europe during 2022–2023 exhibited specific genetic differences compared with H5N5 HPAIVs detected in Europe during autumn 2020, particularly in the N5 NA gene. Those differences included a 66 base pairs nucleotide deletion within the N5 NA gene, which also observed in the H5N5 HPAIVs from Hokkaido. Truncation of the NA stalk has been attributed to the adaptation

of those viruses from wild birds to Galliformes spp. birds [77]. However, most H5N5 HPAIV infections in Europe were detected in wild birds, and no cases have been detected in Galliformes spp. birds since 2022 [78]. Further investigation is needed to clarify whether NA stalk truncation affects the pathogenesis of H5N5 HPAIVs.

During the winter 2023–2024, H5N5 HPAIV infections were confirmed in wild birds, particularly crows, in Erimo (December 19, 2023; south-central Hokkaido) and Kushiro (January 18, 2024; eastern Hokkaido). Infection was also detected in a peregrine falcon (*Falco peregrinus*) in Tamana, Kumamoto Prefecture, Kyushu Island, on January 16, 2024. The isolate from Tamana, A/peregrine falcon/Kumamoto/4301C001/2024 (H5N5), was classified into the G2d subgroup based on its HA gene sequence, whereas its NA gene sequence showed similarity to that of LPAIVs isolated in East Asia (Table 10). Although this combination had not been observed in Japan, reassortment events between the HPAIV H5N1 G2d subgroup and LPAIVs have been documented [72]. H5N5 HPAIVs were detected in Hokkaido in January 2024. A total of 85 crows were found dead in the Sapporo garden, 80 of which were diagnosed as HPAIV positive by the end of April. No HPAIVs were detected in birds within the garden after April 2024. The continuous detection of H5N5 HPAIVs in the Sapporo garden during January–April without unusual deaths of birds other than crows and multiple isolations of H5N5 HPAIVs in other areas of Hokkaido suggest the potential for widespread dissemination of H5N5 HPAIVs within the Hokkaido region.

H5N1 G2d HPAIVs persisted in crows residing in the Sapporo garden even after the introduction of H5N5 G2a viruses, indicating concurrent circulation of genetically distinct viruses within a single crow population. Indeed, the average nanopore sequencing coverage for A/large-billed crow/Hokkaido/B080/2024 (H5N1) was 5497.4 reads for the N1 NA gene (G2d subgroup) and 1943.7 reads for the N5 NA gene (G2a subgroup) (Table 12). This observation suggests single hosts were co-infected with 2 viruses and reassortment occurred between viruses originating from geographically distant areas. Antigenic characterization of H5N5 HPAIVs showed that Cr/Hok/B073/24 (H5N5) exhibited only minor antigenic differences, within a 2–4-fold range in HI titers (Table 11), indicating that H5N5 viruses in subgroup G2a remain antigenically conserved and closely related to other contemporary H5 HPAIVs circulating in Japan, despite genetic

diversification among subgroups (Table 13). H5N5 HPAIVs with unique gene constellations were likely introduced into Japan through stepwise bird migration across northern Eurasia. Cocirculation of two genetically distinct viruses was identified within a single flock of crows. The occurrence of H5N5 HPAIV infections in waterfowl in Japan remains poorly understood, and the absence of reports from neighbouring countries on H5N5 HPAIVs originating from Europe has hindered efforts to reconstruct the spread of this genotype to eastern Asia. Continuous monitoring and timely international information sharing are essential for understanding the global dynamics of HPAIVs and preventing their further dissemination.

**Table 12. Results of whole-genome sequencing of the HPAIV A/large-billed crow/Hokkaido/B080/2024 (H5N1) isolated from a crow in Hokkaido, Japan, in winter 2024[1]**

| Gene segment | A/large-billed crow/Hokkaido/B080/2024 | | | |
|---|---|---|---|---|
| | H5N1 | | H5N5 | |
| | Coverage, % | Mean coverage | Coverage, % | Mean coverage |
| PB2 | 100 | 2761.018 | NR[2] | NR |
| PB1 | 100 | 5578.526 | NR | NR |
| PA | 100 | 7086.121 | NR | NR |
| HA | 100 | 11962.420 | NR | NR |
| NP | 100 | 4856.926 | NR | NR |
| NA | 100 | 5497.429 | 100 | 1943.684 |
| MP | 97.8 | 16003.720 | NR | NR |
| NS | 99.2 | 30145.500 | NR | NR |

[1]Sequencing detected N1 and N5 NA genes in one host, indicating co-infection. [2]NR, no reads.

**Table 13. Genetic homology between HPAIVs Cr/Hok/B073/24 (H5N5; G2a subgroup) and Cr/Hok/B067/23 (H5N1; G2d subgroup)**

| Gene | Homology, % |
|---|---|
| PB2 | 91.9 |
| PB1 | 95.8 |
| PA | 94.8 |
| HA | 98.2 |
| NP | 96.8 |
| NA | 55.7 |
| MP | 98.7 |
| NS | 95.6 |

## Brief summary

HPAI continues to cause substantial mortality among poultry and wild bird populations worldwide. In Hokkaido, northern Japan, detections of H5 HPAIVs in wild birds markedly increased during winters 2021–2023, resulting in spillover to resident birds and poultry. During winter 2023–2024, two genetically distinct HPAIV subtypes, H5N5 and H5N1, were isolated from crows (*Corvus* spp.) in Hokkaido. Phylogenetic analysis of the HA gene classified both isolates within clade 2.3.4.4b, with H5N5 viruses assigned to subgroup G2a and H5N1 viruses to subgroup G2d. The H5N5 viruses in G2a were genetically related to HPAIVs circulating in northern Europe but distinct from those in Asia. In contrast, an additional H5N5 virus isolated from a peregrine falcon (*Falco peregrinus*) in Kumamoto Prefecture belonged to subgroup G2d and possessed a reassorted N5 NA gene derived from LPAIV circulating in East Asia. The H5N1 isolates in subgroup G2d were closely related to Hokkaido strains from winters 2021–2023, suggesting annual reintroduction from neighboring regions. Antigenic analysis using cross-HI assays indicated that the H5N5 viruses retained antigenic similarity with other clade 2.3.4.4b strains. These findings demonstrate the ongoing genetic and antigenic diversification of HPAIVs in Japan and underscore the importance of sustained surveillance and rapid international information exchange to prevent further HPAI dissemination.

# Chapter III

# Introduction and inter-species transmission dynamics of high pathogenicity avian influenza H5N1 viruses in Japan 2021–2025

## Introduction

After H5N1 HPAIV entered Japan in November 2021, successive seasonal outbreaks have occurred among poultry and wild birds. The HA genes of H5N1 and H5N8 HPAIVs circulating in Japan in winter 2021–2022 belonged to G2, which arose from the H5 HPAIVs that circulated in Europe in late 2020 [58]. G2 is further divided into multiple subgroups (G2a–e) based on a naming system specific to Japan, and the origins of these subgroups have been previously described [72, 79]. Among them, G2b and G2d were primarily identified in Japan during winter 2021–2022 [35]. In the following winter season, the outbreak worsened, coinciding with the emergence of multiple G2 subgroups (G2b, G2c, and G2d), indicating increased viral diversity [72]. Despite a temporary decline in the outbreak numbers in winter 2023–2024, a resurgence occurred in the following winter 2024–2025, with viruses in the G2d subgroup remaining prevalent. Unlike in Europe, H5 HPAIVs have not been detected in Japan during the summer, supporting the hypothesis of annual winter introductions from neighboring countries [79]. Moreover, H5N1 HPAIV cases have been reported across multiple host species, including the large-billed crow (*Corvus macrorhynchos*), white-naped cranes (*Grus vipio*), white-tailed sea eagle (*Haliaeetus albicilla*), slaty-backed gull (*Larus schistisagus*), and Galliformes, such as chicken, emu, quail, and guinea fowl [72, 79–81]. Considering the repeated H5N1 HPAIV outbreaks in Japan across multiple host species and the detection of viruses from multiple G2 subgroups, understanding the origin and transmission dynamics of these viruses in different species is imperative. H5N1 HPAIVs were consistently detected in Japan from 2021 to 2025, but other subtypes, such as H5N8 and H5N5 HPAIVs, were limited in Japan. Similar to the pattern observed in Europe, H5N1 HPAIVs were replaced with H5N8 HPAIVs in 2021–2022 and H5N5 HPAIVs were introduced from Europe, mainly in winter 2023–2024, via a distinct bird migration route [35, 82].

Recent phylodynamic analyses have revealed continuous viral exchanges among East Asian countries such as China, Republic of Korea, and Japan, reflecting persistent lineage turnover and gene flow within wild bird populations along the East Asian–Australasian Flyway [83]. Furthermore, H5N1 viruses closely related to East Asian lineages have been found in North America, including Alaska and Canada, indicating

sporadic transcontinental dispersal via the trans-Beringian route or the West Pacific Flyway [25, 84]. Although these introductions have contributed only marginally to the overall viral diversity in North America, this underscores the role of overlapping migratory flyways in linking continental bird populations [85]. Overall, these findings demonstrate how phylodynamic approaches can reveal intercontinental connections and the evolutionary processes driving the global spread of H5N1 HPAIV. In this study, a Bayesian phylodynamic framework was used to analyze a comprehensive sequence dataset of 892 H5N1 HPAIV HA gene sequences collected in Japan from 2021 to 2025, together with additional sequences from other countries that are closely related to Japanese isolates, obtained from a public database. Using this approach, the geographic origins of virus introductions and the transmission patterns between bird species can be inferred. By combining sequence data with host, temporal, and geographic metadata, phylodynamic models can effectively reconstruct viral spread and evolution [86–88], helping establish epidemiological links between wild and domestic bird populations as well as facilitating national surveillance and control strategies.

## Materials and Methods

### Sample collection and virus isolation

Active and passive surveillance is conducted annually at the Laboratory of Microbiology, Faculty of Veterinary Medicine, Hokkaido University, Sapporo, Japan, to monitor the circulation of HPAIV in Hokkaido, the northernmost prefecture of Japan. Detailed information about sampling sites for active surveillance and methods for passive surveillance has been published previously [72, 79]. Tracheal and cloacal swab samples were collected from bird carcasses and immediately mixed with a virus transport medium, consisting of MEM (Shimadzu Diagnostics Corporation) containing 10 mg/mL streptomycin (Meiji Seika Pharma), 10,000 U/mL penicillin G (Meiji Seika Pharma), 250 U/mL nystatin (Sigma-Aldrich), 0.3 mg/mL gentamicin (MSD), and 0.5% bovine serum albumin fraction V (Roche). This mixture was then inoculated into 10-day-old embryonated eggs; the virus was isolated from the allantoic fluid and confirmed using an HA assay [43].

### Genome sequencing

To evaluate the pathogenicity of the isolates, viral RNA was extracted from the allantoic fluid using either TRIzol LS Reagent (Thermo Fisher Scientific) or the QIAamp Viral RNA Mini Kit (Qiagen). The HA gene was amplified by PCR with a specific primer set to confirm the presence of multiple basic amino acid residues at the HA cleavage site, a molecular marker of HPAIV [89]. The PCR products were sequenced using the BigDye Terminator v3.1 Cycle Sequencing Kit (Thermo Fisher Scientific) and analyzed using the 3500 Genetic Analyzer (Thermo Fisher Scientific). Then, NGS was performed using the Flongle adaptor (Oxford Nanopore Technologies) to analyze the genetic background of the HPAIV isolates. The primers used to amplify all eight gene segments, namely PB2, PB1, PA, HA, NP, NA, M, and NS, of these isolates have been described previously [72]. Libraries for Oxford Nanopore were prepared with the NEB Ultra II End Repair/dA-Tailing Module (New England Biolabs) and sequenced on the Flongle adaptor using the Ligation Sequencing Kit V14 (Oxford Nanopore Technologies). The sequencing reads were then mapped and assembled using FluGAS version 2 (World Fusion).

**Phylogenetic tree inferences of H5N1 HPAIV in Japan**

The HA sequences of H5N1 HPAIV (n = 141) obtained by the Laboratory of Microbiology, Hokkaido University, were combined with other sequences acquired from Japan between 2021 and 2025 (n = 309) by the GISAID. To identify genetically similar sequences from other countries, BLAST in GISAID was used to compare the Japanese sequences with global HA sequences to identify the H5N1 HPAIV sequences with high similarity to the Japanese isolates for further analysis. All HA sequences were aligned using MAFFT v7.526 [90], and manually inspected and trimmed with AliView v1.30 [91]. Sequences that were identical (100% sequence homology) and sequences shorter than 1700 base pairs were excluded. The HA gene sequences used in this study contained only the open reading frame region. ML phylogenies were inferred using IQ-TREE 2 [92], with the HKY+G4 nucleotide substitution model [93]. These phylogenies were used to identify monophyletic Japanese clades and evaluate the temporal signal in TempEst v1.5.3 [94]. For visualization and annotation of phylogenies, the R package ggtree v3.14.0 was used [95].

**Bayesian phylodynamic of H5N1 HPAIV in Japan**

A Bayesian phylodynamic approach was used to infer the introduction and inter-species transmission dynamics of H5N1 HPAIV. The Multi-Type Birth-Death (MTBD) model was applied to the phylogenetic tree to explicitly account for structured populations representing different hosts or geographic regions, with separate transmission, sampling, and removal rates [96, 97]. The MTBD model was chosen over simpler birth–death models and discrete phylogeographic approaches because it enables joint estimation of type-specific epidemiological parameters, including the effective reproductive number ($R_e$), becoming-uninfectious rate, sampling proportion, and migration rates between demes. This allows for the inference of virus spread over time in a way that accurately reflects how infections actually occur [98, 99]. Unlike discrete phylogeographic models, which estimate ancestral geographic states without linking to transmission dynamics, MTBD directly models migration as part of the epidemiological process and can adjust for uneven sampling across hosts or regions.

HA sequences were categorized into four epizootic periods (June 2021–May 2022, June 2022–May 2023, June 2023–May 2024, and June 2024–May 2025) and further organized by geographic origin and avian host species. Geographic demes included Europe, Japan, Northeast Asia (Republic of Korea and China), North Asia (Russia), and Northwest America (Canada: British Columbia and Alberta; United States: Alaska). Host demes were grouped as anatidae (ducks, swans, geese), charadriiformes (gulls and curlews), poultry (chickens, ducks, emus, quails, guinea fowl), raptors (eagles, falcons, hawks), cranes, and crows; species with particularly low sample sizes in Japan were combined into a 'Japan birds' category to avoid overparameterization. Table 14 provides the detailed sequence counts and subgroup distributions. The MTBD model was implemented in BEAST v2.6.3 with the BDMM-Prime package, using the BEAGLE library for computational efficiency [100]. Analyses employed an HKY+G4 nucleotide substitution model [93], and a relaxed lognormal molecular clock [101]. Priors for all key model parameters are summarized in Tables 15–18, including the becoming-uninfectious rate, which corresponds to a median infectious period of seven days [102], and migration rates, which are expected to average about two migration events per lineage per year [103].

To mitigate potential sampling bias caused by uneven surveillance efforts among hosts and regions (such as the overrepresentation of poultry outbreaks compared to wild bird detections), deme-specific sampling proportions were calculated within the MTBD framework. For each deme, the sampling proportion reflects the likelihood that an infection was represented in the dataset. It was estimated as the ratio of analyzed sequences to the total number of reported cases in the Food and Agriculture Organization's EMPRES Global Animal Disease Information System (EMPRES-i) (Tables 15–18) [104]. This method partially compensates for uneven sampling coverage by using priors informed by relative surveillance effort and calibrated to avoid overfitting demes with small sample sizes. The MTBD model assumes that transmission, becoming-uninfectious, and sampling rates stay constant within each analysis period and that all relevant demes are included in the dataset; therefore, estimated parameters should be considered as time-averaged values across sampled populations [98]. Phylodynamic parameters and posterior trees were estimated using Markov chain Monte Carlo over 100 million steps, sampling every 10,000 iterations. The first 10% of samples were discarded

as burn-in, and convergence was assessed in Tracer v1.7, ensuring all effective sample sizes exceeded 200 [105]. Maximum clade credibility (MCC) trees were reconstructed with TreeAnnotator v1.10.4 [106], and visualized in R v2.4.2 using the ggtree package [95].

**Table 14. Number of H5N1 HPAIV sequences used in MTBD analyses among regions and among hosts by period and genetic subgroup**

| Period | Total sequences used in MTBD analysis | G2d host-associated sequences | G2c host-associated sequences |
|---|---|---|---|
| Jun 2021–May 2022 | 215 | 75 | NA[1] |
| Jun 2022–May 2023 | 389 | 120 | 242 |
| Jun 2023–May 2024 | 131 | 131 | NA |
| Jun 2024–May 2025 | 161 | 145 | NA |

[1]NA: Not applicable.

**Table 15. Prior values and distributions among different regions and hosts used in the MTBD model in winter 2021–2022**

| Factor | Among regions | | | Among hosts | | |
|---|---|---|---|---|---|---|
| | Parameter | Prior | Rationale | Parameter | Prior | Rationale |
| Molecular evolution model | Nucleotide substitution model | HKY + $\Gamma_4$ | Unequal substitution rates, base bias, and rate heterogeneity (four categories). | Nucleotide substitution model | HKY + $\Gamma_4$ | Unequal substitution rates, base bias, and rate heterogeneity (four categories). |
| | Clock rate | Lognormal | Median substitution rate of 0.001 per site per year | Clock rate | Lognormal | Median substitution rate of 0.001 per site per year |
| MTBD model | Become uninfectious rate | Lognormal (0.0, 52.0) | Median infectious period of 7 days | Become uninfectious rate | Lognormal (0.0, 52.0) | Median infectious period of 7 days |
| | Deme of origins | Distribution | Equal prior among demes | Deme of origins | Distribution | Equal prior among demes |
| | Migration rate among demes | Distribution | Equal prior among demes | $R_e$ among demes | Distribution | Equal prior among demes |
| Sampling proportion | Europe | Uniform (0.0, 0.0095) | 36 sequences/3862 reported cases | Raptor | Uniform (0.0, 0.429) | 3 sequences/7 reported cases |
| | Japan | Uniform (0.0, 0.9) | 90 sequences/100 reported cases | Anatidae | Uniform (0.0, 0.333) | 3 sequences/9 reported cases |
| | North Asia | Uniform (0.0, 1.0) | 14 sequences/10 reported cases | Crow | Uniform (0.0, 0.607) | 34 sequences/56 reported cases |
| | Northeast Asia | Uniform (0.0, 0.728) | 67 sequences/92 reported cases | Poultry | Uniform (0.0, 1.0) | 20 sequences/1 reported cases |
| | Northwest America | Uniform (0.0, 0.0294) | 8 sequences/272 reported cases | North Asia birds | Uniform (0.0, 1.0) | 7 sequences/1 reported case |

**Table 16. Prior values and distributions among different regions and hosts in the G2c and G2d subgroups used in the MTBD model in winter 2022–2023**

| Factor | Among regions | | | Among hosts | | | | | |
|---|---|---|---|---|---|---|---|---|---|
| | Parameter | Prior | Rationale | Parameter | Prior | Rationale | | | |
| Molecular evolution model | Nucleotide substitution model | HKY + $\Gamma_4$ | Unequal substitution rates, base bias, and rate heterogeneity (four categories). | Nucleotide substitution model | HKY + $\Gamma_4$ | Unequal substitution rates, base bias, and rate heterogeneity (four categories). | | | |
| | Clock rate | Lognormal | Median substitution rate of 0.001 per site per year | Clock rate | Lognormal | Median substitution rate of 0.001 per site per year | | | |
| MTBD model | Become uninfectious rate | Lognormal (0.0, 52.0) | Median infectious period of 7 days | Become uninfectious rate | Lognormal (0.0, 52.0) | Median infectious period of 7 days | | | |
| | Deme of origins | Distribution | Equal prior among demes | Deme of origins | Distribution | Equal prior among demes | | | |
| | Migration rate among demes | Distribution | Equal prior among demes | $R_e$ among demes | Distribution | Equal prior among demes | | | |
| Sampling proportion | Japan | Uniform (0.0, 0.650) | 147 sequences/226 reported cases | G2c subgroup | | | G2d subgroup | | |
| | Northwest America | Uniform (0.0, 0.116) | 90 sequences/774 reported cases | Anatidae | Uniform (0.0, 0.462) | 12 sequences/ 26 reported cases | Japan birds | Uniform (0.0, 0.078) | 5 sequences/ 64 reported cases |
| | North Asia | Uniform (0.0, 0.084) | 9 sequences/107 reported cases | Crane | Uniform (0.0, 1.0) | 57 sequences/ 36 reported cases | Crow | Uniform (0.0, 0.256) | 11 sequences/ 43 reported cases |
| | Northeast Asia | Uniform (0.0, 1.0) | 146 sequences/124 reported cases | Crow | Uniform (0.0, 0.209) | 9 sequences/ 43 reported cases | Poultry | Uniform (0.0, 0.615) | 8 sequences/ 13 reported cases |
| | | | | Poultry | Uniform (0.0, 1.0) | 21 sequences/ 13 reported cases | Raptor | Uniform (0.0, 0.148) | 4 sequences/ 27 reported cases |
| | | | | Raptor | Uniform (0.0, 0.185) | 5 sequences/ 27 reported cases | Northwest America birds | Uniform (0.0, 0.763) | 87 sequences/ 114 reported cases |
| | | | | North Asia birds | Uniform (0.0, 1.0) | 4 sequences/ 2 reported cases | | | |
| | | | | Northeast Asia birds | Uniform (0.0, 1.0) | 134 sequences/ 126 reported cases | | | |

**Table 17. Prior values and distributions among different regions and hosts used in the MTBD model in winter 2023–2024**

| Factor | Among regions | | | Among hosts | | |
|---|---|---|---|---|---|---|
| | Parameter | Prior | Rationale | Parameter | Prior | Rationale |
| Molecular evolution model | Nucleotide substitution model | HKY + $\Gamma_4$ | Unequal substitution rates, base bias, and rate heterogeneity (four categories). | Nucleotide substitution model | HKY + $\Gamma_4$ | Unequal substitution rates, base bias, and rate heterogeneity (four categories). |
| | Clock rate | Lognormal | Median substitution rate of 0.001 per site per year | Clock rate | Lognormal | Median substitution rate of 0.001 per site per year |
| MTBD model | Become uninfectious rate | Lognormal (0.0, 52.0) | Median infectious period of 7 days | Become uninfectious rate | Lognormal (0.0, 52.0) | Median infectious period of 7 days |
| | Deme of origins | Distribution | Equal prior among demes | Deme of origins | Distribution | Equal prior among demes |
| | Migration rate among demes | Distribution | Equal prior among demes | $R_e$ among demes | Distribution | Equal prior among demes |
| Sampling proportion | Japan | Uniform (0.0, 0.733) | 107 sequences/146 reported cases | Northeast Asia birds | Uniform (0.0, 1.0) | 6 sequences/5 reported cases |
| | Northwest America | Uniform (0.0, 0.024) | 9 sequences/371 reported cases | Anatidae | Uniform (0.0, 0.588) | 20 sequences/34 reported cases |
| | North Asia | Uniform (0.0, 0.321) | 9 sequences/28 reported cases | Crane | Uniform (0.0, 0.75) | 9 sequences/12 reported cases |
| | Northeast Asia | Uniform (0.0, 0.231) | 6 sequences/26 reported cases | Crow | Uniform (0.0, 0.933) | 56 sequences/60 reported cases |
| | | | | Poultry | Uniform (0.0, 1.0) | 13 sequences/12 reported cases |
| | | | | Raptor | Uniform (0.0, 0.409) | 9 sequences/22 reported cases |
| | | | | Northwest America birds | Uniform (0.0, 0.187) | 9 sequences/48 reported cases |
| | | | | North Asia birds | Uniform (0.0, 0.333) | 9 sequences/27 reported cases |

**Table 18. Prior values and distributions among different regions and hosts used in the MTBD model in winter 2024–2025**

| Factor | Among regions | | | Among hosts | | |
|---|---|---|---|---|---|---|
| | Parameter | Prior | Rationale | Parameter | Prior | Rationale |
| Molecular evolution model | Nucleotide substitution model | HKY + $\Gamma_4$ | Unequal substitution rates, base bias, and rate heterogeneity (four categories). | Nucleotide substitution model | HKY + $\Gamma_4$ | Unequal substitution rates, base bias, and rate heterogeneity (four categories). |
| | Clock rate | Lognormal | Median substitution rate of 0.001 per site per year | Clock rate | Lognormal | Median substitution rate of 0.001 per site per year |
| MTBD model | Become uninfectious rate | Lognormal (0.0, 52.0) | Median infectious period of 7 days | Become uninfectious rate | Lognormal (0.0, 52.0) | Median infectious period of 7 days |
| | Deme of origins | Distribution | Equal prior among demes | Deme of origins | Distribution | Equal prior among demes |
| | Migration rate among demes | Distribution | Equal prior among demes | $R_e$ among demes | Distribution | Equal prior among demes |
| Sampling proportion | Japan | Uniform (0.0, 0.463) | 107 sequences/231 reported cases | Anatidae | Uniform (0.0, 0.346) | 9 sequences/26 reported cases |
| | Northwest America | Uniform (0.0, 0.039) | 48 sequences/1297 reported cases | Charadriiforme | Uniform (0.0, 0.108) | 4 sequences/37 reported cases |
| | Northeast Asia | Uniform (0.0, 0.031) | 3 sequences/97 reported cases | Crane | Uniform (0.0, 0.880) | 44 sequences/50 reported cases |
| | | | | Crow | Uniform (0.0, 0.361) | 22 sequences/61 reported cases |
| | | | | Poultry | Uniform (0.0, 0.462) | 6 sequences/13 reported cases |
| | | | | Raptor | Uniform (0.0, 0.538) | 7 sequences/13 reported cases |
| | | | | Northwest America birds | Uniform (0.0, 0.096) | 51 sequences/531 reported cases |
| | | | | Northeast Asia birds | Uniform (0.0, 0.021) | 2 sequences/9 reported cases |

## Results

### Overview of H5N1 HPAIV epizootics in Japan 2021–2025

During the winter 2021–2022, outbreaks were reported in 22 poultry birds in the first half of the season and 83 wild birds later in the season (Figure 6A). By the following winter, the number of cases increased to 136 wild birds and 88 poultry, mostly early in the season and peaking in midwinter. During winter 2023–2024, the wild bird cases remained high (n = 136), but only 10 poultry outbreaks occurred. In winter 2024–2025, wild bird cases surged to 302, along with 47 poultry outbreaks, with wild bird cases showing a significant rise at the end of winter. Throughout this period, no infections were detected in Japan during the summer months (June–August).

### Genetic analysis

To investigate potential links, an additional 47 European H5N1 HPAIV sequences from 2020–2021 were included in the analysis. Phylogenetic analysis of the H5N1 HPAIV HA genes revealed that Japanese isolates from winter 2021–2022 were genetically distinct from European isolates collected in 2020–2021 (Figure 7). Some Japanese isolates clustered with European viruses from 2021–2022, considered descendants of the 2020–2021 European strains. These clusters also included viruses from Northwest America collected in 2021–2022. Additionally, a subset of Japanese isolates from 2021–2022 clustered with viruses from North Asia and Northeast Asia. Similar clustering patterns were observed in subsequent winter seasons (2022–2023, 2023–2024, and 2024–2025), with Japanese isolates remaining genetically linked to viruses from Northwest America, Northeast Asia, and North Asia, while no European H5N1 isolates were detected in Japan after 2022. This pattern suggests ongoing interregional migration events involving Northeast Asia, Northwest America, and North Asia in each winter season.

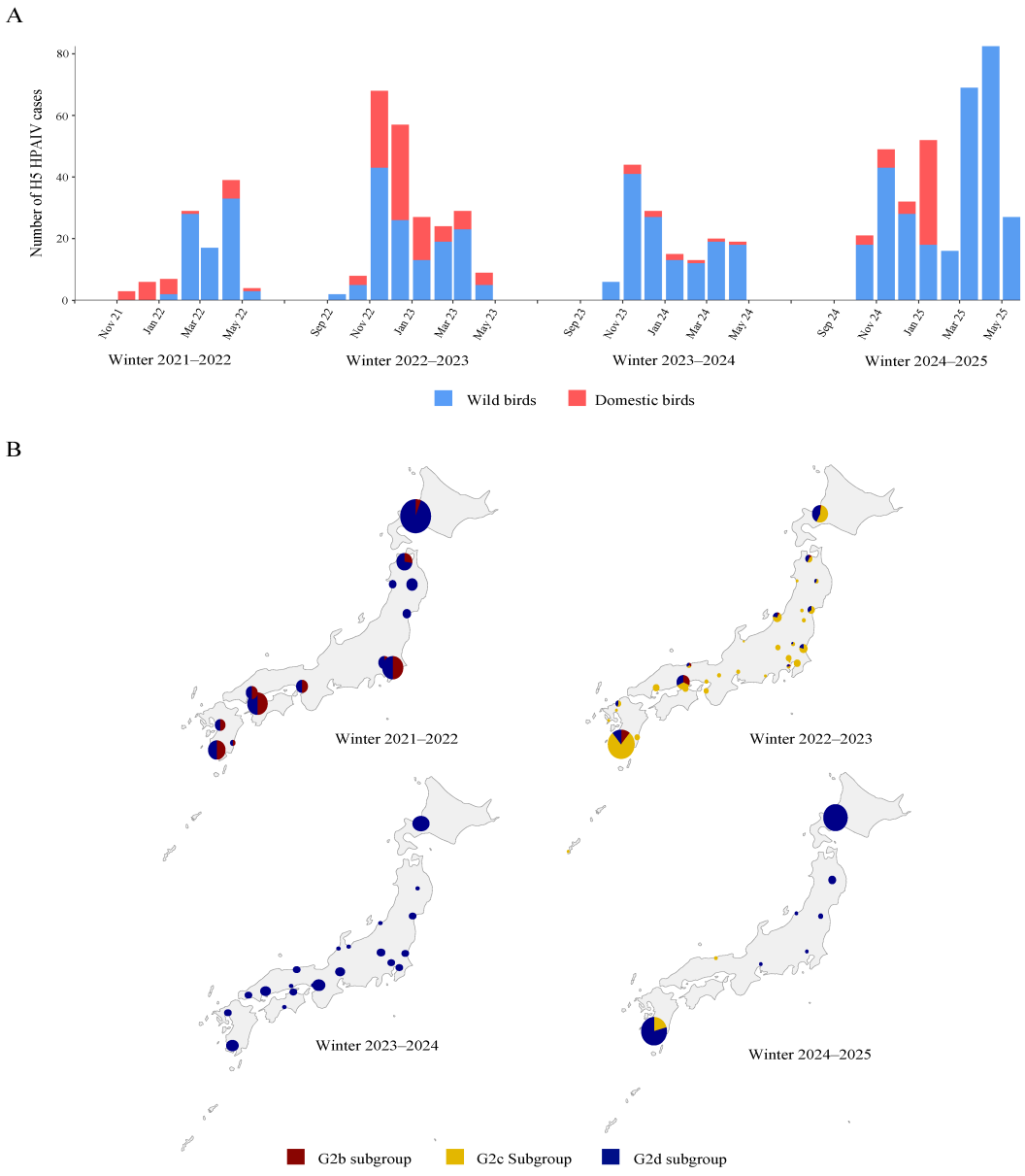


**Figure 6. Temporal and spatial distribution of H5N1 HPAIV cases and genotypes in Japan (2021–2025).** **(A)** The number of H5N1 HPAIV cases in clade 2.3.4.4b outbreaks in Japan from September 2021 to May 2025, detected in wild and domestic birds by month according to EMPRES-i. **(B)** The map shows the distribution of different H5N1 HPAIV genotypes in Japan based on sequences obtained through the GISAID during the four winter seasons from September 2021 to May 2025.

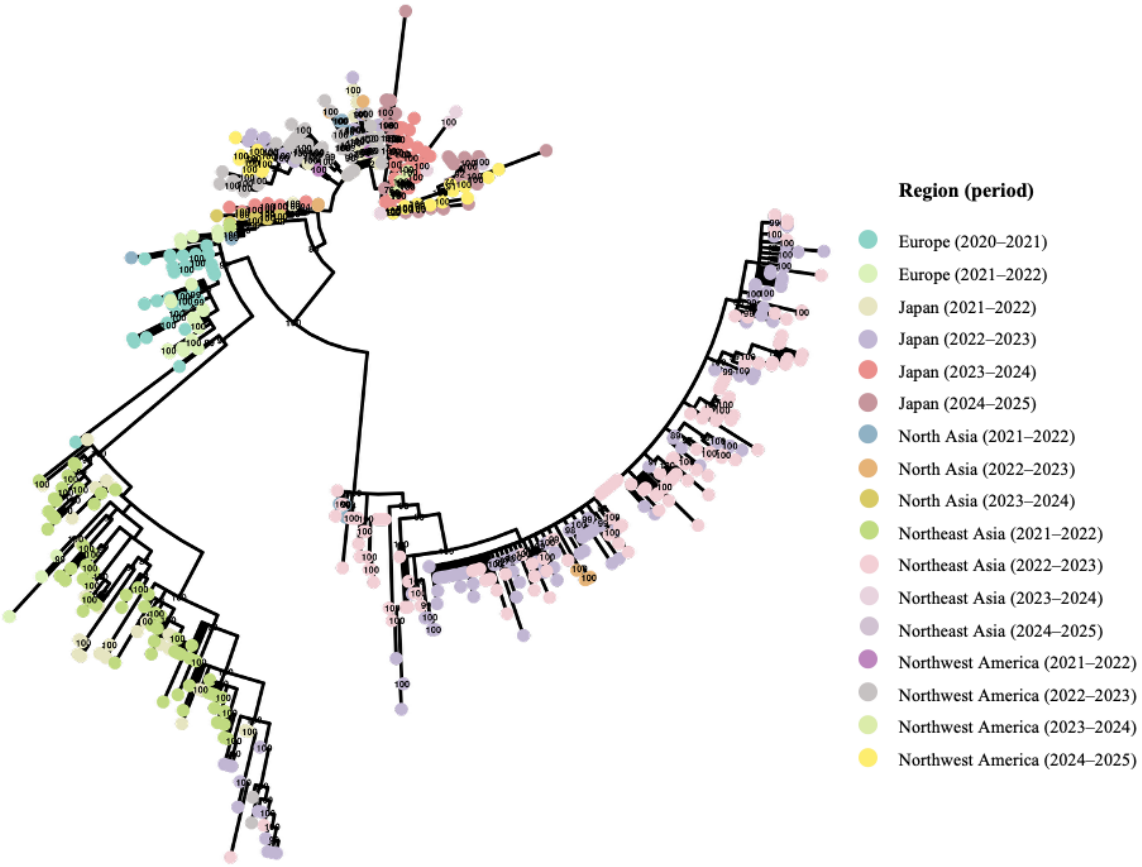


**Figure 7. Phylogenetic tree of the HA gene of H5N1 HPAIVs in winters 2020–2025**. The tree includes 450 H5N1 HPAIVs isolated in Japan during the winters 2021–2025, together with genetically related reference strains obtained from public influenza sequence databases. Reference sequences represent viruses with the highest genetic similarity to Japanese isolates within clade 2.3.4.4b collected during winters 2021–2025, as well as European H5N1 isolates from 2020–2021. The tree was inferred using the ML method implemented in IQ-TREE 2. Node values indicate bootstrap support based on 1,000 replicates, with only values > 70% shown.

**Introduction of H5N1 HPAIV into Japan 2021–2023**

During winter 2021–2022, two independent introductions of H5N1 HPAIV into Japan were observed based on the MCC tree, which were identified as the G2b and G2d subgroups (Figure 8A). The G2b subgroup was predominantly detected in southern Japan through sporadic outbreaks (Figure 6B) at the beginning of the epidemic and probably originated from Northeast Asia (e.g., Republic of Korea and China) because the ancestral strains trace back to this region. Conversely, the G2d subgroup was predominantly detected in northern Japan, specifically in Hokkaido, in the middle of the epidemic. It was most likely introduced from Northwest America (such as the United States and Canada) based on the ancestral strains, leading to multiple outbreaks. For the migration per lineage per year, the mean migration rates indicated Northwest America (1.6, 95% highest posterior density (HPD) [0.7, 2.8]) and Northeast Asia (0.7, 95% HPD [0.3, 1.1]) as major potential sources for introduction into Japan. Conversely, North Asia (1.9, 95% HPD [0.4, 4.0]), Northwest America (2.2, 95% HPD [0.5, 4.7]), and Northeast Asia (2.5, 95% HPD [0.7, 5.0]) were inferred to be major potential destination regions from Japan (Figure 8B). However, the number of inferred migration events showed that most of the viral movements to Japan occurred from Northwest America (30.2, 95% HPD [16, 43]), with fewer events originating in Northeast Asia (10.5, 95% HPD [6.0, 16.0]) (Figure 8C). This suggests that while some routes exhibit high potential migration rates, they may have contributed to fewer introductions, possibly due to shorter lineage time spent in Japan or sparse sampling. Indeed, the viruses spent comparable amounts of time across the following regions: Northeast Asia (6.5, 95% HPD [5.4, 7.8]), followed by Europe (6.2, 95% HPD [4.8, 7.7]), and Northwest America (4.0, 95% HPD [2.4, 5.5]). However, the viruses spent the least amount of time in Japan (1.5, 95% HPD [1.0, 2.1]) and North Asia (0.6, 95% HPD [0.3, 1.0]) (Figure 8D).

H5N1 HPAIV was reintroduced in winter 2022–2023, and was categorized into three distinct subgroups (G2b, G2c, and G2d) based on the MCC tree. The G2c subgroup was primarily seen in southern Japan, likely originating from Northeast Asia. Viruses in the G2d subgroup were primarily detected in northern Japan, in Hokkaido Prefecture (Figure 6B), and were likely introduced from Northwest America. The G2b subgroup, which was detected in Hokkaido in autumn 2022, likely originated from North Asia

(Figure 9A). The mean migration rates indicated that North Asia (1.9, 95% HPD [0.7, 3.3]) and Northeast Asia (1.5, 95% HPD [0.5, 2.6]) were major potential sources for introduction into Japan, while Northeast Asia (1.7, 95% HPD [0.4, 5.1]) and North Asia (1.4, 95% HPD [0.3, 2.7]) were potential destination regions for viral lineages originating from Japan (Figure 9B). Regarding the number of inferred migration events, a high number of viral movements from North Asia (21.7, 95% HPD [6.0, 38.0]), followed by Northeast Asia (10.8, 95% HPD [2.0, 2.0]) to Japan, was observed but with fever inferred events involving Northwest America (7.9, 95% HPD [2.0, 13.0]) (Figure 9C). Based on the detection of multiple subgroups of the viruses in Japan, it can be deduced that the amount of time these viruses spend in Japan (11.7, 95% HPD [8.6, 15.0]) is comparable to that in other regions such as Northwest America (10.7, 95% HPD [8.8, 12.9]), followed by Northeast Asia (9.3, 95% HPD [7.1, 11.9]). The viruses seem to spend the least amount of time in North Asia (5.7, 95% HPD [2.6, 8.9]) (Figure 9D).

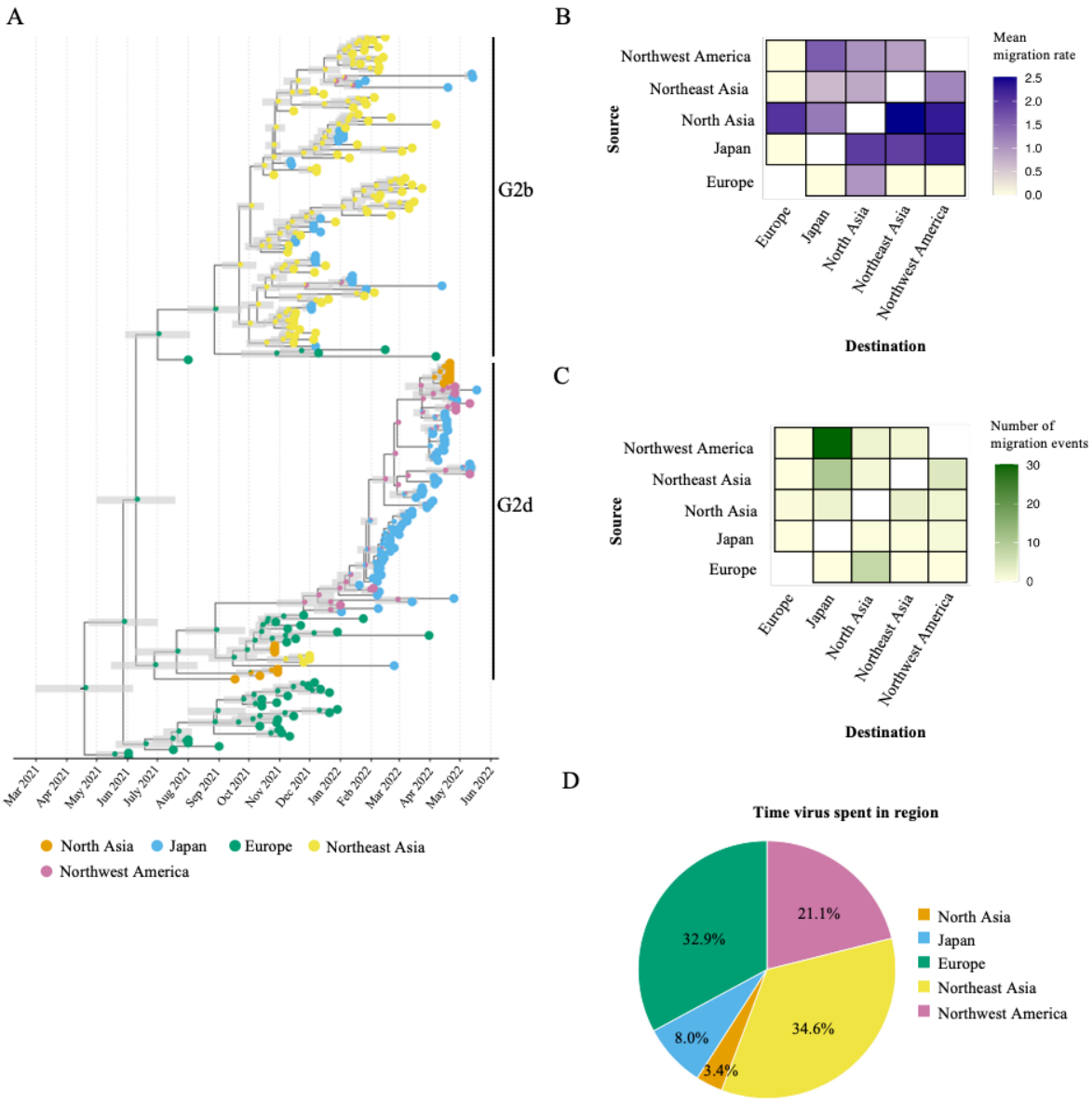


**Figure 8. Phylogeographic analysis of H5N1 HPAIV clade 2.3.4.4b in Japan during winter 2021–2022**. **(A)** The MCC tree was constructed using the HA gene of the H5N1 HPAIV from clade 2.3.4.4b in Japan from June 2021 to May 2022. It was supplemented with other H5N1 HPAIV samples from different regions during the same period, represented by different colors for the internal and external nodes of the MCC tree. **(B)** Heatmaps showing the average per-lineage virus migration rates and **(C)** the number of inferred virus migrations between different geographic regions in winter 2021–2022. **(D)** The pie chart displays the percentage of time the viruses spent in each geographic region during winter 2021–2022.

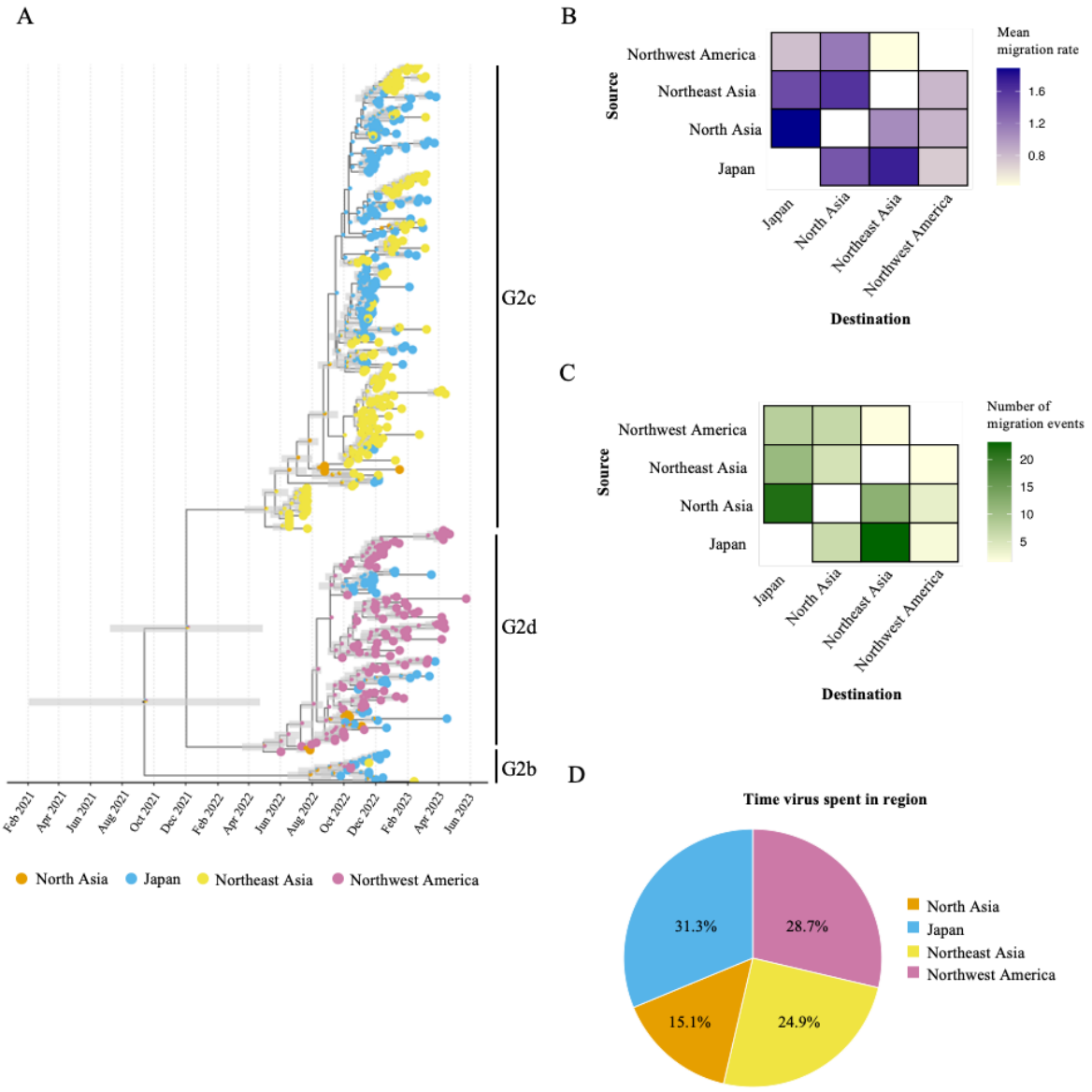


**Figure 9. Phylogeographic analysis of H5N1 HPAIV clade 2.3.4.4b in Japan during winter 2022–2023**. **(A)** The MCC tree was constructed using the HA gene of the H5N1 HPAIV from clade 2.3.4.4b in Japan from June 2022 to May 2023. It was supplemented with other H5N1 HPAIV samples from different regions during the same period, represented by different colors for the internal and external nodes of the MCC tree. **(B)** Heatmaps showing the average per-lineage virus migration rates and **(C)** the number of inferred virus migrations between different geographic regions in winter 2022–2023. **(D)** The pie chart displays the percentage of time viruses spent in each geographic region during winter 2022–2023.

**Shift in the geographic origins of H5N1 HPAIV during winters 2023–2025**

H5N1 HPAIVs from the G2c and G2d subgroups were reintroduced during winters 2023–2024 and 2024–2025, with a shift in the geographic origin of the viruses in the G2d subgroup. While introductions in winters 2021–2022 and 2022–2023 were primarily linked to ancestral strains from Northwest America, those in the later winters were more likely to have originated from Northeast Asia (Figures 10A and 11A). In winter 2023–2024, North Asia (1.6, 95% HPD [0.5, 3.2]), Northeast Asia (1.4, 95% HPD [0.7, 2.3]), and Northwest America (1.3, 95% HPD [0.4, 2.5]) had similar rates of virus introduction into Japan (Figure 10B). Meanwhile, Northeast Asia (2.2, 95% HPD [0.4, 4.4]) was inferred as the major potential destination from Japan. Based on the number of inferred migration events, most of the viral movement was observed from Northeast Asia (65.8, 95% HPD [50.0, 80.0]) to Japan with fewer inferred events involving Northwest America (4.0, 95% HPD [0.0, 10.0]) and North Asia (2.1, 95% HPD [0.0, 6.0]) (Figure 10C), as evidenced by the substantial duration of time these viruses spend in Northeast Asia (11.8, 95% HPD [8.8, 15.6]). However, they spend the least amount of time in Japan (2.4, 95% HPD [1.4, 3.6]), followed by Northwest America (1.1, 95% HPD [0.3, 2.0]), and North Asia (0.7, 95% HPD [0.2, 1.3]) (Figure 10D).

In winter 2024–2025, introductions into Japan were again mainly from Northeast Asia (1.0, 95% HPD [0.5, 1.6]) and Northwest America (1.6, 95% HPD [0.4, 3.2]), with most inferred migration events traced to Northeast Asia (38.0, 95% HPD [29.0, 46.0]), and only limited inferred events involving the Northwest America (0.6, 95% HPD [0.0, 2.0]) (Figure 11B–C). Viruses also spent considerably more time in Northeast Asia (8.3, 95% HPD [6.0, 10.9]) than in Japan (1.6, 95% HPD [1.0, 2.2]) or Northwest America (0.7, 95% HPD [0.3, 1.2]) (Figure 11D), which suggest that Northeast Asia remained the dominant source and reservoir of viruses during these consecutive winters.

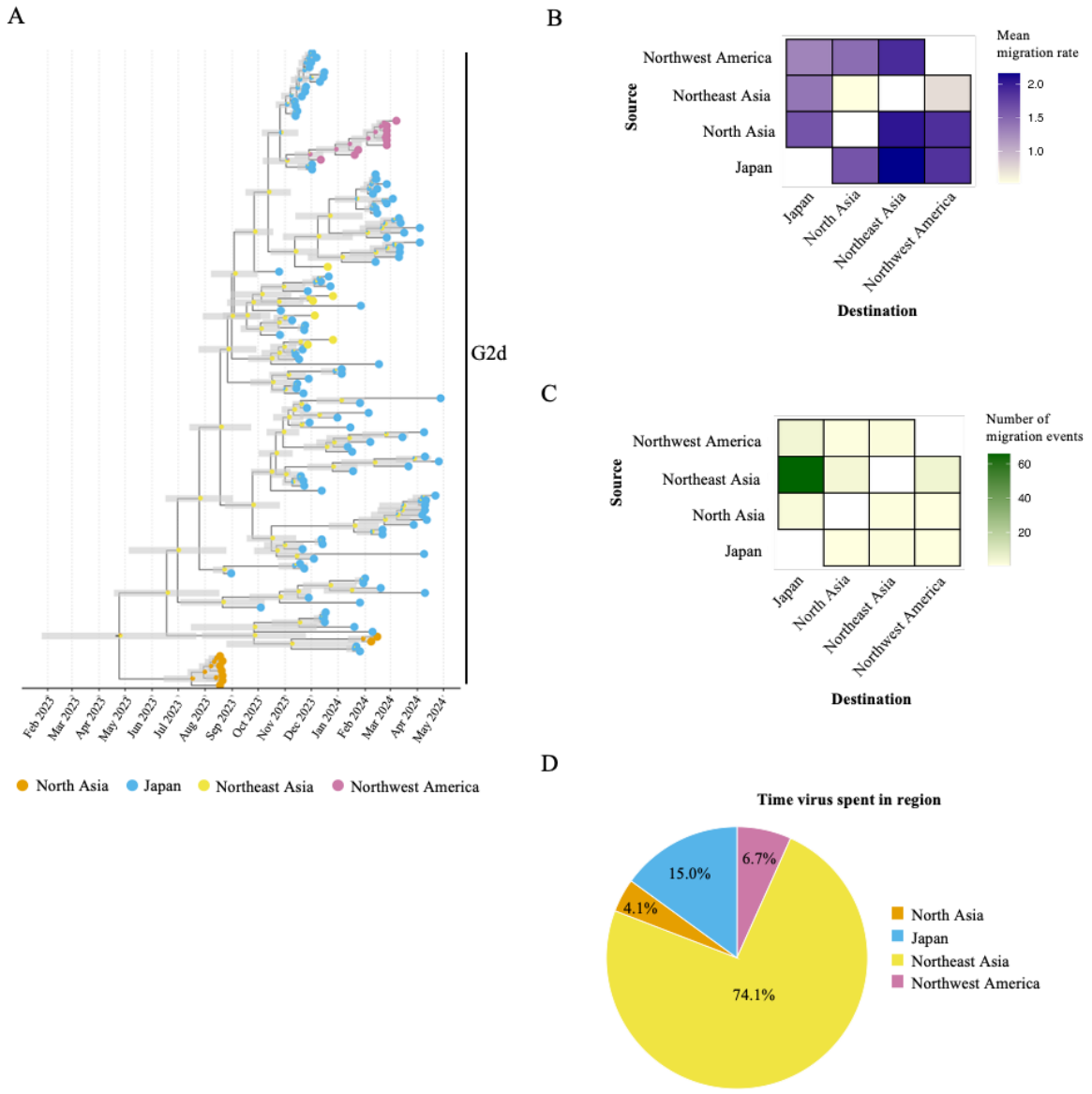


**Figure 10. Phylogeographic analysis of H5N1 HPAIV clade 2.3.4.4b in Japan during winter 2023–2024**. **(A)** The MCC tree was constructed using the HA gene of the H5N1 HPAIV from clade 2.3.4.4b in Japan from June 2023 to May 2024. It was supplemented with other H5N1 HPAIV samples from different regions during the same period, represented by different colors for the internal and external nodes of the MCC tree. **(B)** Heatmaps showing the average per-lineage virus migration rates and **(C)** the number of inferred virus migrations between different geographic regions in winter 2023–2024. **(D)** The pie chart displays the percentage of time the viruses spent in each geographic region during winter 2023–2024.

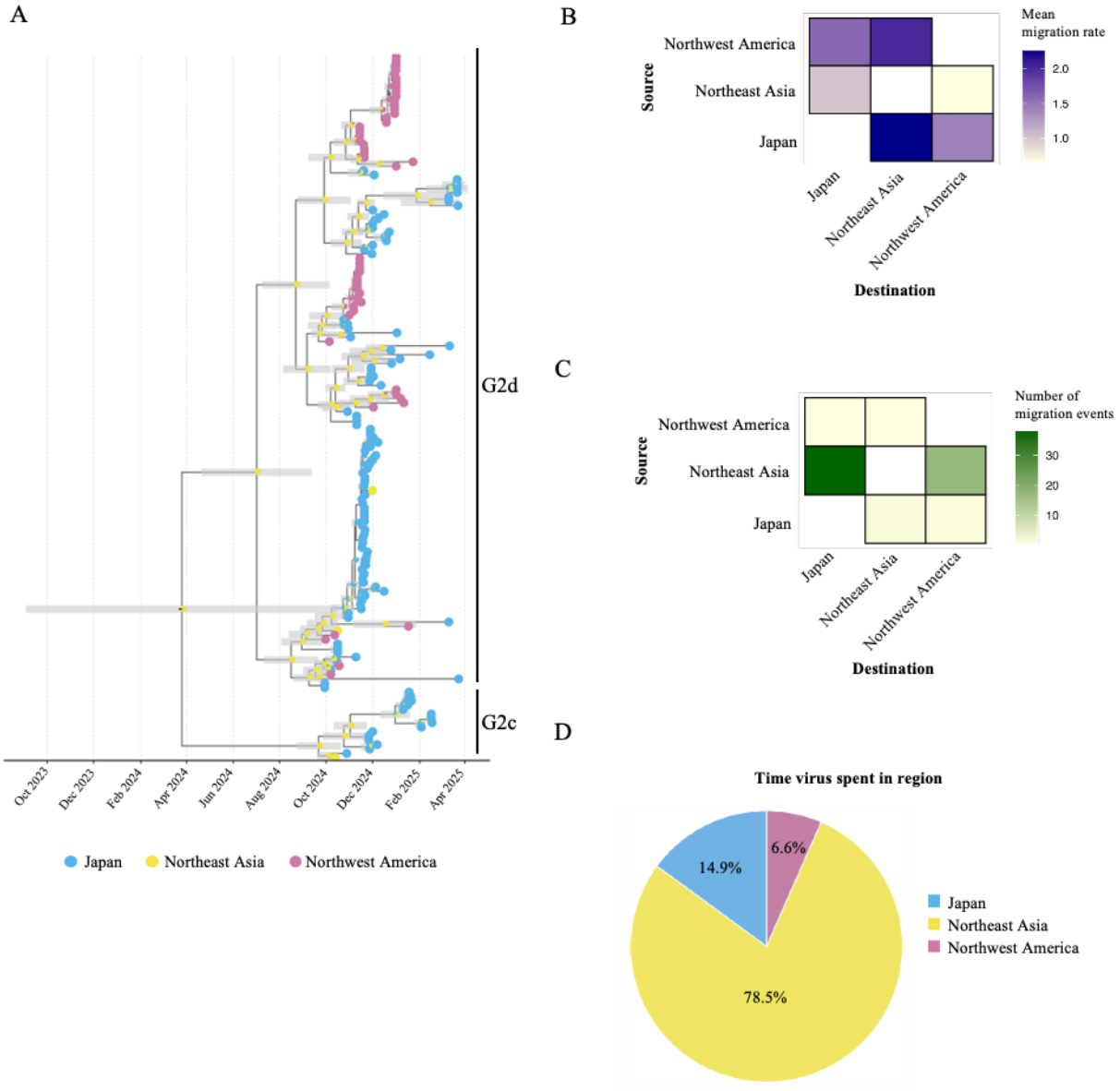


**Figure 11. Phylogeographic analysis of H5N1 HPAIV clade 2.3.4.4b in Japan during winter 2024–2025**. **(A)** The MCC tree was constructed using the HA gene of the H5N1 HPAIV from clade 2.3.4.4b in Japan from June 2023 to May 2024. It was supplemented with other H5N1 HPAIV samples from different regions during the same period, represented by different colors for the internal and external nodes of the MCC tree. **(B)** Heatmaps showing the average per-lineage virus migration rates and **(C)** the number of inferred virus migrations between different geographic regions in winter 2024–2025. **(D)** The pie chart displays the percentage of time the viruses spent in each geographic region during winter 2024–2025.

**Inter-species transmission dynamics of H5N1 HPAIV in Japan during winters 2021–2025**

In winter 2021–2022, the analyses focused on avian hosts within the G2d subgroup, including raptors, crows (*Corvidae*), anatidae (e.g., ducks and geese), and poultry. The mean $R_e$ within the host groups, which indicates the average number of secondary infections within a host group, exceeded 1 in poultry (3.1, 95% HPD [0.9, 5.7]) and crows (1.3, 95% HPD [0.1, 2.8]) (Figure 12A), suggesting sustained transmission among these populations. Conversely, the mean $R_e$ between host groups, called inter-species transmission, was lower, indicating more limited inter-species spread. The highest mean $R_e$ was from raptors (1.8, 95% HPD [0.0, 6.4]) and anatidae (1.6, 95% HPD interval [0.0, 5.7]) to crows (Figures 12B and 13A). This is consistent with the number of inferred inter-species transmission events, which was the highest in raptors (8.1, 95% HPD [0.0, 29.0]), followed by anatidae (8.0, 95% HPD [0.0, 29.0]) to crows (Figure 12C). In contrast, transmission from crows to other host groups was rare, with few inferred events to raptors, poultry, or anatidae. This directional asymmetry was also reflected in the MCC tree, where most crow isolates formed a monophyletic clade, indicating limited transmission to other species (Figure 13B). In winter 2022–2023, the G2c and G2d subgroups were analyzed separately. In the G2c subgroup, the mean $R_e$ within the host groups exceeded 1 only in the cranes (1.6, 95% HPD [1.0, 2.2]), while this value was below 1 in the other host groups (Figure 14A). The mean $R_e$ between host groups remained consistently below 1, suggesting very limited inter-species transmission (Figures 14B and 15A). In the G2d subgroup, the mean $R_e$ values within and between host groups were also below 1 (Figures 14D–E, 16A), supported by the low number of inferred inter-species transmission events (Figure 14F).

In winter 2023–2024, the mean $R_e$ within host groups in the G2d subgroup exceeded 1 in several bird species, with the highest value observed in crows (4.8, 95% HPD [1.0, 8.2]), followed by poultry (2.5, 95% HPD [0.1, 5.3]), cranes (2.0, 95% HPD [0.2, 4.0]) and anatidae (1.7, 95% HPD [0.1, 3.8]) (Figure 17A), indicating ongoing within-group transmission. Although the mean $R_e$ between host groups remained below 1, it was closer to this threshold compared to that seen in previous winters, for instance, from raptors to crows (0.9, 95% HPD [0.0, 2.3]) and anatidae (0.9, 95% HPD [0.0, 2.4]) (Figures 17B and 18A). This pattern aligns with the number of transmission events

estimated between those groups (Figure 17C) and is also reflected in the MCC tree (Figure 18B). In winter 2024–2025, the mean $R_e$ within host groups in the G2d subgroup exceeded 1 in several bird species, with the highest in cranes (9.5, 95% HPD [5.5, 14.1]), followed by crows (6.2, 95% HPD [0.2, 10.4]), poultry (2.1, 95% HPD [0.0, 15.1]), anatidae (1.1, 95% HPD [0.0, 3.2]) and charadriiformes (1.2, 95% HPD [0.0, 3.4]) (Figure 19A). Meanwhile, the mean $R_e$ between host groups exceeded 1 from raptors to anatidae (1.2, 95% HPD [0.0, 3.4]) and charadriiformes (1.1, 95% HPD [0.0, 3.3]), as well from anatidae to raptors (1.0, 95% HPD [0.0, 2.8]) and charadriiformes (1.0, 95% HPD [0.0, 2.9]). Interestingly, transmission from crows to charadriiformes (1.1, 95% HPD [0.0, 3.2]) also showed a mean $R_e$ exceeding 1 (Figures 19B and 20A). This pattern matches the estimated number of transmission events observed between these groups (Figure 19C), as shown in the MCC tree (Figure 20B).

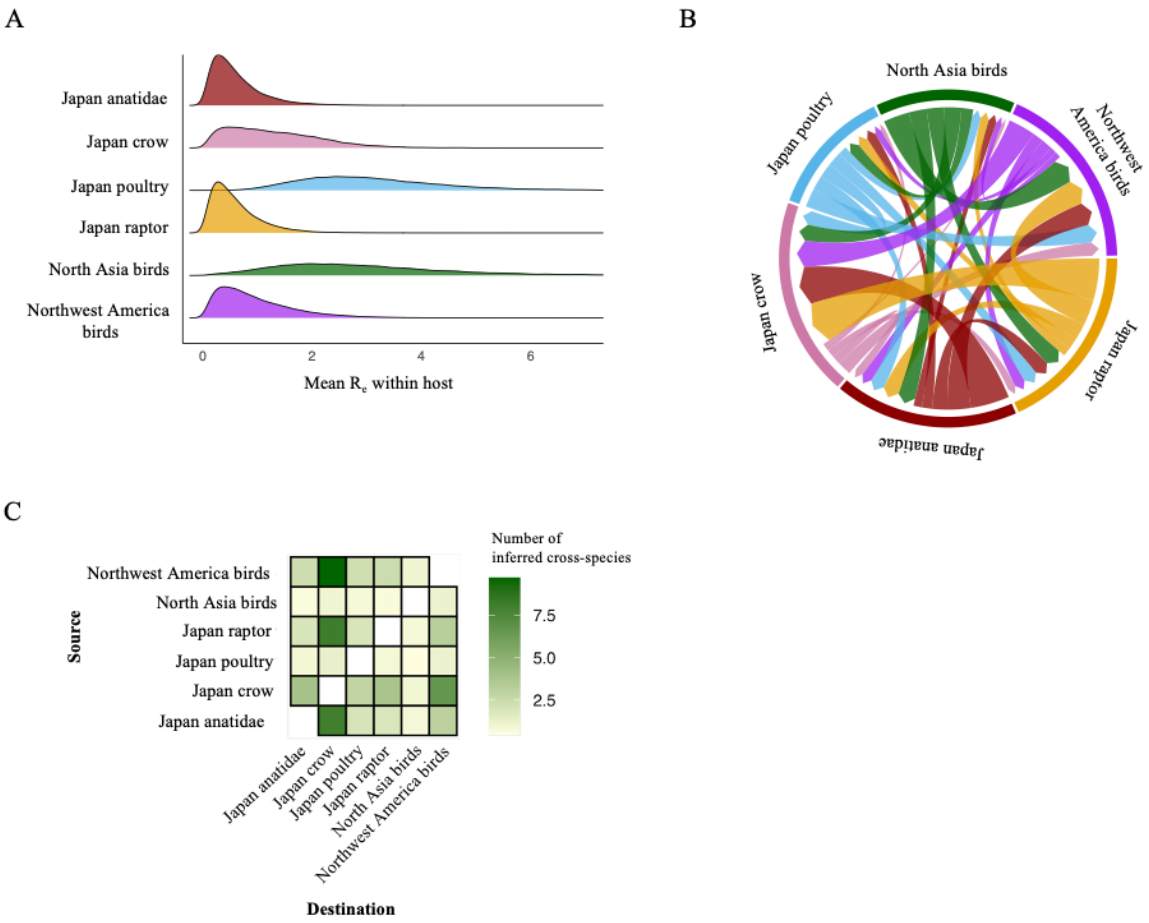


**Figure 12. Host-associated $R_e$ and cross-species transmission dynamics of H5N1 HPAIV among avian hosts in Japan during winter 2021–2022**. **(A)** The ridge plot for each host type (x-axis) shows the density distribution of the mean $R_e$ (x-axis) within the hosts during winter 2021–2022. **(B)** The chord diagram displays transmission events between different bird species in Japan and other regions during the winter 2021–2022, indicating the mean $R_e$ among host groups. The line thickness reflects the magnitude of the mean $R_e$ between hosts, and the arrows show the direction of host transmission. **(C)** The heatmap displays the inferred cross-species transmissions among hosts in Japan and between other regions during winter 2021–2022.

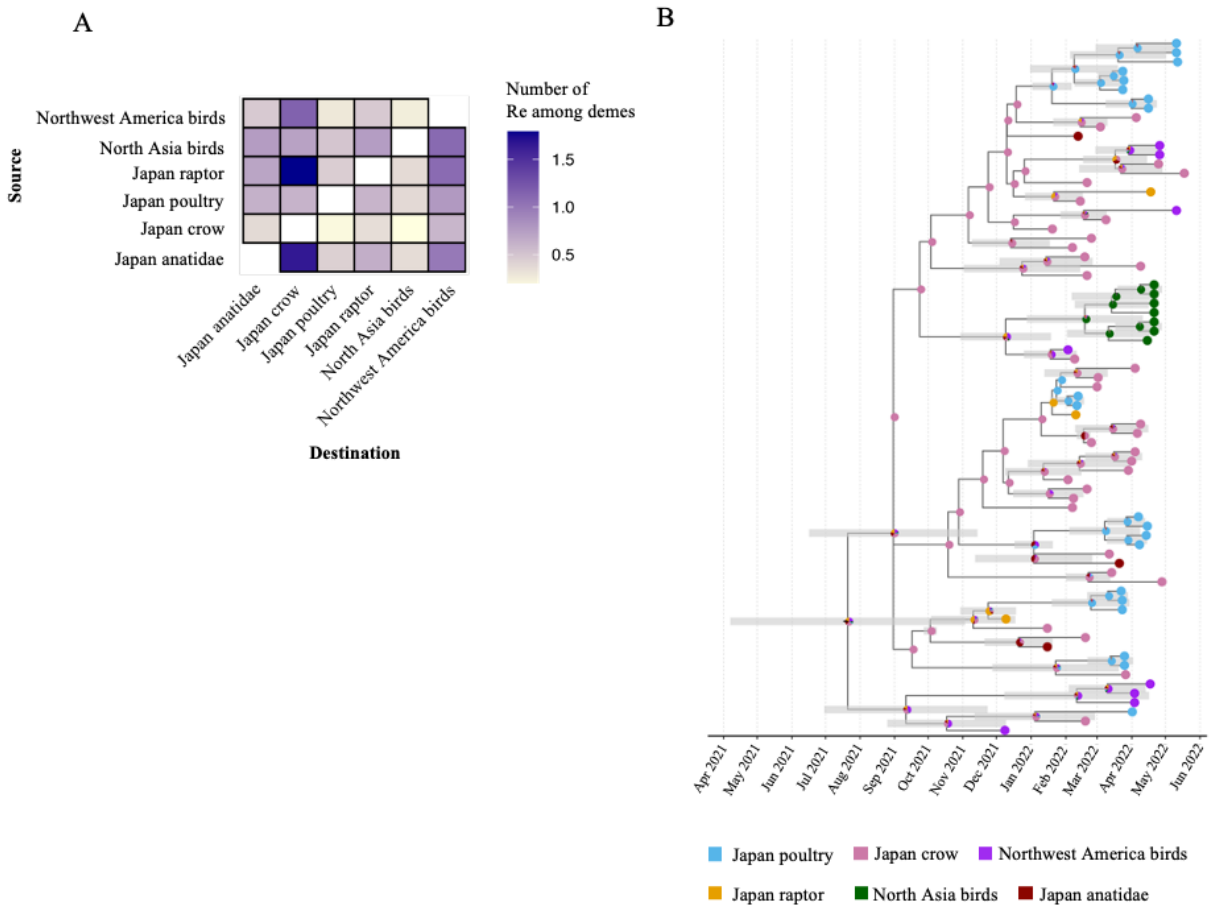


**Figure 13. Host-associated $R_e$ and phylogenetic relationships of H5N1 HPAIV among avian hosts in Japan during winter 2021–2022**. **(A)** Heatmap showing the mean $R_e$ among host groups in Japan and between other regions during winter 2021–2022. **(B)** The MCC tree was constructed using the HA gene of the H5N1 HPAIV in clade 2.3.4.4b in Japan from June 2021 to May 2022. It was supplemented with other H5N1 HPAIV samples from different regions during the same period. The internal and external nodes of the MCC tree are colored by the host type.

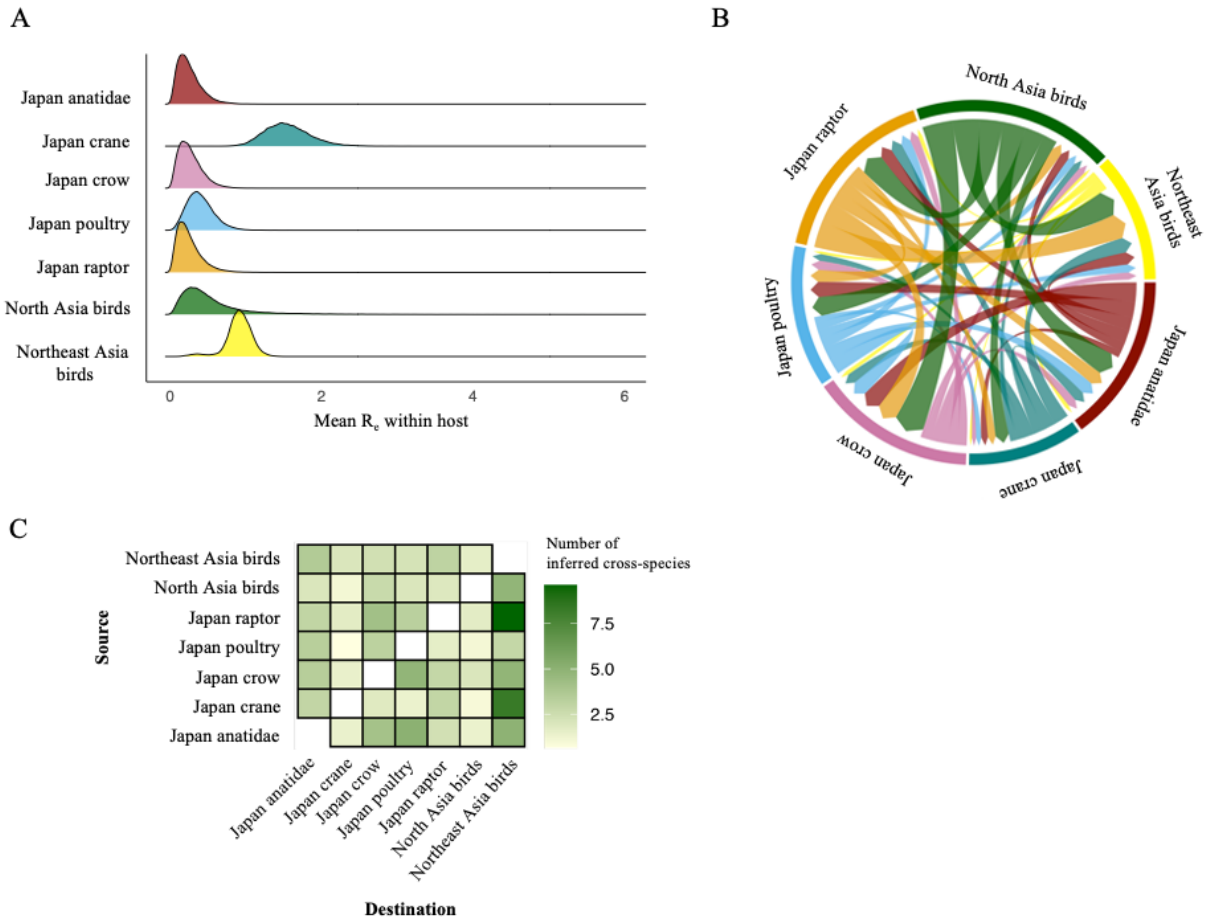


**Figure 14. Host-associated $R_e$ and cross-species transmission dynamics of H5N1 HPAIV among avian hosts in Japan during winter 2022–2023**. Ridge plots for each host type (x-axes) showing the density distribution of the mean $R_e$ (x-axes) within hosts in the **(A)** G2c subgroups during winter 2022–2023. Chord diagrams displaying the transmission events between different bird species in Japan in the **(B)** G2c subgroups and other regions during winter 2022–2023, indicating the mean $R_e$ among host groups. The line thickness reflects the magnitude of the mean $R_e$ between hosts, and the arrows show the direction of transmission. Heatmaps denoting the inferred cross-species transmissions among hosts in Japan in the **(C)** G2c subgroups, and between other regions during winter 2022–2023.

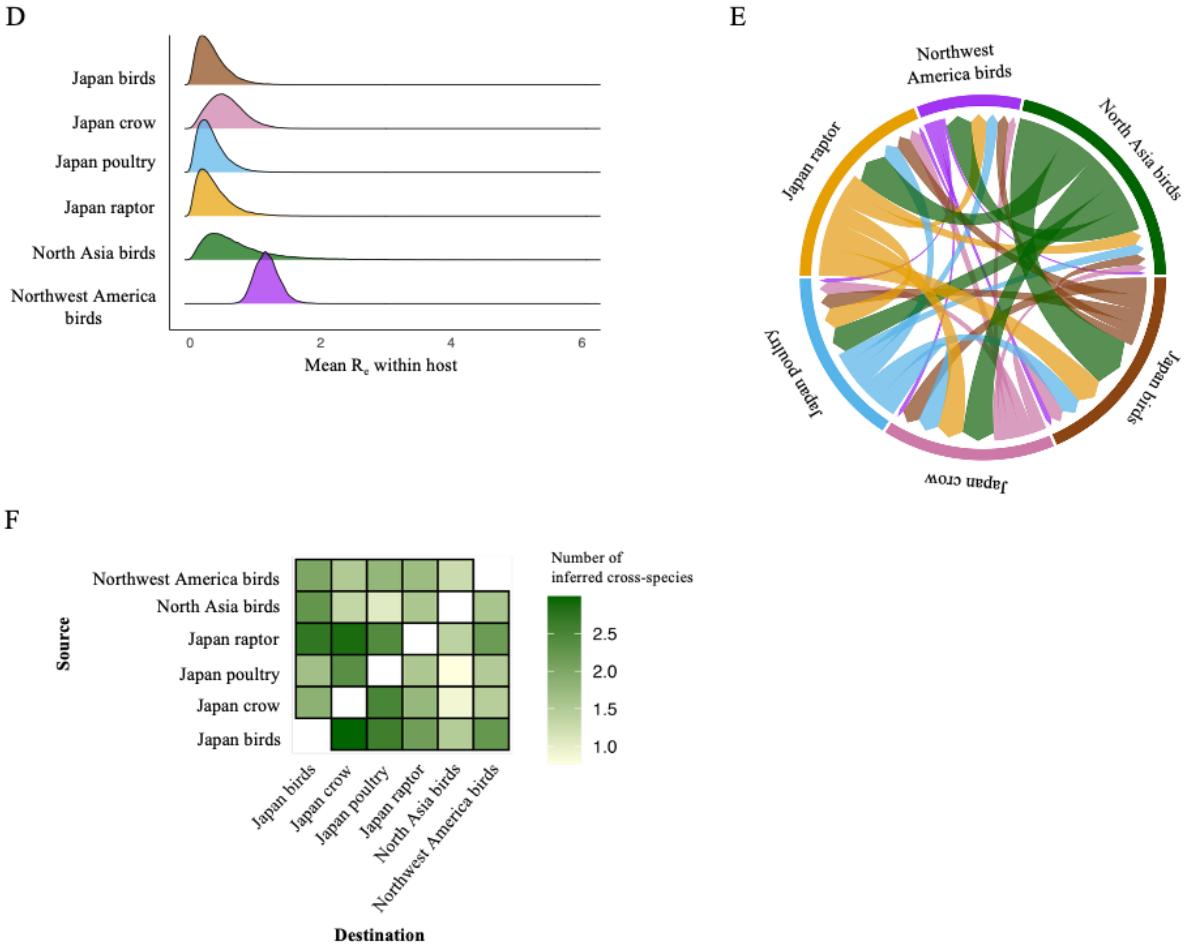


**Figure 14** (*cont*)**. Host-associated $R_e$ and cross-species transmission dynamics of H5N1 HPAIV among avian hosts in Japan during winter 2022–2023**. Ridge plots for each host type (x-axes) showing the density distribution of the mean $R_e$ (x-axes) within hosts in the **(D)** G2d subgroups during winter 2022–2023. Chord diagrams displaying the transmission events between different bird species in Japan in the **(E)** G2d subgroups and other regions during winter 2022–2023, indicating the mean $R_e$ among host groups. The line thickness reflects the magnitude of the mean $R_e$ between hosts, and the arrows show the direction of transmission. Heatmaps denoting the inferred cross-species transmissions among hosts in Japan in the **(F)** G2d subgroups, and between other regions during winter 2022–2023.

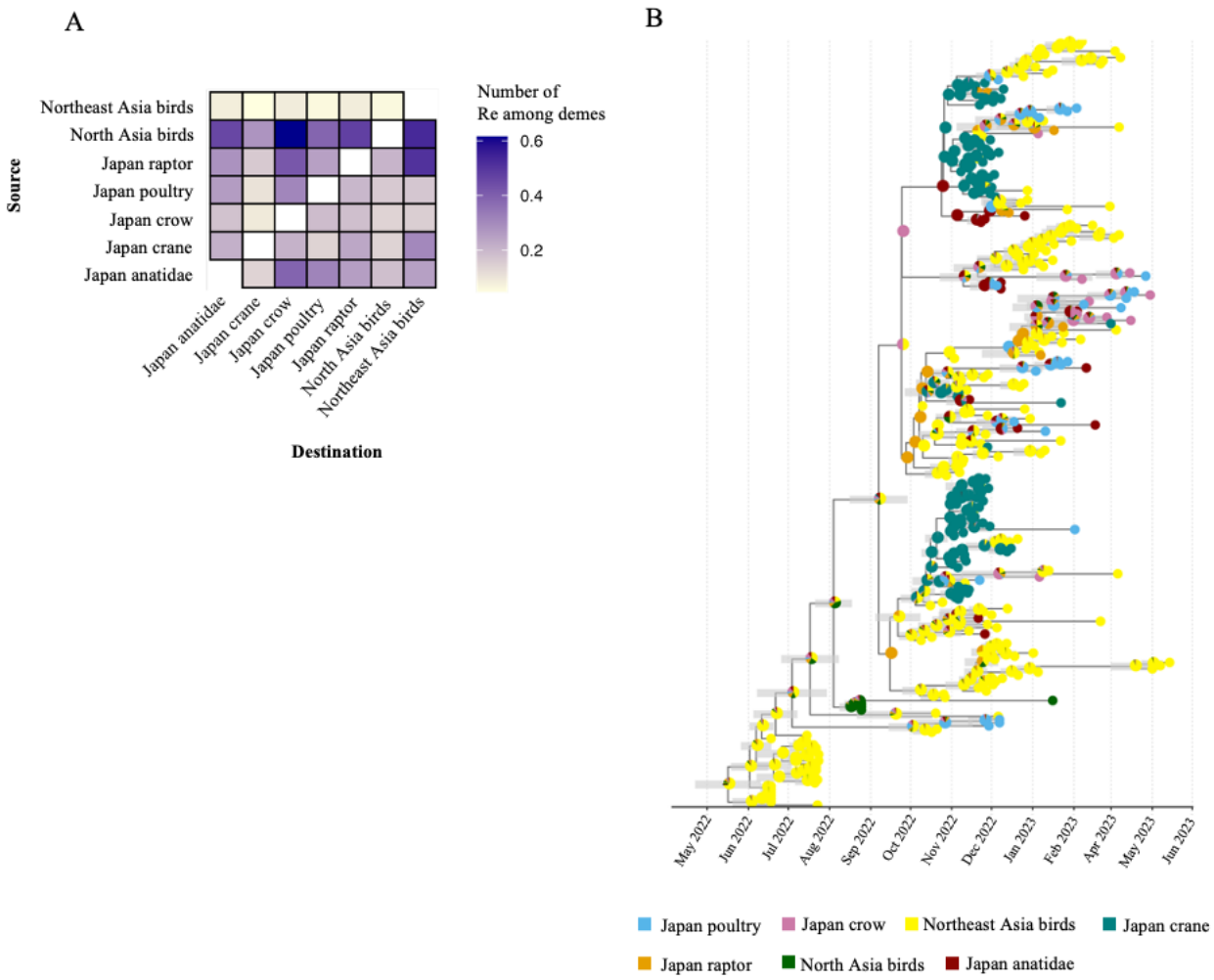


**Figure 15. Host-associated $R_e$ and phylogenetic relationships of H5N1 HPAIV (G2c subgroup) among avian hosts in Japan during winter 2022–2023**. **(A)** Heatmap showing the mean $R_e$ number among host groups in Japan and between other regions during winter 2022–2023. **(B)** The MCC tree was constructed using the HA gene of the H5N1 HPAIV in clade 2.3.4.4b, specifically for the viruses in the G2c subgroup in Japan from June 2022 to May 2023. It was supplemented with other H5N1 HPAIV samples from different regions during the same period. The internal and external nodes of the MCC tree are colored by the host type.

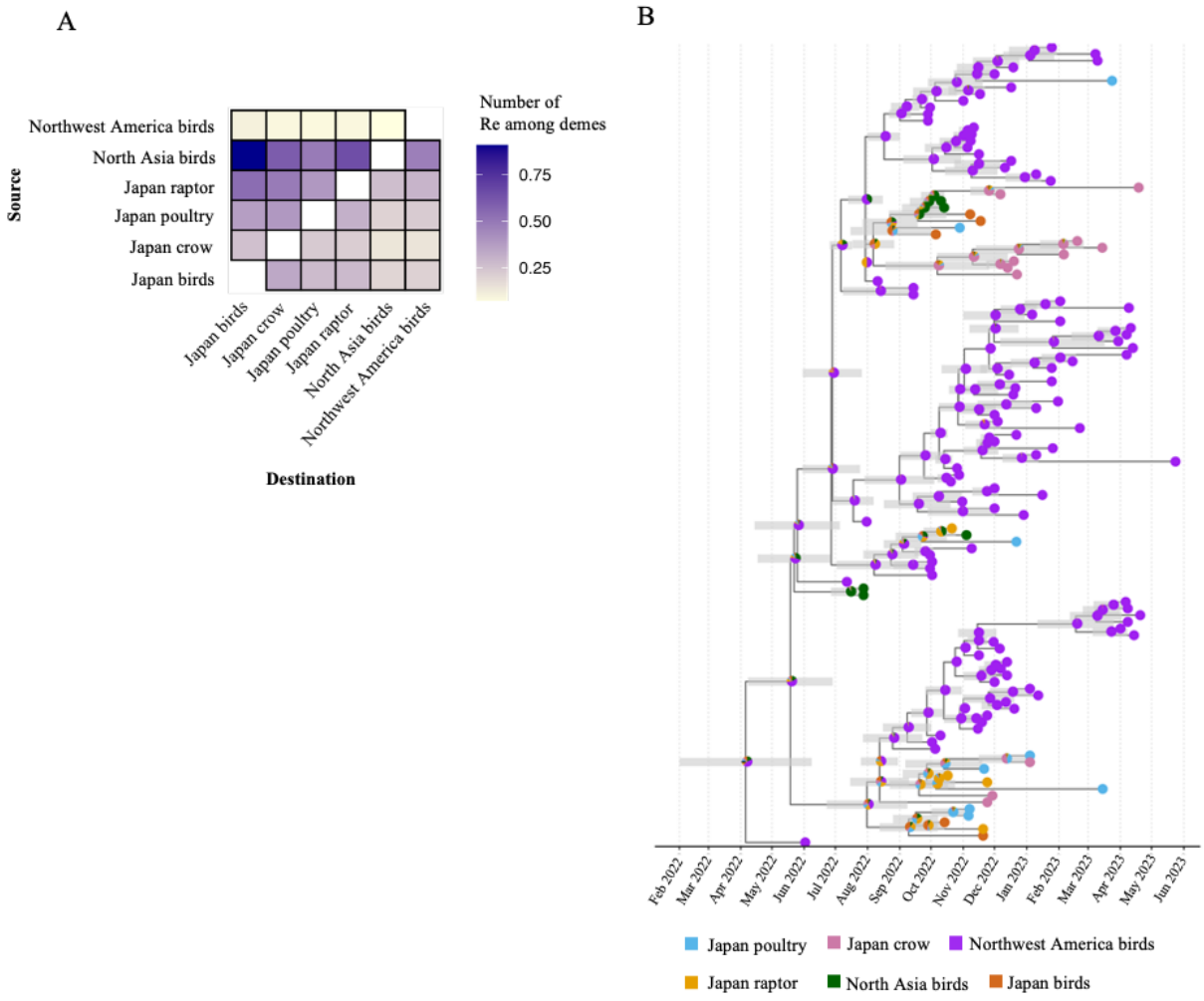


**Figure 16. Host-associated $R_e$ and phylogenetic relationships of H5N1 HPAIV (G2d subgroup) among avian hosts in Japan during winter 2022–2023**. **(A)** Heatmap showing the mean $R_e$ among host groups in Japan and between other regions during winter 2022–2023. **(B)** The MCC tree was constructed using the HA gene of the H5N1 HPAIV in clade 2.3.4.4b, specifically for the viruses in the G2d subgroup in Japan from June 2022 to May 2023. It was supplemented with other H5N1 HPAIV samples from different regions during the same period. The internal and external nodes of the MCC tree are colored by the host type.

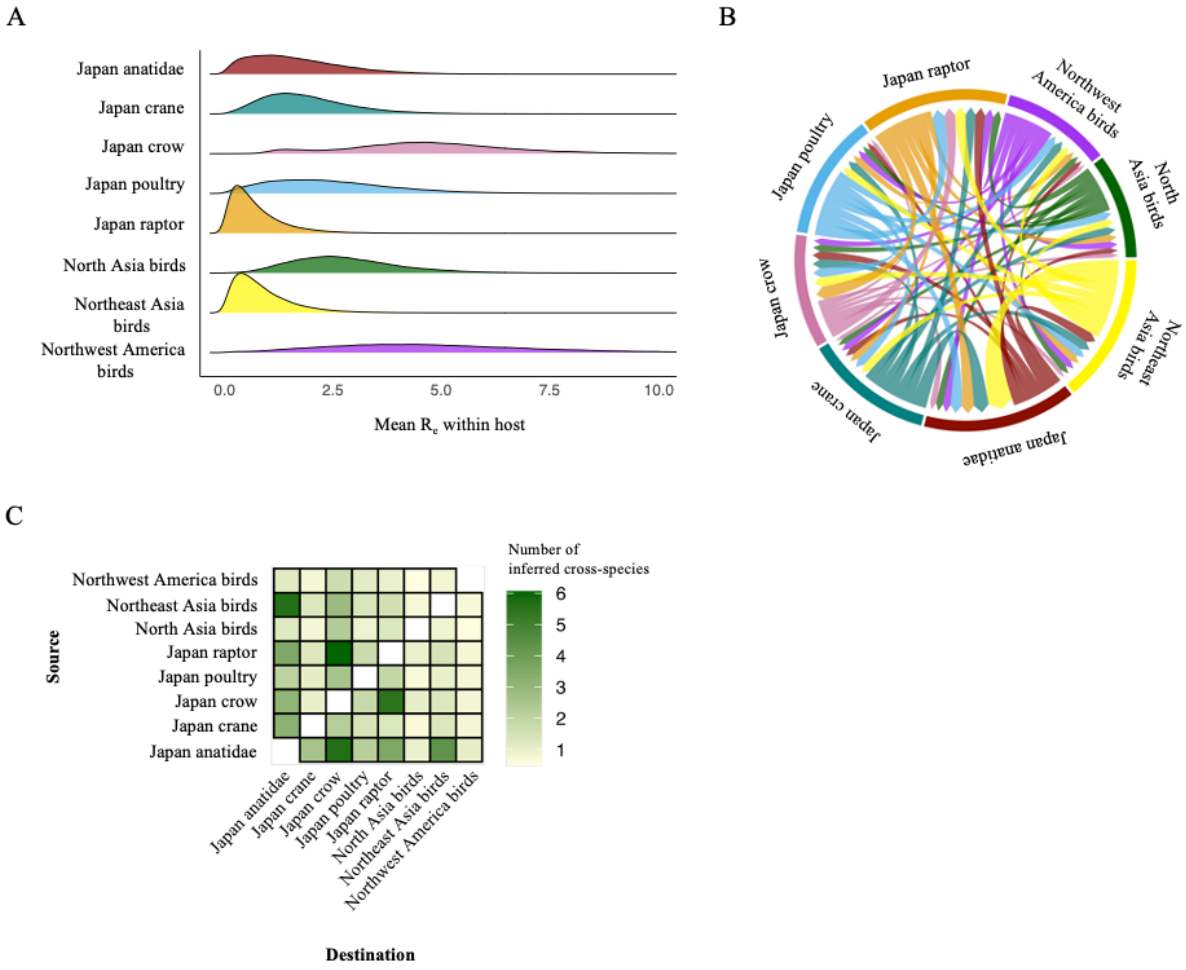


**Figure 17. Host-associated $R_e$ and cross-species transmission dynamics of H5N1 HPAIV among avian hosts in Japan during winter 2023–2024**. **(A)** The ridge plot for each host type (x-axis) shows the density distribution of the mean $R_e$ (x-axis) within hosts during winter 2023–2024. **(B)** The chord diagram displays transmission events between different bird species in Japan and other regions during winter 2023–2024, indicating the mean $R_e$ among host groups. The line thickness reflects the magnitude of the mean $R_e$ between hosts, and the arrows show the direction of host transmission. **(C)** The heatmap displays the inferred cross-species transmissions among hosts in Japan and between other regions during winter 2023–2024.

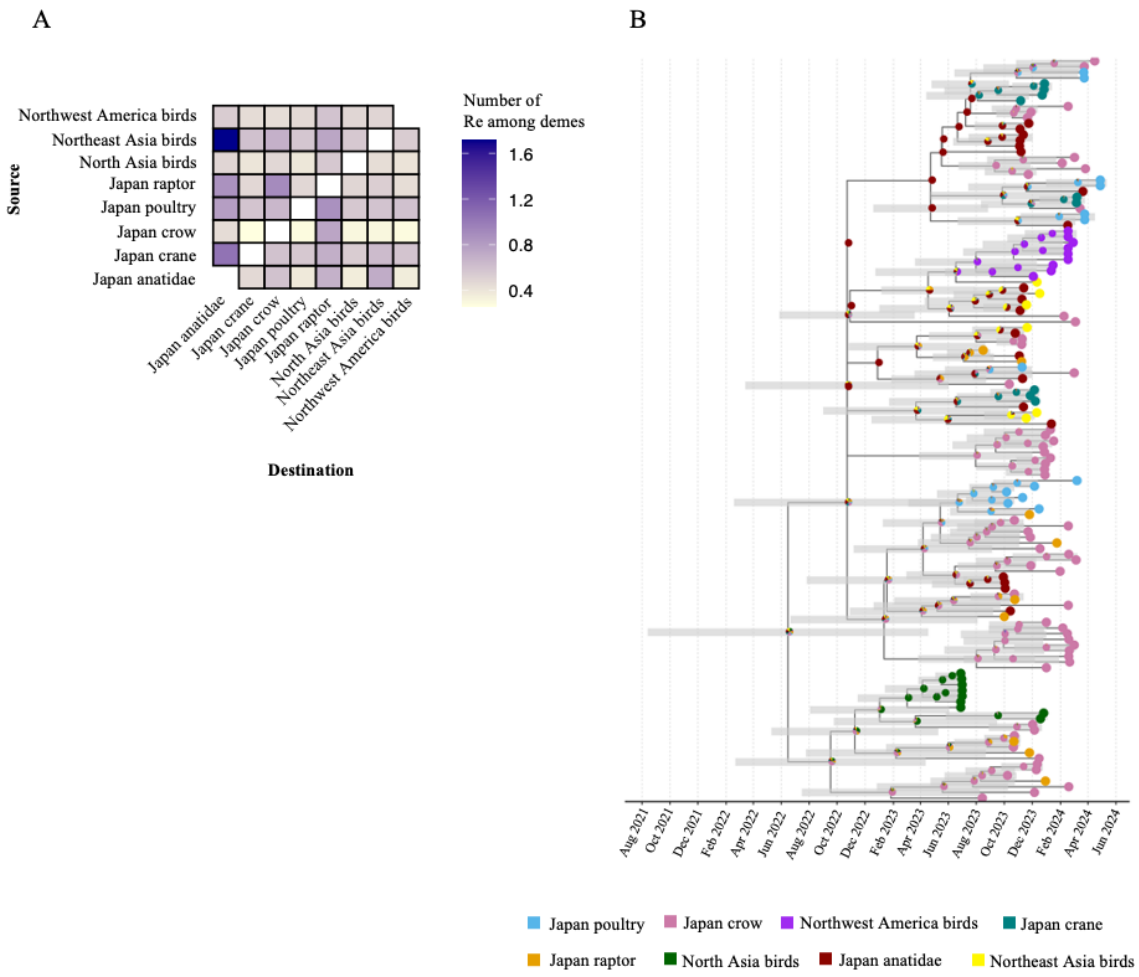


**Figure 18. Host-associated $R_e$ and phylogenetic relationships of H5N1 HPAIV among avian hosts in Japan during winter 2023–2024**. **(A)** Heatmap showing the mean $R_e$ among host groups in Japan and between other regions during winter 2023–2024. **(B)** The MCC tree was constructed using the HA gene of the H5N1 HPAIV in clade 2.3.4.4b in Japan from June 2023 to May 2024. It was supplemented with other H5N1 HPAIV samples from different regions during the same period. The internal and external nodes of the MCC tree are colored by the host type.

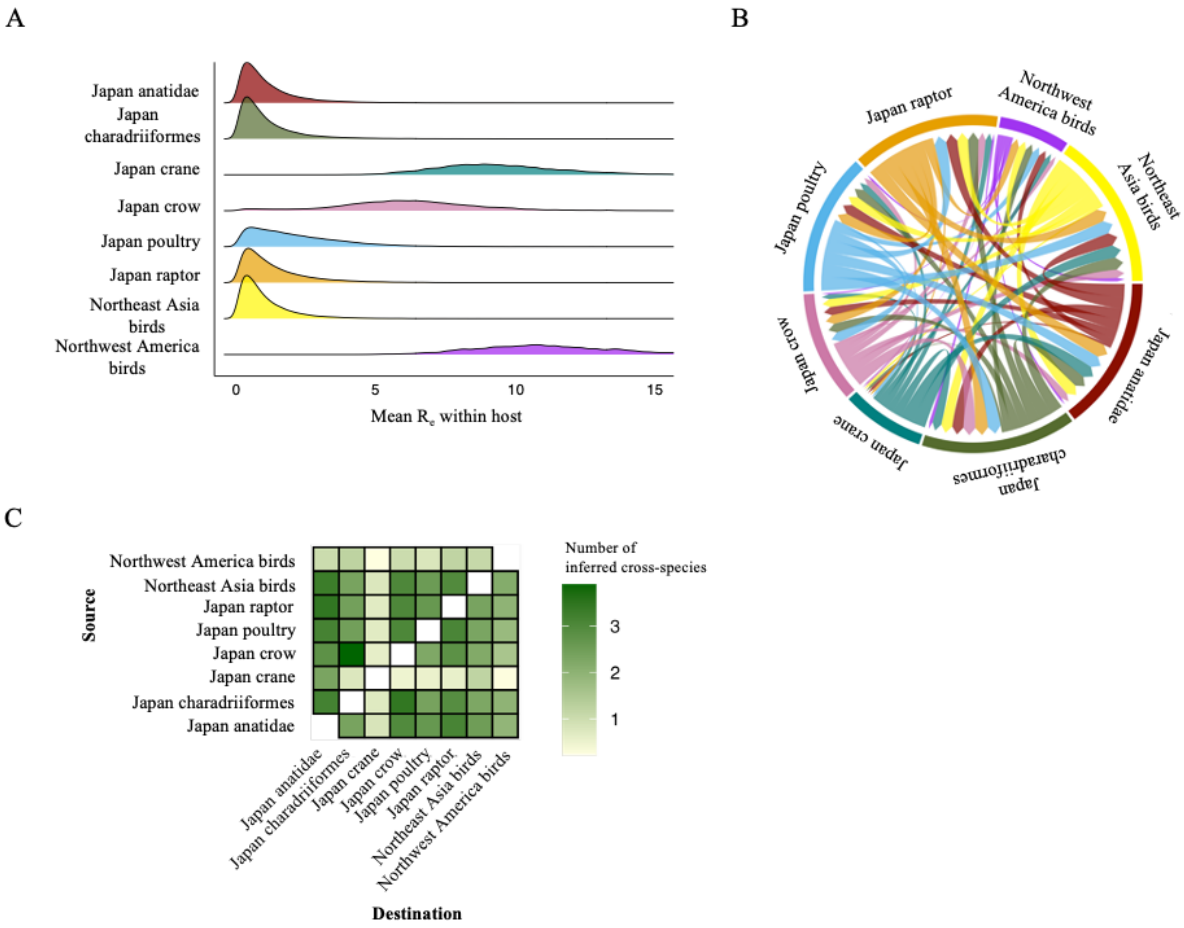


**Figure 19. Host-associated $R_e$ and cross-species transmission dynamics of H5N1 HPAIV among avian hosts in Japan during winter 2024–2025**. **(A)** The ridge plot for each host type (x-axis) shows the density distribution of the mean $R_e$ (x-axis) within hosts during winter 2024–2025. **(B)** The chord diagram displays transmission events between different bird species in Japan and other regions during winter 2024–2025, indicating the mean $R_e$ among host groups. The line thickness reflects the magnitude of the mean $R_e$ between hosts, and the arrows show the direction of host transmission. (**C)** The heatmap displays the inferred cross-species transmissions among hosts in Japan and between other regions during winter 2024–2025.

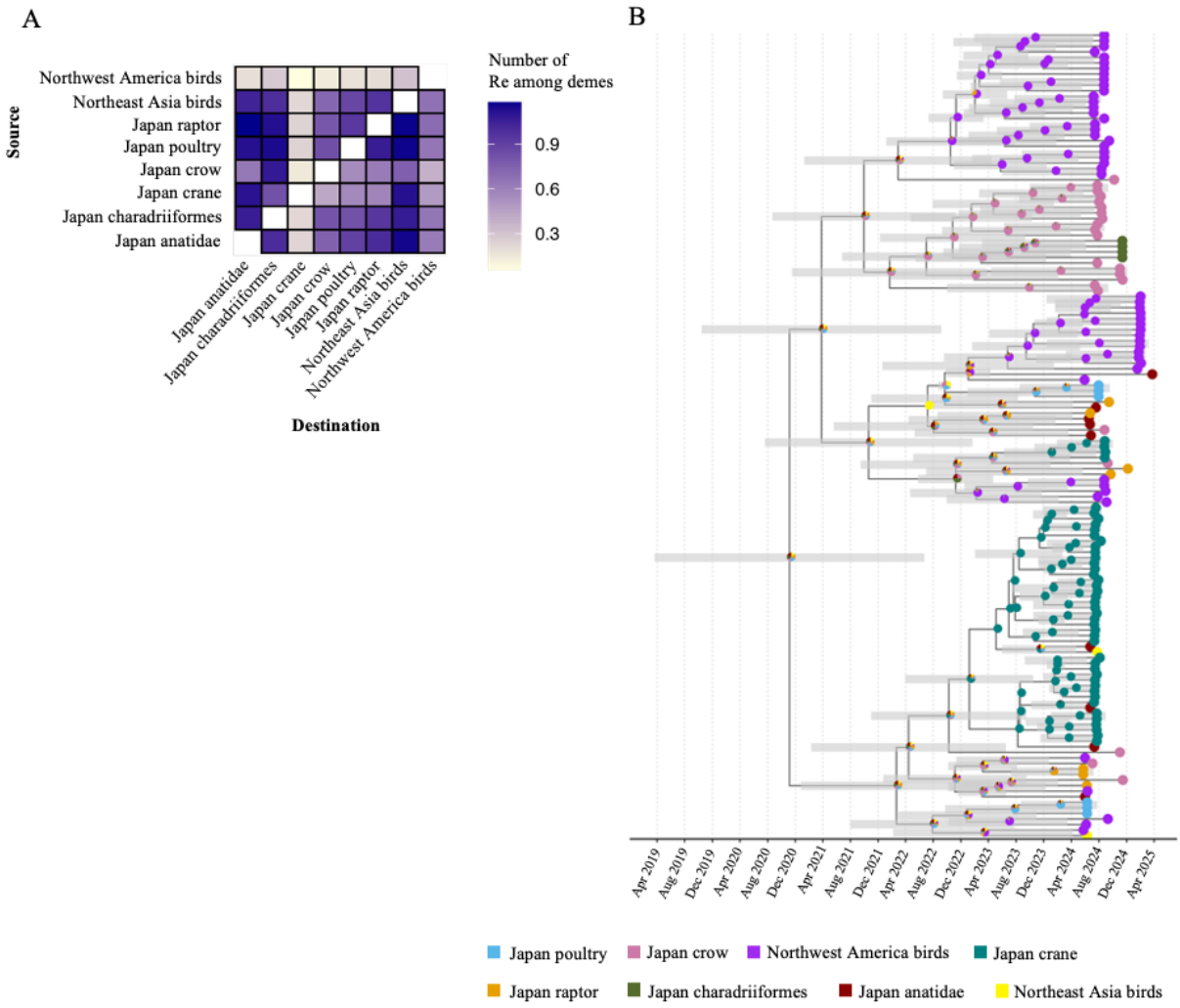


**Figure 20. Host-associated $R_e$ and phylogenetic relationships of H5N1 HPAIV among avian hosts in Japan during winter 2024–2025**. **(A)** Heatmap showing the mean $R_e$ among host groups in Japan and between other regions during winter 2024–2025. **(B)** The MCC tree was constructed using the HA gene of the H5N1 HPAIV in clade 2.3.4.4b in Japan from June 2024 to May 2025. It was supplemented with other H5N1 HPAIV samples from different regions during the same period. The internal and external nodes of the MCC tree are colored by the host type.

## Discussion

This study examined the geographic origins and transmission patterns of H5N1 HPAIVs belonging to clade 2.3.4.4b across different bird species, which have been repeatedly introduced to Japan each winter from 2021 to 2025. The results showed that the HA gene sequences in Japan diverged into multiple subgroups, such as G2b, G2c, and G2d, as reported previously [72]. The G2b subgroup detected in winter 2021–2022 likely originated from Northeast Asia. When it re-emerged in winter 2022–2023, it was probably introduced from North Asia. H5N1 HPAIV in the G2c subgroup, first identified in Japan in winter 2022–2023, was likely introduced from Northeast Asia, and reappeared in winter 2024–2025, again originating from Northeast Asia, indicating consistent virus movement between Northeast Asia and Japan [72, 107, 108]. The presence of G2b and G2c in Japan from winters 2021–2025 further indicates that HPAIV spreads along the East Asian-Australasian flight route, primarily through wild migratory birds during autumn. Multiple phylogenetic studies support a primary west-to-east transmission pattern, with East Asian viruses being more closely related to those from Europe and Central Asia than to North American lineages [9, 84, 109].

In contrast, the G2d subgroup was first identified in Japan during winter 2021–2022 and has been detected annually since then [21, 72, 79]. This study shows that during winters 2021–2023, common ancestral strains were found in North Asia, Northwest America, and Japan, as evidenced by frequent viral migration events among these regions. Notably, phylodynamic analyses suggest that the ancestral strains of the G2d subgroup may have originated from viruses circulating in Northwest America during winters 2021–2023, suggesting a trans-Beringian introduction of viruses from North America to Japan. Such a transmission route has historically been considered unlikely due to limited migratory bird overlap and sparse surveillance in critical regions such as Alaska and Siberia [9, 84, 110]. However, a distinct cluster in the MCC tree for winter 2022–2023 further supports this hypothesis by revealing North Asia as an intermediate region before the virus transmission into Japan. Despite the possibility of a direct introduction from Northwest America to Japan, the limited availability of genomic data from North Asia constrains definitive conclusions. Nevertheless, previous studies have shown genetic similarities between HPAIVs detected in Northwest America and those isolated in Japan, indicating possible transmission through migratory birds along the West Pacific flight

path [25]. Additionally, a bidirectional viral flow might exist, as viruses detected in East Asia in autumn 2022 were closely related to those identified in North America, although current evidence is limited [111]. From winter 2023–2024, the likely geographical origin of the G2d subgroup appeared to have shifted, with evidence suggesting its Northeast Asian origin. This implies that the changes in transmission patterns for this group of viruses may result from ongoing viral migration events among North Asia, Northwest America, and Northeast Asia, with North Asia serving as a major viral hub, given its role as a key breeding ground for many migratory birds and its location at the intersection of multiple flight paths [112]. This may promote the spread of G2d viruses to Northeast Asia, as shown by the increased viral migration events from North Asia. Furthermore, the extended presence of the virus in Northeast Asia in winters 2023–2025 suggests a potential local presence of G2d viruses in that region. These findings suggest that Japan could act as a hub for intercontinental virus introductions, as multiple virus entries from different regions, including North Asia, Northwest America, and Northeast Asia, have been detected, reflecting its strategic location along the East Asia–Australasian and West Pacific migratory flyways. This is particularly concerning given that, despite the seemingly distinct introduction routes for each subgroup (G2b, G2c, and G2d), their entry patterns appear to change across the years, reflecting the unpredictable nature of HPAIV spread and complicating control strategies.

This study revealed variations in the transmission patterns of H5N1 HPAIVs across different bird species (Figure 21). Poultry showed consistent within-$R_e$ during several seasons, notably during the winters 2021–2022 ($R_e$ = 3.1), 2023–2024 ($R_e$ = 2.5), and 2024–2025 ($R_e$ = 2.1), suggesting sustained intraspecies transmission. Farm-to-farm transmission of HPAIV is relatively rare in Japanese HPAIV outbreaks, according to the post-outbreak investigations by the national authorities. The high mean $R_e$ observed in poultry may result from duplicate sequence submissions from multiple laboratories in Japan for the same poultry cases. This might result in the reporting of multiple sequences for a single event, leading to an overestimation of the mean $R_e$ values within the poultry population. However, HPAI outbreaks occurred continuously at high rates in poultry farms during winter 2024–2025, which theoretically matches the high mean $R_e$ in these birds. Overall, between group transmission from poultry to wild birds remained rare throughout, suggesting that poultry most likely act as recipients rather than drivers of

inter-species transmission. Crows emerged as a key host group with divergent roles across the seasons. In the winters of 2021–2022, 2023–2024, and 2024–2025, the mean $R_e$ within crows exceeded 1 ($R_e$ = 1.3, 4.8, and 6.2, respectively), indicating sustained intraspecies transmission. While onward transmission from crows to other species remained limited early on, an increasing transmission potential was observed in later seasons, including to charadriiformes in winter 2024–2025. These findings suggest a shift in the role of crows from primarily dead-end hosts (as seen with G2c) to potential intermediate hosts (notably for G2d), possibly driven by ecological factors such as regional overwintering behavior in Hokkaido and the environmental persistence of viruses. Nevertheless, crows may still function as opportunistic transmitters, as evidenced by the higher number of inferred events between crows and poultry in the winters 2022–2023 and 2024–2025, based on the presence of dead crows near infected poultry farms [113]. Experimental studies also indicate variable susceptibility to different H5 HPAIV subgroups [114], which warrants further investigation for the G2b, G2c, and G2d subgroups, as shown by the differences in pathogenicity in chickens across these subgroups [72].

Raptors significantly contribute to inter-species transmission, with the highest between-host $R_e$ observed in the earlier seasons, especially toward crows ($R_e$ = 1.8 in winter 2021–2022; $R_e$ = 0.9 in winter 2023–2024) and toward anatidae and charadriiformes ($R_e$ = 1.1 in winter 2024–2025). Transmission from raptors to anatidae is generally considered uncommon because these two species occupy different ecological niches. Viruses are not easily detectable in waterfowl, which are considered to be asymptomatic carriers. In contrast, raptors are highly susceptible to HPAIV infection because they sometimes scavenge on infected birds, including waterfowl. This typically causes early death [115], leading to earlier detection and reporting of their HPAIV infection. The difference in disease notifications after HPAIV infection among anatidae and raptors could also indirectly affect the interpretation of the disease dynamics. Furthermore, crows are also susceptible to HPAIV infection due to scavenging or habitat sharing with waterfowl. However, they are usually not assessed until their mass die-off, unlike that in the raptors. Although raptors are typically regarded as spillover hosts, acquiring infection through predation or scavenging infected birds, the results suggest that they may contribute to local transmission to other host groups before succumbing to the virus infection. Though their limited mobility after infection restricts their long-

distance spread [116], their role in local amplification and transmission, especially to crows and other wild birds, warrants further study. Anatidae played a dual role across the seasons. Notably, the within-group $R_e$ values were often above 1 ($R_e$ = 1.7 in winter 2023–2024, $R_e$ = 1.1 in winter 2024–2025), suggesting sustained transmission within wild waterfowl populations, these birds were recurrently identified as sources of cross-species transmission, especially to crows, raptors, cranes, and charadriiformes, consistent with their capacity for long-distance migration even when infected or asymptomatic [117]. In contrast, cranes showed a progressive increase in epidemiological significance throughout the study period. In winter 2022–2023, they were the only host group in the G2c subgroup with a mean $R_e$ above 1 ($R_e$ = 1.6). Their transmission potentials increased further in winter 2023–2024 ($R_e$ = 2.0) and peaked in winter 2024–2025 ($R_e$ = 9.5) within the G2d subgroup, likely because of virus introduction via shared habitats with anatidae [118], which facilitated cross-species transmission. However, transmission from cranes to other wild birds remained rare, indicating that cranes are more often recipients than drivers of inter-species spread.

Although this study provides valuable insights into the geographic origins and inter-species transmission dynamics of H5N1 HPAIV in Japan, several limitations remain. As the available surveillance data relies mainly on deceased birds or environmental samples in Japan, rather than live-captured birds, it may not accurately reflect the real-time dynamics of virus circulation because it overlooks subclinical infections and asymptomatic carriers. Additionally, delays in data sharing or inadequate surveillance efforts across countries can hinder a prompt understanding of the broader HPAIV situation. In the context of phylodynamic analyses, sampling biases and limited sequence availability are setbacks for the accurate depiction of virus transmission. The MTBD model was appropriate for this study because it connects the phylogenetic tree with the underlying epidemiological processes of transmission, migration, and sampling among structured populations. MTBD enables estimation of specific transmission and migration rates, helping to distinguish repeated introductions from local persistence and partially accounting for uneven sampling across host types [98]. While discrete-trait phylogeographic approaches can describe lineage movements, they do not offer mechanistic insights into transmission dynamics [119]. However, the limitation of MTBD is that it assumes that transmission, removal, and migration rates are constant within each

analysis period and does not explicitly account for unsampled populations [96, 98]. Therefore, the estimated rates should be viewed as averages over the period rather than exact figures. Nonetheless, the observed clustering and virus migration patterns among regions and hosts remained consistent across all analyses, supporting the robustness of the inferred transmission and migration dynamics. Consequently, ongoing efforts to improve global surveillance, including sampling live-captured wild birds and sharing data promptly, are essential for refining phylodynamic inferences and better understanding of H5 HPAIV transmission dynamics.

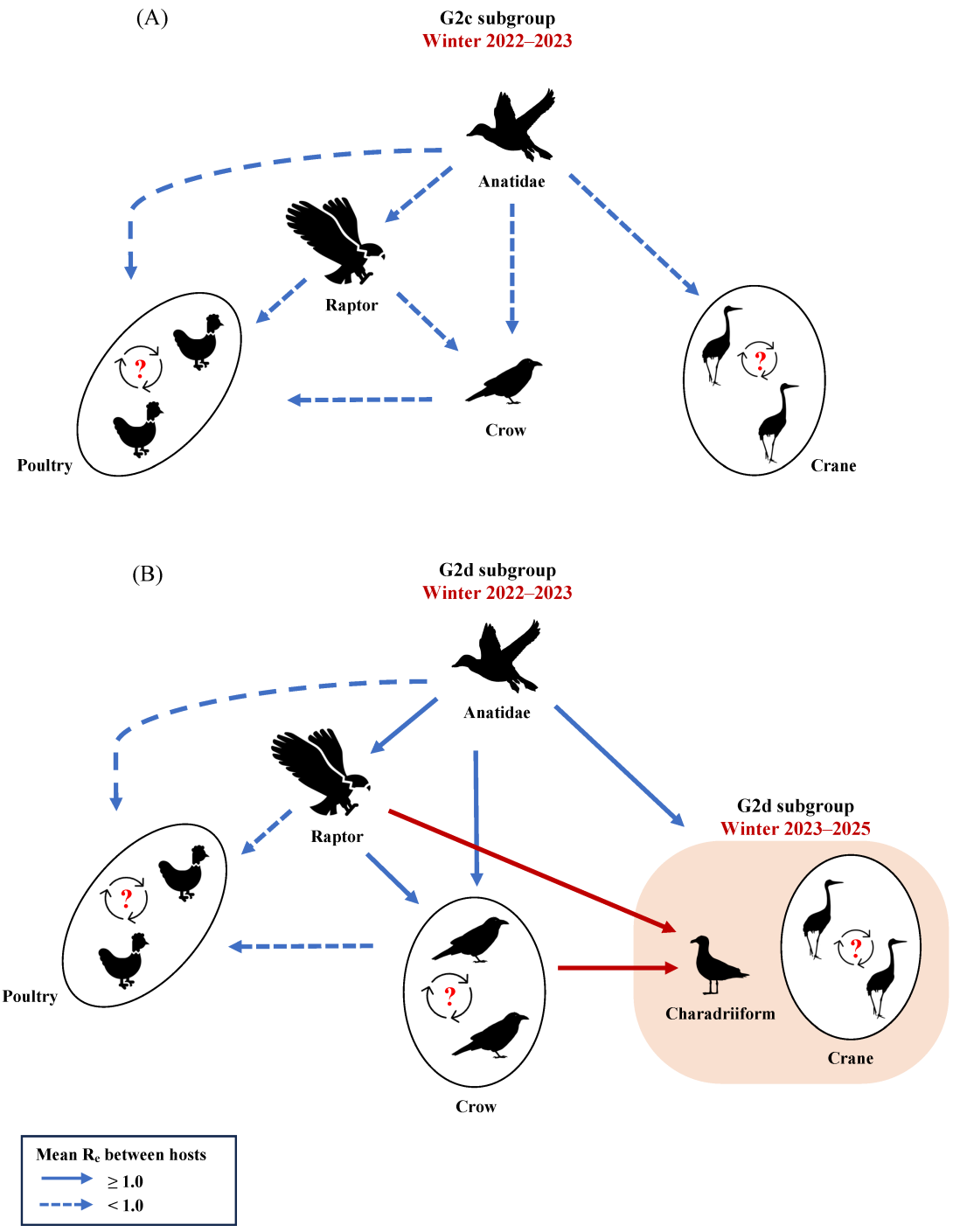


**Figure 21. Transmission dynamics among hosts in the G2c and G2d subgroups (2021–2025)**. Graphical abstract depicting the transmission events between hosts in **(A)** the G2c subgroup during winter 2022–2023 and **(B)** the G2d subgroup during winters 2021–2025, based on the mean $R_e$. The arrow indicates the direction of transmission. The solid and dotted lines represent mean $R_e$ greater than or equal to 1.0 and $R_e$ less than 1.0, respectively.

## Brief summary

HPAIV impacts poultry and wild birds worldwide. Since the introduction of clade 2.3.4.4b H5N1 isolates in Japan in late 2021, new cases have been reported in domestic birds and poultry each winter. To understand the role of wild birds in introducing these viruses in Japan, a phylodynamic analysis based on geography and host species was conducted using H5N1 isolates in Japan from 2021–2025. A total of 892 HA gene sequences of H5N1 viruses derived from birds collected between June 2021 and May 2025, along with additional sequences that were highly similar to those of Japanese isolates, were obtained from a public database. The role of wild birds in the transmission dynamics of H5N1 isolates in Japan across four winter seasons (2021–2025) was assessed using a Bayesian phylodynamic approach with an MTBD model. Phylodynamic analysis revealed that the clade 2.3.4.4b comprised three distinct subgroups, G2b, G2c, and G2d, which were prevalent during the winter seasons. Isolates from G2b and G2c were linked to common ancestral strains from North Asia and Northeast Asia, respectively. Meanwhile, G2d, the dominant strain in Japan from 2021 to 2025, shared an ancestral strain from the Northwest America. During winters 2023–2025, the ancestral strain was traced to Northeast Asia, indicating a shift in the viral origin. This transition suggests increased virus migration among regions and infection of a broader range of avian hosts, implying that Japan may function as a hub for intercontinental virus introductions, receiving multiple independent viral entries from North Asia, Northeast Asia, and Northwest America. Additionally, waterfowl and possibly raptors may have introduced viruses into Japan, whereas poultry and crows were infected but did not appear to contribute to onward transmission. However, the continuous introduction of H5N1 into Japan each winter can alter the disease transmission pattern observed in crows, resulting in more virus spillover from crows to other hosts, such as poultry and charadriiformes. These findings emphasize the importance of continuous monitoring and prompt information sharing to better understand the global dynamics of viruses.

# Chapter IV

# Evaluation of the efficacy of low-concentration gaseous chlorine dioxide in inactivating airborne H5 high pathogenicity avian influenza virus *in vivo* model

## Introduction

The introduction of HPAIV to poultry farms was believed to result from exposure to virus-contaminated excretions or secretions from wild birds. This process is facilitated by the movement of people, contaminated equipment, and vehicles [120]. In addition, the detection of wild waterbird-derived DNA in the atmosphere of farms demonstrated that the airborne dispersal of HPAIV might contribute to introducing viruses into the flock [121]. Therefore, biosecurity measures remain a top priority for controlling HPAI outbreaks on poultry farms. Segregation, cleaning, and disinfection are fundamental biosecurity principles that prevent the intrusion of people, wild animals (such as rodents or crows, which interact with both wild birds and poultry), or vehicles that can carry pathogens into the farm. Additionally, disinfectants that inactivate pathogens on farm surfaces and equipment can reduce the risk of HPAI outbreaks in poultry [122]. Although current biosecurity measures are considered crucial in minimizing HPAI introduction, outbreaks in poultry farms have been continuously reported, underscoring the need to continually enhance these measures, including the adaptation of new technologies, as H5 HPAIV can be introduced through aerosolized contaminants from infected birds directly, through other animals, or by human activities. Safe and effective disinfectants are additional options to reduce the level of contamination by pathogens, and they are applicable to poultry farms, markets, and their surrounding environments. Disinfectants such as sodium hypochlorite (NaOCl) and quaternary ammonium compounds (QACs) are commonly used in poultry farms. NaOCl is known for its broad-spectrum disinfectant properties, as it effectively eliminates a variety of viruses, including feline calicivirus, human influenza virus, and measles virus, as well as bacteria such as *Pseudomonas aeruginosa* and *Acinetobacter* spp. [123, 124]. In conjunction with QACs, NaOCl has also displayed significant virucidal activity against severe acute respiratory syndrome coronavirus 2 (SARS-CoV-2) and H7N1 LPAIV [125, 126]. However, NaOCl is less effective in the presence of organic matter, and this compound can corrode the metal surface [127, 128]. Similarly, QACs lose virucidal properties under these conditions and at low temperatures [129]. Therefore, another disinfectant, such as $ClO_2$, might be considered to improve biosecurity on poultry farms.

$ClO_2$ is a yellow, water-soluble gas with a characteristic chlorine-like odor and strong oxidizing properties. It is classified as an A-1 level disinfectant and recognized by the WHO as safe and effective, and it is commonly used in commercial settings [130, 131]. Additionally, $ClO_2$ is typically less corrosive to metals during disinfection-level exposure, making it more suitable for environments with sensitive equipment [132]. Several studies have demonstrated the wide range of antimicrobial activities of liquid and gaseous $ClO_2$ against bacteria, fungi, and viruses, including *Staphylococcus aureus*, *Penicillium chrysogenum*, SARS-CoV-2, and H7N1 LPAIV [133–136]. Numerous studies found that gaseous $ClO_2$ exhibits virucidal efficacy against several influenza viruses, including H1N1 seasonal influenza in a mouse model [0.03 ppmv (0.084 mg/$m^3$) after 15 min] and H7N9 HPAIV *in vitro* (5.0 ppmv after 1 h) [137, 138]. The antimicrobial effects of $ClO_2$ are likely associated with the peroxidation of viral lipids, thereby disrupting the lipid envelope and protein shell [139]. This capability has been demonstrated through the ability of $ClO_2$ to inactivate influenza viruses by oxidizing the tryptophan residue (W153) to *N*-formylkynurenine in the HA protein, which is crucial for viral attachment to host cell receptors [140]. Despite the recognized broad-spectrum antimicrobial properties of $ClO_2$, the virucidal efficacy of gaseous $ClO_2$ against H5 HPAIV has not been thoroughly investigated *in vivo* settings. Therefore, this study represents the first comprehensive investigation of the efficacy of gaseous $ClO_2$ against H5 HPAIV using a chick model as *in vivo* model, providing novel empirical data to support its application. The obtained data will be applied to additional options in biosecurity measures to reduce HPAI risks on poultry farms.

## Materials and Methods

### Virus preparation

An H5N1 HPAIV WTE/Hok/R22/22 (H5N1) strain previously isolated from a deceased white-tailed eagle (*Haliaeetus albicilla*) [21], was propagated into 10-day-old embryonated eggs. Following virus propagation in allantoic fluid as confirmed by the HA assay [43], the collected allantoic fluid was used as the viral stock. The final titer of the viral stock was determined as $10^{9.0}$ $TCID_{50}$/mL.

### Cells and virus quantification

MDCK cells were cultured in a 96-well plate, with each well containing 100 μL of MEM (Shimadzu Diagnostics Corporation) supplemented with 10% bovine fetal serum (Merck KGaA, Darmstadt, Germany), 100 U/mL penicillin G (Meiji Seika Pharma), 0.3 mg/mL L-glutamine (Nacalai Tesque, Kyoto, Japan), 0.1 mg/mL streptomycin (Meiji Seika Pharma), and 8 mg/mL gentamicin (MSD). Once the MCDK cells reached 90% confluency, each virus sample was diluted 10-fold with MEM and inoculated onto the cells, which were incubated at 37 °C in a 5% $CO_2$ incubator for 3 days to observe CPE in the infected cells. Using the Reed and Muench method, virus infectivity was quantified as $TCID_{50}$ [141].

### Experimental setup for the efficacy of gaseous $ClO_2$

Two isolators, designated as isolators A and B, with dimensions of 46 × 40 × 26 $cm^3$ (47.8 L) were used in this experimental setting within the class IIA biosafety cabinet (Figure 22). The two isolators were connected by a polyvinyl chloride tube with a radius of 5 cm. Gaseous $ClO_2$, produced by an $ClO_2$ generator (elecloorer SS, Fujicom, Aichi, Japan), or negative-control air (0 ppmv $ClO_2$) was introduced into isolator A through an additional opening. A battery-powered fan was installed inside isolator A to improve air circulation, whereas nebulizers (Omron, Kyoto, Japan) were employed to generate aerosol from a suspension of phosphate-buffered saline or viruses suspended in sterilized distilled water. Following the interaction of the delivered gas with the nebulized viruses, the air mixture was expelled by an oil air pump into isolator B. The MD8 air sampler (Sartorius, Gottingen, Germany) collected airborne microorganisms by suctioning a

specific air volume through a gelatin membrane filter (Sartorius) installed in isolator B. A sampling tube for $ClO_2$ measurement was inserted into isolator A to concurrently measure and monitor the gaseous $ClO_2$ concentration using a $ClO_2$ gas detector (New Cosmos Electric, Osaka, Japan). The concentration of gaseous $ClO_2$ inside isolator A was manually controlled to 0.010 (the lowest limit of the $ClO_2$ generator), 0.025, 0.050, or 0.100 ppmv by adjusting the gas supply from the $ClO_2$ generator while monitoring the concentration with the $ClO_2$ gas detector.

The inactivation efficacy of gaseous $ClO_2$ and *in vivo* experiments were evaluated under the following conditions. A specific concentration of gaseous $ClO_2$ (0.010, 0.025, 0.050, or 0.100 ppmv) was introduced for 2 min to maintain the gaseous $ClO_2$ levels in isolator A. After nebulizing a certain concentration of viruses for 2 min, the gaseous $ClO_2$ concentration in isolator A was maintained at the target level for a designated inactivation time (1 or 5 min, Figure 22A). The air mixture was pumped from isolator A to isolator B by the air pump, and the air introduced into isolator B was collected by the air sampler at each sampling interval for subsequent infectivity virus quantification by $TCID_{50}$ (Figure 22B). For *in vivo* setting, chicks in isolator B were exposed to the introduced air for each exposure duration (Figure 22C). In all experiments, temperature and relative humidity were controlled within the ranges of 22 °C–27 °C and 62–98%, respectively.

**Evaluation of the efficacy of gaseous $ClO_2$ against aerosol H5 HPAIV**

Viruses from various air mixture conditions were collected using a gelatin membrane filter from the air sampler located in isolator B at a sampling velocity of 20 L/min. The filter was dissolved in 10 mL of a transport medium containing MEM (Shimadzu Diagnostics Corporation) containing 10 mg/mL streptomycin (Meiji Seika Pharma), 0.3 mg/mL gentamicin (MSD), 10,000 U/mL penicillin G, 0.5% bovine serum albumin fraction V (Roche), and 250 U/mL nystatin (Sigma-Aldrich). Then, the infectivity of the virus collected on the filter in MDCK cells under each experimental condition was expressed as $TCID_{50}$/mL. The effectiveness of gaseous $ClO_2$ against H5 HPAIV was evaluated by quantifying viral inactivation using the $TCID_{50}$ method. Experiments were conducted independently in five rounds, primarily on different days, and viral inactivation was expressed as a $\log_{10}$ reduction, calculated as the difference

between the virus titer in the absence of gaseous $ClO_2$ (0 ppmv) and the titer after exposure to gaseous $ClO_2$ at a specified concentration for a specified time.

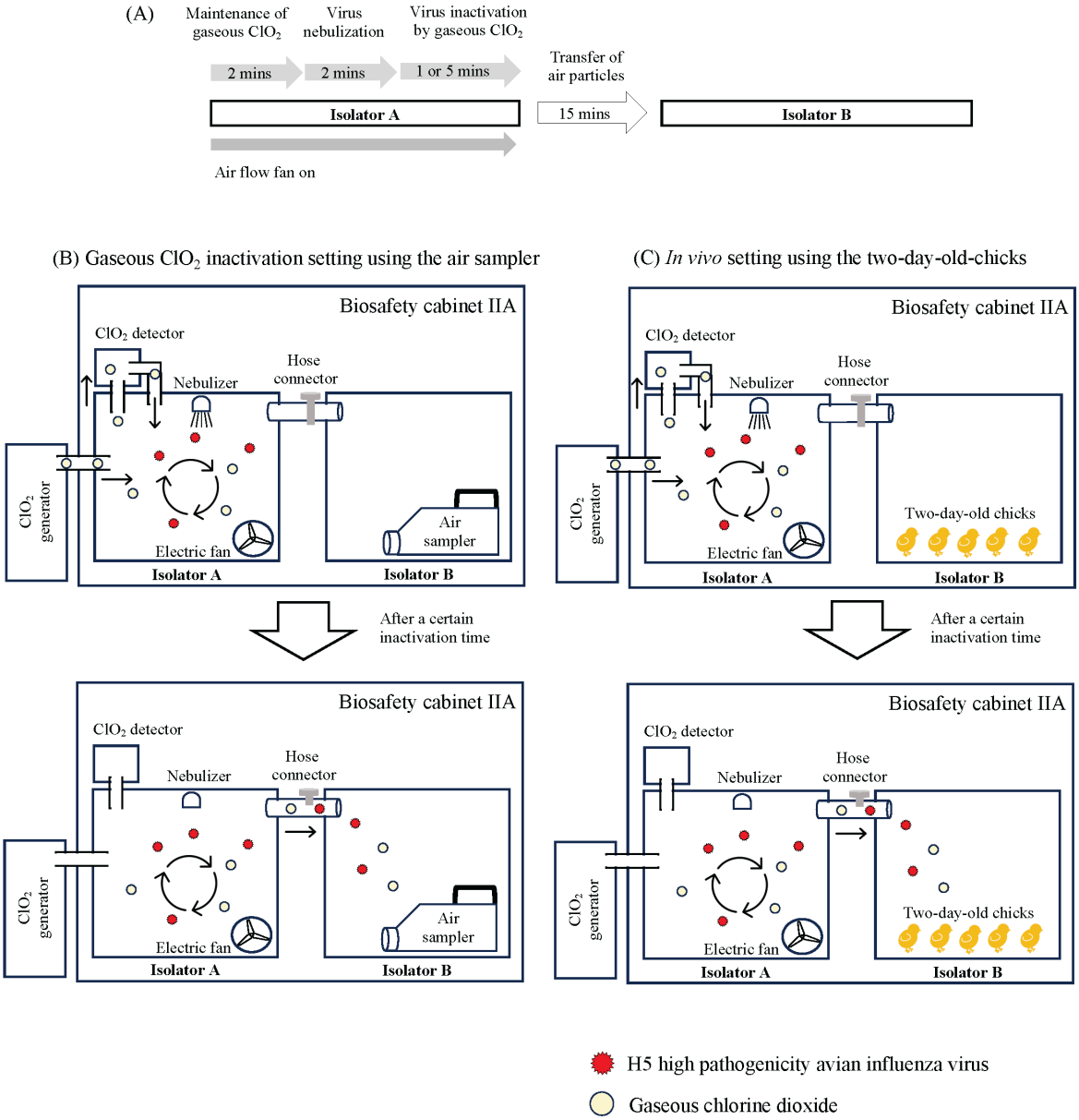


**Figure 22. Experimental setup for evaluating gaseous $ClO_2$ inactivation of aerosolized H5 HPAIV.** **(A)** Workflow of the experiment setup for inactivating aerosolized H5 HPAIV using gaseous $ClO_2$. **(B–C)** The experimental setup used to evaluate the effectiveness of gaseous $ClO_2$ under aerosolized H5 HPAIV conditions **(B)** and *in vivo* **(C)**.

**Evaluation of the sensitivity of chicks to H5 HPAIV**

The sensitivity of chicks to H5 HPAIV was evaluated using the $CLD_{50}$. Two-day-old white leghorn chicks were purchased from Iwamura Poultry (Niigata, Japan), randomly assigned into five groups (five chicks per group), and intranasally inoculated with 30 μL of WTE/Hok/R22/22 (H5N1). The infectious dosage ranged from $10^{0.0}$ to $10^{5.0}$ $TCID_{50}$, and the mortality rate of the chicks was monitored for 14 dpc.

**Evaluation of the efficacy of gaseous $ClO_2$ against H5 HPAIV in 2-day-old chicks**

Five 2-day-old white leghorn chicks purchased from Iwamura Poultry were placed in isolator B and exposed to the air mixture from each experimental condition. After disconnecting all tubes from isolator B, the clinical condition of the chicks was monitored daily for 14 dpc.

**Antibody detection in the chicks 14 days after virus nebulization**

Serum was extracted from the blood of chicks that survived 14 dpc and subjected to an HI assay to determine the antibody titer against WTE/Hok/R22/22 (H5N1). The virus was mixed with serial dilutions of serum from each surviving chick and incubated for 30 min at 37 °C, followed by the addition of 0.5% chicken erythrocytes, which were mixed for 30 min at room temperature. The HI antibody titers were expressed as the lowest concentrations of antibodies capable of completely inhibiting four HA units of the virus.

**Ethic statements**

All animal experiments were conducted at the Animal BSL-3 Facility, Faculty of Veterinary Medicine, Hokkaido University, which has been accredited by the AAALAC International since 2007. The Institutional Animal Care and Use Committee of the Faculty of Veterinary Medicine, Hokkaido University approved the experiments (approval number: 23-0121). Additionally, the study was approved by the Biosafety Management Committee on Pathogens and Other Hazardous Agents at the Faculty of Veterinary Medicine, Hokkaido University (approval no. 2022-1-78).

## Results

### Efficacy of gaseous $ClO_2$ against aerosol H5 HPAIV

In isolator A, gaseous $ClO_2$ or air produced by the gaseous $ClO_2$ generator was allowed to mix evenly with aerosolized H5 HPAIV generated by the nebulizer at an infectious dose of $10^{8.0}$ $TCID_{50}$/mL, a significantly higher virus titer than typically used in experimental conditions, as described in Table 19. To facilitate virus nebulization, the original viral stock was diluted 10-fold with sterilized distilled water, as the allantoic fluid-derived stocks contain abundant proteins that could hinder the nebulizing process. In the absence of gaseous $ClO_2$, the virus particles collected by the air sampler placed in isolator B exhibited virus recovery with mean titers of 2.8 ± 0.3 and 3.3 ± 0.9 $log_{10}$ $TCID_{50}$/mL after 0 and 5 min of inactivation, respectively. For this reason, the 5 min inactivation period, which yielded the lowest dispersion of infectious virus particles, was considered suitable for assessing the effectiveness of gaseous $ClO_2$ against H5 HPAIV at an infectious dose of $10^{8.0}$ $TCID_{50}$/mL. To evaluate the inactivation efficacy of gaseous $ClO_2$, virus aerosols were mixed with gaseous $ClO_2$ at a concentration of 0.100 ppmv for an inactivation time of 5 min. No infectious viruses were recovered by the air sampler, demonstrating the inactivation efficacy of gaseous $ClO_2$ against H5 HPAIV.

### Minimum conditions required for the efficacy of gaseous $ClO_2$ against aerosol H5 HPAIV

The minimum conditions required for gaseous $ClO_2$ to be effective against H5 HPAIV were evaluated using the same experimental setup. Different concentrations of gaseous $ClO_2$ (0.010, 0.025, 0.050, and 0.100 ppmv) and two inactivation times (1 and 5 min) were tested. Under different gas concentration settings, the measured concentration of gaseous $ClO_2$ was 0.013 ± 0.005, 0.027 ± 0.006, 0.052 ± 0.003, and 0.104 ± 0.005 ppmv. Variances in virus recovery titers observed under identical experimental conditions could be attributed to the evaluation of gaseous $ClO_2$ inactivation setting being conducted on different days (rounds). Nevertheless, the overall $log_{10}$ reduction observed under each round was consistent across all outcomes. To address this variability, all subsequent results are presented as individual values from three or more independent replicate experiments rather than as mean titers. In the absence of gaseous $ClO_2$, virus titers of 2.7,

4.5, and 4.5 $\log_{10}$ $TCID_{50}$/mL were recovered after 1 min inactivation, while titers of 3.3, 2.5, 2.7, and 4.5 $\log_{10}$ $TCID_{50}$/mL were recovered after 5 min inactivation, using the air sampler at an infectious dose of $10^{8.0}$ $TCID_{50}$/mL (Table 20). In contrast, when viruses were exposed to 0.100 ppmv of gaseous $ClO_2$, a marked decrease in virus recovery was observed, with only < 0.5, 1.0, and 1.5 $\log_{10}$ $TCID_{50}$/mL (2.2–3.5 $\log_{10}$ reduction) of infectious particles recovered after 1 min inactivation, and < 0.5 $\log_{10}$ $TCID_{50}$/mL (2.0–2.8 $\log_{10}$ reduction) after 5 min inactivation. As the concentration of gaseous $ClO_2$ decreased, titers of virus recovery increased accordingly. At 0.050 ppmv, virus titers of < 0.5, 2.0, and 2.0 $\log_{10}$ $TCID_{50}$/mL (2.2–2.5 $\log_{10}$ reduction) and < 0.5, < 0.5, and 1.5 $\log_{10}$ $TCID_{50}$/mL (2.0–3.0 $\log_{10}$ reduction) were confirmed after 1 and 5 min inactivation, respectively. Further reductions in gaseous $ClO_2$ levels resulted in increased titers of viral recovery. At 0.025 ppmv, viruses with titers of < 0.5, 3.5, and 2.5 $\log_{10}$ $TCID_{50}$/mL (1.0–2.2 $\log_{10}$ reduction), as well as < 0.5, < 0.5, and 2.3 $\log_{10}$ $TCID_{50}$/mL (2.0–2.2 $\log_{10}$ reduction), were recovered after 1 and 5 min inactivation, respectively. Similarly, at 0.010 ppmv, viruses with titers of < 0.5, 3.5, and 3.3 $\log_{10}$ $TCID_{50}$/mL (1.0–2.2 $\log_{10}$ reduction) after 1 min inactivation and < 0.5, 2.5, and 2.5 $\log_{10}$ $TCID_{50}$/mL (2.0–2.2 $\log_{10}$ reduction) after 5 min inactivation were recovered, respectively.

**Infectivity of WTE/Hok/R22/22 (H5N1) in chicks**

To estimate the $CLD_{50}$ of WTE/Hok/R22/22 (H5N1) in chicks, various doses of the virus were intranasally inoculated into 2-day-old chicks, which were then monitored for 14 days (Table 21). Chicks challenged intranasally with the virus at $10^{4.0}$ and $10^{5.0}$ $TCID_{50}$/0.03 mL died within 2 dpc (Table 21). Meanwhile, four of five chicks died within 3 dpc when challenged intranasally with $10^{2.0}$ or $10^{3.0}$ $TCID_{50}$/0.03 mL. The remaining chicks challenged with $10^{0.0}$–$10^{1.0}$ $TCID_{50}$/0.03 mL survived for 14 dpc. Based on these observations, the $CLD_{50}$ of the chicks to H5 HPAIV was estimated to be $10^{2.5}$ $TCID_{50}$.

**Table 19. Infectious virus recovered by the air sampler after treatment with gaseous $ClO_2$**

| Input dose ($log_{10}$ $TCID_{50}$/mL) | $ClO_2$ (ppmv) | Inactivation time (min) | Sampling time (min) | Recovery dose ($log_{10}$ $TCID_{50}$/mL) | Temperature (°C) | Relative humidity (%) |
|---|---|---|---|---|---|---|
| 8.0 | 0 | 0 | 10 | 2.8 ± 0.3 | 23.4 ± 2.6 | 64.3 ± 8.9 |
| 8.0 | 0 | 5 | 10 | 3.3 ± 0.9 | 25.2 ± 1.9 | 81.6 ± 5.9 |
| 8.0 | 0.100 | 5 | 10 | < 0.5 ± 0.0[1] | 26.1 ± 2.2 | 77.9 ± 4.5 |

[1]< 0.5 $log_{10}$ $TCID_{50}$/mL is the lowest detection limit of the virus titers.

**Table 20. Assessment of minimum conditions for the efficacy of gaseous $ClO_2$ against H5 HPAIV**

| Input dose ($log_{10}$ $TCID_{50}$/mL) | $ClO_2$ (ppmv) | Inactivation time (min) | Sampling time (min) | Recovery dose in each round ($log_{10}$ $TCID_{50}$/mL) | | | | | $Log_{10}$ reduction from no gaseous $ClO_2$ in each round ($Log_{10}$ $TCID_{50}$/mL) | | | | | Temperature (°C) | Relative humidity (%) |
|---|---|---|---|---|---|---|---|---|---|---|---|---|---|---|---|
| | | | | 1[1] | 2 | 3 | 4[2] | 5 | 1 | 2 | 3 | 4 | 5 | | |
| 8.0 | 0 | 1 | 10 | NT[3] | NT | 2.7 | 4.5 | 4.5 | NA[4] | NA | NA | NA | NA | 24.8 ± 1.9 | 70.7 ± 4.9 |
| 8.0 | 0 | 5 | 10 | 3.3 | 2.5 | 2.7 | 4.5 | -[5] | NA | NA | NA | NA | NA | 25.2 ± 1.9 | 81.6 ± 5.9 |
| 8.0 | 0.010 | 1 | 10 | NT | NT | < 0.5[6] | 3.5 | 3.3 | NT | NT | > 2.2 | 1.0 | 1.2 | 26.4 ± 0.6 | 67.8 ± 3.0 |
| 8.0 | 0.010 | 5 | 10 | NT | NT | < 0.5 | 2.5 | 2.5 | NT | NT | > 2.2 | 2.0 | 2.0 | 26.8 ± 0.9 | 67.3 ± 9.0 |
| 8.0 | 0.025 | 1 | 10 | NT | NT | < 0.5 | 3.5 | 2.5 | NT | NT | > 2.2 | 1.0 | 2.0 | 26.5 ± 0.6 | 62.4 ± 6.8 |
| 8.0 | 0.025 | 5 | 10 | NT | < 0.5 | < 0.5 | 2.3 | - | NT | > 2.0 | > 2.2 | 2.2 | - | 26.8 ± 0.9 | 63.7 ± 11.7 |
| 8.0 | 0.050 | 1 | 10 | NT | NT | < 0.5 | 2.0 | 2.0 | NT | NT | > 2.2 | 2.5 | 2.5 | 26.9 ± 0.2 | 63.9 ± 4.9 |
| 8.0 | 0.050 | 5 | 10 | NT | < 0.5 | < 0.5 | 1.5 | - | NT | > 2.0 | > 2.2 | 3.0 | - | 26.2 ± 1.2 | 72.4 ± 5.8 |
| 8.0 | 0.100 | 1 | 10 | NT | NT | < 0.5 | 1.0 | 1.5 | NT | NT | > 2.2 | 3.5 | 3.0 | 26.1 ± 0.9 | 64.0 ± 6.5 |
| 8.0 | 0.100 | 5 | 10 | < 0.5 | < 0.5 | < 0.5 | NT | NT | > 2.8 | > 2.0 | > 2.2 | NT | NT | 26.1 ± 2.2 | 77.9 ± 4.5 |

[1]Number indicates the order of independent rounds.
[2]Rounds 4 and 5 were performed on the same day.
[3]NT: Not tested.
[4]NA: Not applicable.
[5]-: Indicates that virus titers in Round 4 applied to Round 5, as both rounds were conducted under identical conditions on the same day.
[6]< 0.5 $log_{10}$ $TCID_{50}$/mL is the lowest detection limit of the virus titers.

**Table 21. Determination of the $CLD_{50}$ by intranasally challenged with WTE/Hok/R22/22 (H5N1) in two-day-old chicks (n = 5)**

| Infectious dose ($log_{10}$ $TCID_{50}$) | Number of surviving chicks |
|---|---|
| 0.0 | 5 |
| 1.0 | 5 |
| 2.0 | 1 |
| 3.0 | 1 |
| 4.0 | 0 |
| 5.0 | 0 |

**Minimum conditions for the efficacy of gaseous $ClO_2$ against H5 HPAIV *in vivo***

To determine the minimum conditions for the efficacy of gaseous $ClO_2$ against H5 HPAI *in vivo* setting, the same experimental setup was used to evaluate its inactivation efficacy. The measured concentrations of gaseous $ClO_2$ under these conditions were 0.012 ± 0.002, 0.027 ± 0.003, 0.054 ± 0.003, and 0.104 ± 0.003 ppmv. All chicks died when exposed to aerosolized H5 HPAIV at $10^{8.0}$ $TCID_{50}$/mL in the absence of gaseous $ClO_2$ (Table 4). However, all chicks survived exposure to aerosolized H5 HPAIV that had been treated with 0.100 ppmv gaseous $ClO_2$ for 1 or 5 min, consistent with the results observed in the gaseous $ClO_2$ inactivation setting. Nevertheless, different outcomes emerged when the gaseous $ClO_2$ concentration was reduced to 0.050, 0.025, or 0.010 ppmv. Gaseous $ClO_2$ at 0.050 ppmv protected most chicks against aerosolized H5 HPAIV, with four of five chicks surviving after 5 min of inactivation, whereas only one chick survived when the inactivation time was 1 min. Conversely, only one and two chicks survived when the inactivation time was 5 min for $ClO_2$ concentrations of 0.025 and 0.010 ppmv, respectively, whereas no chicks survived when the inactivation time was 1 min. No antibody against H5 HPAIV was detected in the surviving chicks by the HI test after 14 dpc. Thus, the minimum concentration (0.050 ppmv) of gaseous $ClO_2$ at an inactivation time of 5 min can quickly protect against H5 HPAIV infection in chicks.

**Table 22. Assessment of minimum conditions for the efficacy of gaseous $ClO_2$ against H5 HPAIV *in vivo* setting**

| Input dose ($log_{10}$ $TCID_{50}$/mL) | $ClO_2$ (ppmv) | Inactivation time (min) | Sampling time (min) | Number of surviving chicks (n = 5) | HI[1] titer | Temperature (°C) | Relative humidity (%) |
|---|---|---|---|---|---|---|---|
| 8.0 | 0 | 1 | 10 | 0 | NA[2] | 23.7 ± 0.0 | 73.8 ± 2.6 |
| 8.0 | 0 | 5 | 10 | 0 | NA | 23.8 ± 0.1 | 86.1 ± 3.5 |
| 8.0 | 0.010 | 1 | 10 | 0 | NA | 23.7 ± 0.1 | 85.6 ± 1.1 |
| 8.0 | 0.010 | 5 | 10 | 2 | < 2[3] | 25.8 ± 0.1 | 98.1 ± 0.8 |
| 8.0 | 0.025 | 1 | 10 | 0 | NA | 24.9 ± 0.1 | 84.2 ± 1.5 |
| 8.0 | 0.025 | 5 | 10 | 1 | < 2 | 24.0 ± 0.0 | 90.8 ± 3.0 |
| 8.0 | 0.050 | 1 | 10 | 1 | < 2 | 25.6 ± 0.0 | 82.0 ± 1.6 |
| 8.0 | 0.050 | 5 | 10 | 4 | < 2 | 24.4 ± 0.0 | 89.8 ± 3.9 |
| 8.0 | 0.100 | 1 | 10 | 5 | < 2 | 23.4 ± 0.0 | 78.6 ± 2.1 |
| 8.0 | 0.100 | 5 | 10 | 5 | < 2 | 22.8 ± 0.2 | 87.7 ± 4.5 |

[1]Antiserum was collected from surviving chicks 14 dpc to detect the presence of antibodies against H5 HPAIV.
[2]NA: Not applicable.
[3]Average hemagglutination inhibition (HI) titer collected from the surviving chicks.

## Discussion

Biosecurity measures remain a top priority for preventing avian influenza outbreaks in the poultry industry. However, even with intensive implementation of these measures, HPAI outbreaks can still occur in poultry. Therefore, effective and safe disinfectants represent additional options to halt the spread of pathogens because of their ability to decontaminate poultry farms, markets, and the surrounding environment, including surfaces and air, thereby supplementing biosecurity efforts. This study demonstrated that gaseous $ClO_2$ at 0.100 ppmv can inactivate aerosolized H5 HPAIV within 1 to 5 minutes, achieving approximately 2.0–3.5 $\log_{10}$ reduction. Notably, a lower concentration of gaseous $ClO_2$ (0.010 ppmv) with 5 min inactivation can also effectively inactivate aerosolized H5 HPAIV, achieving 2.0–2.2 $\log_{10}$ reduction, in contrast to studies evaluating the effects of gaseous $ClO_2$ on various IAV strains. Numerous studies highlighted the effectiveness of gaseous $ClO_2$ in suppressing multiple IAV strains, such as H1N1, achieving approximately 0.77 and 1.43 $\log_{10}$ reductions at concentrations of 0.02 and 0.1 ppmv, respectively, over 10 min [133]. Additionally, significant effects were noted against H7N9 at gaseous $ClO_2$ concentrations exceeding 5.0 ppmv for 1 h of exposure [138]. The difference in the effectiveness of gaseous $ClO_2$ against IAVs might be attributed to experimental settings, such as humidity, the presence of organic matter, and temperature, which must be considered. In the current *in vivo* study, chicks, known to be the most sensitive animals to H5 HPAIV, were used as an animal model to assess the efficacy of gaseous $ClO_2$ against H5 HPAIV. According to the survival of chicks challenged with different dosages of the virus, the $CLD_{50}$ was calculated as $10^{2.5}$ $TCID_{50}$, as shown in Table 21. In comparison, the $CLD_{50}$ of a viral strain genetically similar to WTE/Hok/R22/22 (H5N1) was estimated to be approximately $10^{4.5}$ $EID_{50}$ in 6-week-old chickens [21], indicating that younger chicks are more susceptible than older birds.

This study found that gaseous $ClO_2$ at 0.100 ppmv, whether used for 1 or 5 min, can completely protect chicks against aerosolized H5 HPAIV infection. In the meantime, the minimum effective concentration of gaseous $ClO_2$ against aerosolized H5 HPAIV was 0.050 ppmv for 5 min of inactivation, as most chicks survived exposure to viruses treated with this concentration of gaseous $ClO_2$ for 5 min. Conversely, chicks exposed to H5 HPAIV without gaseous $ClO_2$ treatment succumbed to viral infection, as demonstrated in

Table 22. The clear distinction in chick mortality between the presence and absence of gaseous $ClO_2$ highlights its high efficacy in inactivating H5 HPAIV in the atmosphere. This finding aligns with the virus recovery results observed in the gaseous $ClO_2$ inactivation setting, as lower amounts of virus were detected in the air sample after exposure to 0.100 or 0.050 ppmv $ClO_2$ for 5 min, as shown in Table 20. In addition to *in vivo* results, such as chick mortality rates that closely matched the virus reduction observed in the gaseous $ClO_2$ inactivation efficacy, chick mortality increased as the concentration of gaseous $ClO_2$ decreased. Based on the inactivation efficacy of gaseous $ClO_2$, the virus recovery at 0.100 ppmv (1 and 5 min) and 0.050 ppmv (5 min) ranged < 0.5–1.5 $\log_{10}$ $TCID_{50}$/mL, remaining insufficient to infect the chicks since the $CLD_{50}$ is approximately 2.5 $\log_{10}$ $TCID_{50}$. However, as the concentration of gaseous $ClO_2$ declined, chick mortality increased, as observed at 0.050 ppmv (1 min) and 0.010–0.025 ppmv (1 and 5 min), where the virus recovery in the gaseous $ClO_2$ inactivation setting ranged from < 0.5–3.5 $\log_{10}$ $TCID_{50}$/mL. Although some discrepancies were noted between the inactivation efficacy of gaseous $ClO_2$ and *in vivo* results, these are likely due to host-related and experimental factors. *In vivo*, variability in host susceptibility can lead to different mortality outcomes even within the same species. In addition, differences in sensitivity between the cell culture system used for viral quantification and *in vivo* settings may also have contributed to the varying susceptibility observed. For example, a study by Al-Dalawi et al reported that AIV replicates more efficiently *in ovo* setting than *in vitro* setting [142], indicating that different infection models can exhibit different sensitivities and may therefore yield results that do not fully align with *in vitro* findings. Conversely, the gaseous $ClO_2$ inactivation setting used in the present study may have facilitated more effective interactions between gaseous $ClO_2$ and viral particles, potentially due to better mixing during the vacuuming process via air sampling in isolator B. In contrast, *in vivo* setup exposed chicks only to the mixed air delivered from isolator A, which may have reduced the efficiency of viral inactivation. Nonetheless, despite these differences between experimental models, the overall trends observed in both settings were consistent with the conclusions of the study.

In prior research, viral concentrations in the air of $10^{4.3}$–$10^{6.4}$ RNA copies/$m^3$ were detected during an H5N8 HPAI outbreak on a poultry farm [143]. Given that exposure to $10^{3.8}$–$10^{4.7}$ $EID_{50}$ H5 HPAIVs is sufficient to cause death in chickens [35], 2.7 $\log_{10}$

reduction ($10^{6.4}$ to approximately $10^{3.7}$ RNA copies/$m^3$) in the infectivity of H5 HPAIV in the atmosphere is necessary to protect birds from HPAI on farms. 3.0 $\log_{10}$ reduction was obtained based on virus titers above the detection limit (1.5 $\log_{10}$ $TCID_{50}$/mL) following exposure to 0.100 ppmv gaseous $ClO_2$ for 1 min, as shown in Table 20. Therefore, this can be achieved using gaseous $ClO_2$ at 0.100 ppmv for 1 min. However, this estimate should be interpreted with caution, as it assumes a direct relationship between RNA copies and infectious particles and it does not consider host inhalation patterns or viral deposition in the respiratory system. Regardless, it offers a helpful benchmark for assessing the effectiveness of disinfection methods. When comparing the antimicrobial efficacy of various air disinfectants, gaseous $ClO_2$ also exhibited antimicrobial activity against SARS-CoV-2 in the atmosphere, achieving a 100-fold reduction within 10 min at 1.0 ppmv [133]. Similar levels of infectivity reduction were observed in SARS-CoV-2 following treatment with ozone at 1.0 ppmv (2 mg/$m^3$) over the same timeframe [133]. Moreover, the infectivity of aerosolized IAV was reduced by 4-fold after exposure to 1.70 ppmv ozone at 76% relative humidity for 80 min. However, a major drawback of ozone as an air disinfectant is that its effective concentration exceeds the threshold limit (0.100 ppmv), necessitating decontamination in leak-proof rooms or the absence of humans for 80 min during its use [144]. Contrarily, the gaseous $ClO_2$ concentrations (0.100 ppmv) assessed in this study met the permissible exposure limits for public health set by the Occupational Safety and Health Administration of the United States Department of Labor (Occupational Safety and Health Administration, 1978). Furthermore, this study found that gaseous $ClO_2$ was effective against viruses even at concentrations as low as 0.010 ppmv, indicating that such low and safe levels are ideal for public areas.

The efficacy of gaseous $ClO_2$ in inactivating aerosolized H5 HPAIV aerosol was demonstrated in this study, providing an additional option for disinfecting aerosolized H5 HPAIV in the atmosphere and reducing viral contamination in the farm environment, thereby preventing HPAI outbreaks. In addition, the safety of gaseous $ClO_2$ at 0.100 ppmv was demonstrated by the survival of chicks for 14 days with no clinical symptoms after 15 min of exposure in the same isolator (data not shown). The lack of adverse effects observed in 2-day-old chicks, which are likely more sensitive to chemical toxicity than adult birds, suggests that both chicks and chickens can generally tolerate 0.100 ppmv

gaseous $ClO_2$. Because 0.100 ppmv gaseous $ClO_2$ is also recognized as an acceptable level for humans, applying gaseous $ClO_2$ at this concentration to activate H5 HPAIVs in environments in which humans are present or chickens live, such as inside chicken farm barns, is a viable strategy. Some studies revealed the possibility of windborne transmission of HPAIV between commercial poultry outbreaks, and the tunnel ventilation system might have played a role in amplifying the infection risk [121, 146]. Outside open-type chicken farms, the airflow within farms is well-controlled by ventilation systems, which introduce outside air through ventilation ducts. In such farms, spraying gaseous $ClO_2$ in front of the duct effectively reduces the risk of potential HPAIV invasion. Although constant spraying is required, the very short time needed for gaseous $ClO_2$ to inactivate viruses might not necessitate spraying it throughout the entire atmosphere of the farm; instead, spraying $ClO_2$ at the duct should be sufficient. Positive data on H5 HPAIV inactivation by gaseous $ClO_2$ under experimental conditions should be further applied to field settings, including poultry farms.

This study had some limitations, as the efficacy of gaseous $ClO_2$ might be influenced by the presence of organic matter. Generally, the effect of humidity on virucidal gas is an important consideration for evaluating virucidal efficacy. Similar to other gases, the virucidal effect of gaseous $ClO_2$ can be affected by humidity, as humidity also includes organic matter. In the present study, as the aerosolized virus and gaseous $ClO_2$ were sprayed in an airtight small isolator, humidity was maintained mostly in the range of 62–98% during the inactivation of HPAIV. This humidity level is generally higher than that in environments in which humans and chickens comfortably reside, indicating that the virucidal effect observed in this study might be overestimated compared with its effectiveness under field conditions. Although humidity was not the focus of this study, future study should examine gaseous $ClO_2$ efficacy under conditions that better reflect field environments. Even at lower gaseous $ClO_2$ concentrations such as 0.010 ppmv, 1 min of inactivation resulted in a 1.0–2.2 $\log_{10}$ reduction, still implying partial inactivation, whereas 5 min of inactivation resulted in a 2.0–2.2 $\log_{10}$ reduction, indicating effective inactivation. Therefore, extending exposure time or improving mixing efficiency may further enhance efficacy under low-dose conditions and facilitate easier maintenance in large, open environments. However, the atmospheric temperature should also be considered as it could also impact the effectiveness of gaseous $ClO_2$ [147,

148]. The present study demonstrated the virucidal effect of gaseous $ClO_2$ against H5 HPAIV, which was confirmed for the first time, its efficacy in both gaseous $ClO_2$ inactivation setting and *in vivo* model, as summarized in Figure 23. The concentration of H5 HPAIV suppressed by gaseous $ClO_2$ in the experimental conditions was insufficient to infect 2-day-old chicks, providing the first indication that gaseous $ClO_2$ can protect chickens from HPAIV infection, and this strategy could be applied to enhance biosecurity measures in poultry. Future research should focus on testing gaseous $ClO_2$ in farms and homes to assess its practical use for improving sanitation and enhancing biosecurity.

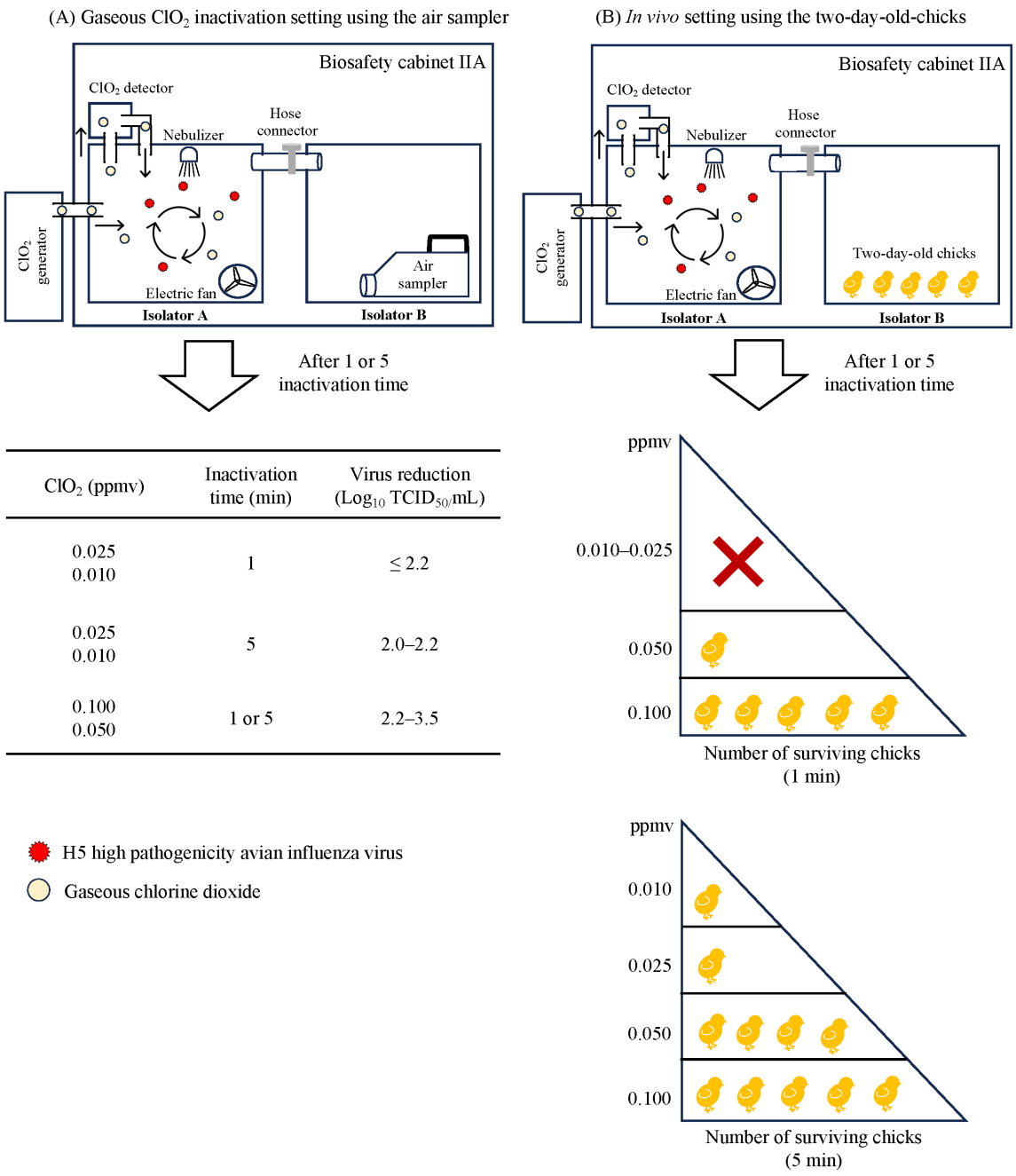


**Figure 23. Inactivation efficacy of gaseous $ClO_2$ against aerosolized H5 HPAIV**. Summary of the inactivation efficacy of gaseous $ClO_2$ in the gaseous $ClO_2$ exposure system **(A)** and *in vivo* model **(B)**.

## Brief summary

H5 HPAIV continues to spread globally, causing several HPAI outbreaks in poultry and significant economic losses. Biosecurity measures that prevent the introduction of HPAIV represent a top priority for controlling HPAI outbreaks on poultry farms. Although these measures are crucial for minimizing HPAI introduction, outbreaks of viral infection on poultry farms persist, underscoring the importance of continuously improving biosecurity protocols. Therefore, safe and effective microbicide disinfectants could play an essential role in reducing viral spread by inactivating viral particles on surfaces and in the air. This study assessed the efficacy of gaseous $ClO_2$ against H5 HPAIV under both gaseous $ClO_2$ inactivation setting and *in vivo* conditions. In the gaseous $ClO_2$ inactivation setting, only low virus titers were recovered (< 0.5–1.5 $\log_{10}$ $TCID_{50}$/mL) when H5 HPAIV aerosols were exposed to gaseous $ClO_2$ (0.050 ppmv, 0.14 $mg/m^3$) for 5 min, corresponding to an approximately 2.0–3.0 $\log_{10}$ reduction. Furthermore, *in vivo*, all chicks exposed to aerosolized H5 HPAIV, which were treated with 0.100 ppmv gaseous $ClO_2$, survived for 14 dpc, demonstrating complete protection against the virus. The minimum effective concentration of gaseous $ClO_2$ was 0.010 ppmv for 5 min of inactivation in the inactivation setting, and 0.050 ppmv for 5 min *in vivo*, indicating that relatively low concentrations are sufficient for effective viral inactivation. Therefore, gaseous $ClO_2$ was effective at inactivating aerosolized H5 HPAIV and has potential for use as a disinfectant to prevent HPAIV introduction into poultry.

## Conclusion

The spread of clade 2.3.4.4b H5N1 HPAIV from 2021 to 2025 is an unprecedented event, marked by ongoing circulation among wild birds and expansion into the Americas and Antarctica. H5 HPAIV has been introduced to Japan annually since late 2021, primarily driven by migratory birds, resulting in frequent spillovers into domestic poultry and, in some cases, into mammalian hosts. Thus, understanding the genetic, antigenic, pathogenic, and transmission patterns of these viruses, as described in Chapters I through III, is essential for developing effective control and mitigation strategies. During winters 2022–2024, multiple genetically distinct H5 HPAIVs were detected in Japan. Based on HA gene analyses, these viruses were classified into four subgroups: G2a, G2b, G2c, and G2d. Each subgroup was linked to different geographic origins, such as Europe, Northeast Asia, North Asia, and Northwest America. These findings indicate that Japan could serve as a hub for multiple independent viral introductions each winter. Despite the genetic diversity of the viruses, all subgroups retained high pathogenicity in chickens, as demonstrated by the experimentally infected birds dying within 5 dpc. Additionally, the differences in disease severity seen in broilers and layers suggest varying levels of host susceptibility. The characterization of viral antigenicity also revealed that the clade 2.3.4.4b viruses circulating in recent years remain antigenically similar to another and show limited divergence from strains identified over the past decade. This indicates minimal antigenic drift and low selective pressure on the HA surface glycoprotein.

Phylodynamic analyses offered key insights into the origins and host transmission routes of H5N1 HPAIVs in Japan from 2021 to 2025. Different geographic sources were identified for each subgroup. For instance, the G2c subgroup was mainly associated with Northeast Asia, while the G2b subgroup was introduced from both Northeast and North Asia. The G2d subgroup initially shared a common ancestor with viruses found in Northwest America and North Asia during 2021 to 2023. However, more recent detections were linked to Northeast Asia, showing a shift over time in the viral population. These findings highlight the constantly changing nature of global HPAIV transmission networks, which complicate outbreak preparedness. Interspecies transmission analyses revealed that waterfowl in the family Anatidae and possibly raptor species serve as key

spreaders of the virus within Japan. While poultry, crows, charadriiformes, and cranes typically act as terminal hosts, the roles of certain species shifted as viral incursions increased after 2021. For instance, crows, once thought to be dead-end hosts, later became intermediate transmitters capable of spreading the virus to other bird species. Substantial poultry and economic losses have resulted from the continuous spread of H5 HPAIV worldwide, and current control strategies rely on rapid culling, movement restrictions, biosecurity measures, and strict disinfection procedures. Among these measures, disinfection and biosecurity remain the most effective for limiting viral introduction through contaminated equipment, vehicles, or personnel. In Chapter IV, this study evaluated gaseous $ClO_2$, as a potential biosecurity tool. The results showed that gaseous $ClO_2$ effectively inactivated aerosolized H5 HPAIV under both gaseous $ClO_2$ inactivation setting and *in vivo* conditions, even at low concentrations. Although maintaining a stable concentration of gaseous $ClO_2$ in large environments can be challenging, targeted applications in ventilation systems or enclosed farm entry points may provide a practical means to reduce the risk of viral introduction into poultry facilities.

In summary, this thesis offers a detailed assessment of the epidemiology, evolution, and transmission dynamics of clade 2.3.4.4b H5 HPAIV, focusing on repeated introductions into Japan in recent years. The integration of molecular, pathogenic, and phylodynamic data highlights the importance of ongoing surveillance to track viral evolution, evaluate emerging risks, and enable timely interventions. The proven effectiveness of gaseous $ClO_2$ for inactivation also provides a valuable addition to existing biosecurity measures and emphasizes the need for innovative strategies to prevent viral incursions. Overall, the findings deepen understanding of the global ecology of H5 HPAIV and support future risk assessments, surveillance, and control efforts in Japan and other affected regions.

**Acknowledgements**

The completion of this Ph.D. thesis has been made possible through the support, collaboration, and patience of many remarkable individuals. I am deeply indebted to all who have guided, encouraged, and stood by me throughout this challenging yet rewarding journey.

First and foremost, I would like to express my profound gratitude to my principal supervisor, Professor Yoshihiro Sakoda, from the Laboratory of Microbiology, Department of Disease Control, Faculty of Veterinary Medicine, Hokkaido University. His steadfast support, inspiring leadership, and exceptional mentorship have shaped not only this work but also my growth as a researcher. His insightful guidance and boundless enthusiasm provided clarity and motivation at every stage of this journey. My sincere thanks go to my vice-supervisors, Associate Professor Norizaku Isoda (Laboratory of Microbiology, Department of Disease Control, Faculty of Veterinary Medicine, Hokkaido University) and Associate Professor Takahiro Hiono (One Health Research Center, Hokkaido University). Their expert advice, thoughtful discussions, and unwavering encouragement have been invaluable throughout the course of my studies. Their mentorship has greatly contributed to the scientific rigor and depth of this thesis.

I am also deeply thankful to my academic advisors, Professor Satoru Konnai (Laboratory of Infectious Diseases, Department of Disease Control, Faculty of Veterinary Medicine, Hokkaido University) and Professor Ayato Takada (Division for Global Epidemiology, International Institute for Zoonosis Control, Hokkaido University), for their constructive feedback, kind guidance, and continued support, which have significantly strengthened the quality of my research. My heartfelt appreciation extends to Dr. Takanori Miura (Department of Molecular Biochemistry and Clinical Investigation, Osaka University Graduate School of Medicine), and to Dr. Claire Guinat, Manon Couty, and Diletta Fornasiero (Hosts–Pathogens Interactions, University of Toulouse, National Research Institute for Agriculture, Food and Environment, and the National Veterinary School of Toulouse, France). Their collaboration, expertise, and generosity made our joint research both productive and inspiring.

I am deeply grateful to all members of the Laboratory of Microbiology, Department of Disease Control, Faculty of Veterinary Medicine, Hokkaido University, for their support and assistance in both research and daily life in Japan. I wish to particularly thank Dr. Huynh Tan Loc, my colleague Daiki Kobayashi, and my juniors Nguyen Bao Linh, Yo Shimazu, Gan Shiqi, Kazuki Nishikawa, Han Sehei, Tatsuru Morita, and Maya Kobayashi for their kindness, cooperation, and friendship, and lastly my special friend, Khanh Van Vo for the continuous support and care for this past two years. I also wish to express my sincere respect and remorse for the animals and cells used in this study. Their sacrifice has contributed to the advancement of scientific knowledge, and I honor them with deep gratitude.

Finally, to everyone who has supported, inspired, or encouraged me in any way during this journey, including mentors, collaborators, family, colleagues, and friends, please accept my deepest thanks. Your guidance and kindness have made this achievement possible. I remain forever grateful and wish each of you continued success and happiness in your future endeavors.

## References


1. Peter M. Howley, David M. Knipe, et al. 2021. Fields Virology: Emerging Viruses, 7th ed., Wolters Kluwer.
2. Fouchier, R. A. M., Munster, V., Wallensten, A., Bestebroer, T. M., Herfst, S., Smith, D., Rimmelzwaan, G. F., Olsen, B. and Osterhaus, A. D. M. E. 2005. Characterization of a novel influenza A virus hemagglutinin subtype (H16) obtained from black-headed gulls. *J Virol.* **79**: 2814–2822.
3. Tong, S., Li, Y., Rivailler, P., Conrardy, C., Castillo, D. A. A., Chen, L. M., Recuenco, S., Ellison, J. A., Davis, C. T., York, I. A., Turmelle, A. S., Moran, D., Rogers, S., Shi, M., Tao, Y., Weil, M. R., Tang, K., Rowe, L. A., Sammons, S., Xu, X., Frace, M., Lindblade, K. A., Cox, N. J., Anderson, L. J., Rupprecht, C. E. and Donis, R. O. 2012. A distinct lineage of influenza A virus from bats. *Proc Natl Acad Sci.* **109**: 4269–4274.
4. Fereidouni, S., Starick, E., Karamendin, K., Di Genova, C., Scott, S. D., Khan, Y., Harder, T. and Kydyrmanov, A. 2023. Genetic characterization of a new candidate hemagglutinin subtype of influenza A viruses. *Emerg Microbes Infect.* **12**: 2225645.
5. Govorkova, E. A., Baranovich, T., Seiler, P., Armstrong, J., Burnham, A., Guan, Y., Peiris, M., Webby, R. J. and Webster, R. G. 2013. Antiviral resistance among highly pathogenic influenza A (H5N1) viruses isolated worldwide in 2002–2012 shows need for continued monitoring. *Antiviral Res.* **98**: 297–304.
6. Alexander, D. J. 2007. An overview of the epidemiology of avian influenza. *Vaccine*. **25**: 5637–5644.
7. Dhingra, M. S., Artois, J., Dellicour, S., Lemey, P., Dauphin, G., von Dobschuetz, S., van Boeckel, T. P., Castellan, D. M., Morzaria, S. and Gilbert, M. 2018. Geographical and historical patterns in the emergences of novel highly pathogenic avian influenza (HPAI) H5 and H7 viruses in poultry. *Front Vet Sci.* **5**: 84.
8. Escalera-Zamudio, M., Golden, M., Gutiérrez, B., Thézé, J., Keown, J. R., Carrique, L., Bowden, T. A. and Pybus, O. G. 2020. Parallel evolution in the emergence of highly pathogenic avian influenza A viruses. *Nat Commun.* **11**: 5511.
9. The Global Consortium for H5N8 and Related Influenza Viruses 2016. Role for migratory wild birds in the global spread of avian influenza H5N8. *Science*. **354**: 213–217.

10. Li, K. S., Guan, Y., Wang, J., Smith, G. J. D., Xu, K. M., Duan, L., Rahardjo, A. P., Puthavathana, P., Buranathai, C., Nguyen, T. D., Estoepangestie, A. T. S., Chaisingh, A., Auewarakul, P., Long, H. T., Hanh, N. T. H., Webby, R. J., Poon, L. L. M., Chen, H., Shortridge, K. F., Yuen, K. Y., Webster, R. G. and Peiris, J. S. M. 2004. Genesis of a highly pathogenic and potentially pandemic H5N1 influenza virus in eastern Asia. *Nature*. **430**: 209–213.
11. Chen, H., Li, Y., Li, Z., Shi, J., Shinya, K., Deng, G., Qi, Q., Tian, G., Fan, S., Zhao, H., Sun, Y. and Kawaoka, Y. 2006. Properties and dissemination of H5N1 viruses isolated during an influenza outbreak in migratory waterfowl in western China. *J Virol*. **80**: 5976–5983.
12. Lycett, S. J., Pohlmann, A., Staubach, C., Caliendo, V., Woolhouse, M., Beer, M., Kuiken, T., Global Consortium for H5N8 and Related Influenza Viruses, Lycett, S. J., Pohlmann, A., Staubach, C., Caliendo, V., van Borm, S., Breed, A., Briand, F. X., Brown, I., Dán, Á., DeLiberto, T., von Dobschuetz, S., Fouchier, R., Gilbert, M., Hill, S., Hjulsager, C. K., Ip, H., Koopmans, M., Larsen, L. E., Lee, D. H., Naguib, M. M., Monne, I., Pybus, O., Ramey, A., Savic, V., Sharshov, K., Shestopalov, A., Song, C. S., Steensels, M., Swayne, D., Świętoń, E., Wan, X., Zohari, S., Woolhouse, M., Beer, M. and Kuiken, T. 2020. Genesis and spread of multiple reassortants during the 2016/2017 H5 avian influenza epidemic in Eurasia. *Proc Natl Acad Sci.* **117**: 20814–20825.
13. Fusaro, A., Zecchin, B., Vrancken, B., Abolnik, C., Ademun, R., Alassane, A., Arafa, A., Awuni, J. A., Couacy-Hymann, E., Coulibaly, M. B., Gaidet, N., Go-Maro, E., Joannis, T., Jumbo, S. D., Minoungou, G., Meseko, C., Souley, M. M., Ndumu, D. B., Shittu, I., Twabela, A., Wade, A., Wiersma, L., Akpeli, Y. P., Zamperin, G., Milani, A., Lemey, P. and Monne, I. 2019. Disentangling the role of Africa in the global spread of H5 highly pathogenic avian influenza. *Nat Commun.* **10**: 5310.
14. World Health Organization. 2021. Zoonotic influenza vaccine viruses and candidate vaccine viruses for pandemic preparedness. https://cdn.who.int/media/docs/default-source/influenza/who-influenza-recommendations/vcm-southern-hemisphere-recommendation-2022/202110_zoonotic_vaccinevirusupdate.pdf [accessed on: 24 March 2024].

15. Li, Y. T., Su, Y. C. F. and Smith, G. J. D. 2021. H5Nx viruses emerged during the suppression of H5N1 virus populations in poultry. *Microbiol Spectr.* **9**: e01309-21.
16. Pohlmann, A., King, J., Fusaro, A., Zecchin, B., Banyard, A. C., Brown, I. H., Byrne, A. M. P., Beerens, N., Liang, Y., Heutink, R., Harders, F., James, J., Reid, S. M., Hansen, R. D. E., Lewis, N. S., Hjulsager, C., Larsen, L. E., Zohari, S., Anderson, K., Bröjer, C., Nagy, A., Savič, V., van Borm, S., Steensels, M., Briand, F. X., Swieton, E., Smietanka, K., Grund, C., Beer, M. and Harder, T. 2022. Has epizootic become enzootic? Evidence for a fundamental change in the infection dynamics of highly pathogenic avian influenza in Europe, 2021. *mBio*. **13**: e00609-22.
17. European Food Safety Authority, European Centre for Disease Prevention, Control, European Union Reference Laboratory for Avian Influenza, Adlhoch, C., Fusaro, A., Gonzales, J. L., Kuiken, T., Marangon, S., Niqueux, É., Staubach, C., Terregino, C., Aznar, I., Muñoz Guajardo, I. and Baldinelli, F. 2021. Avian influenza overview September – December 2021. *EFSA J.* **19**.
18. European Food Safety Authority, European Centre for Disease Prevention and Control, European Union Reference Laboratory for Avian Influenza, Alexakis, L., Fusaro, A., Kuiken, T., Mirinavičiūtė, G., Ståhl, K., Staubach, C., Svartström, O., Terregino, C., Willgert, K., Delacourt, R., Goudjihounde, S. M., Grant, M., Tampach, S. and Kohnle, L. 2024. Avian influenza overview March–June 2024. *EFSA J.* **22**.
19. Abolnik, C., Phiri, T. P., van der Zel, G., Anthony, J., Daniell, N. and de Boni, L. 2022. Wild bird surveillance in the Gauteng province of South Africa during the high-risk period for highly pathogenic avian influenza virus introduction. *Viruses*. **14**: 2027.
20. Lo, F. T., Zecchin, B., Diallo, A. A., Racky, O., Tassoni, L., Diop, A., Diouf, M., Diouf, M., Samb, Y. N., Pastori, A., Gobbo, F., Ellero, F., Diop, M., Lo, M. M., Diouf, M. N., Fall, M., Ndiaye, A. A., Gaye, A. M., Badiane, M., Lo, M., Youm, B. N., Ndao, I., Niaga, M., Terregino, C., Diop, B., Ndiaye, Y., Angot, A., Seck, I., Niang, M., Soumare, B., Fusaro, A. and Monne, I. 2022. Intercontinental spread of Eurasian highly pathogenic avian influenza A (H5N1) to Senegal. *Emerg Infect Dis.* **28**: 234–237.

21. Isoda, N., Onuma, M., Hiono, T., Sobolev, I., Lim, H., Nabeshima, K., Honjyo, H., Yokoyama, M., Shestopalov, A. and Sakoda, Y. 2022. Detection of new H5N1 high pathogenicity avian influenza viruses in winter 2021–2022 in the Far East, which are genetically close to those in Europe. *Viruses*. **14**: 2168.
22. Zhang, X., Wu, J., Wang, Y., Hao, M., Liu, H., Fan, S., Li, J., Sun, J., He, Y., Zhang, Y. and Chen, J. 2024. Highly pathogenic avian influenza A virus in wild migratory birds, Qinghai Lake, China, 2022. *Emerg Infect Dis*. **30**: 2135–2139.
23. Sagong, M., Lee, Y., Song, S., Cha, R. M., Lee, E., Kang, Y., Cho, H., Kang, H., Lee, Y. and Lee, K. 2022. Emergence of clade 2.3.4.4b novel reassortant H5N1 high pathogenicity avian influenza virus in South Korea during late 2021. *Transbound Emerg Dis.* **69**: e3255–e3260.
24. Caliendo, V., Lewis, N. S., Pohlmann, A., Baillie, S. R., Banyard, A. C., Beer, M., Brown, I. H., Fouchier, R. A. M., Hansen, R. D. E., Lameris, T. K., Lang, A. S., Laurendeau, S., Lung, O., Robertson, G., van der Jeugd, H., Alkie, T. N., Thorup, K., van Toor, M. L., Waldenström, J., Yason, C., Kuiken, T. and Berhane, Y. 2022. Transatlantic spread of highly pathogenic avian influenza H5N1 by wild birds from Europe to North America in 2021. *Sci Rep.* **12**: 11729.
25. Alkie, T. N., Lopes, S., Hisanaga, T., Xu, W., Suderman, M., Koziuk, J., Fisher, M., Redford, T., Lung, O., Joseph, T., Himsworth, C. G., Brown, I. H., Bowes, V., Lewis, N. S. and Berhane, Y. 2022. A threat from both sides: Multiple introductions of genetically distinct H5 HPAI viruses into Canada via both East Asia-Australasia/Pacific and Atlantic flyways. *Virus Evol*. **8**: veac077.
26. Banyard, A. C., Bennison, A., Byrne, A. M. P., Reid, S. M., Lynton-Jenkins, J. G., Mollett, B., De Silva, D., Peers-Dent, J., Finlayson, K., Hall, R., Blockley, F., Blyth, M., Falchieri, M., Fowler, Z., Fitzcharles, E. M., Brown, I. H. and James, J. 2024. Detection and spread of high pathogenicity avian influenza virus H5N1 in the Antarctic Region. *Nat Commun.* **15**: 7433.
27. Kandeil, A., Patton, C., Jones, J. C., Jeevan, T., Harrington, W. N., Trifkovic, S., Seiler, J. P., Fabrizio, T., Woodard, K., Turner, J. C., Crumpton, J. C., Miller, L., Rubrum, A., de Beauchamp, J., Russell, C. J., Govorkova, E. A., Vogel, P., Kim-Torchetti, M., Berhane, Y., Stallknecht, D., Poulson, R., Kercher, L. and Webby, R.

J. 2023. Rapid evolution of A (H5N1) influenza viruses after intercontinental spread to North America. *Nat Commun.* **14**: 3082.

28. Ruiz-Saenz, J., Martinez-Gutierrez, M. and Pujol, F. H. 2023. Multiple introductions of highly pathogenic avian influenza H5N1 clade 2.3.4.4b into South America. *Travel Med Infect Dis.* **53**: 102591.
29. Yang, Q., Wang, B., Lemey, P., Dong, L., Mu, T., Wiebe, R. A., Guo, F., Trovão, N. S., Park, S. W., Lewis, N., Tsui, J. L. H., Bajaj, S., Cheng, Y., Yang, L., Haba, Y., Li, B., Zhang, G., Pybus, O. G., Tian, H. and Grenfell, B. 2024. Synchrony of bird migration with global dispersal of avian influenza reveals exposed bird orders. *Nat Commun.* **15**: 1126.
30. Moriguchi, S., Hosoda, R., Ushine, N., Kato, T. and Hayama, S. 2021. Surveillance system for avian influenza in wild birds and implications of its improvement with insights into the highly pathogenic avian influenza outbreaks in Japan. *Prev Vet Med.* **187**: 105234.
31. Nam, J. H., Españo, E., Song, E. J., Shim, S. M., Na, W., Jeong, S. H., Kim, J., Jang, J., Song, D. and Kim, J. K. 2021. Surveillance of avian influenza viruses from 2009 to 2013 in South Korea. *Sci Rep.* **11**: 23991.
32. Hill, N. J., Bishop, M. A., Trovão, N. S., Ineson, K. M., Schaefer, A. L., Puryear, W. B., Zhou, K., Foss, A. D., Clark, D. E., MacKenzie, K. G., Gass, J. D., Borkenhagen, L. K., Hall, J. S. and Runstadler, J. A. 2022. Ecological divergence of wild birds drives avian influenza spillover and global spread. *PLoS Pathog*. **18**: e1010062.
33. Harvey, J. A., Mullinax, J. M., Runge, M. C. and Prosser, D. J. 2023. The changing dynamics of highly pathogenic avian influenza H5N1: Next steps for management & science in North America. *Biol Conserv*. **282**: 110041.
34. Salaheldin, A. H., Elbestawy, A. R., Abdelkader, A. M., Sultan, H. A., Ibrahim, A. A., Abd El-Hamid, H. S. and Abdelwhab, E. M. 2022. Isolation of genetically diverse H5N8 avian influenza viruses in poultry in Egypt, 2019–2021. *Viruses*. **14**: 1431.
35. Takadate, Y., Tsunekuni, R., Kumagai, A., Mine, J., Kikutani, Y., Sakuma, S., Miyazawa, K. and Uchida, Y. 2023. Different infectivity and transmissibility of H5N8 and H5N1 high pathogenicity avian influenza viruses isolated from chickens in Japan in the 2021/2022 season. *Viruses*. **15**: 265.

36. WHO/OIE/FAO H5N1 Evolution Working Group 2008. Toward a unified nomenclature system for highly pathogenic avian influenza virus (H5N1). *Emerg Infect Dis.* **14**: e1.
37. Lycett, S. J., Duchatel, F. and Digard, P. 2019. A brief history of bird flu. *Philos Trans R Soc B Biol Sci.* **374**: 20180257.
38. Yang, J., Zhang, C., Yuan, Y., Sun, J., Lu, L., Sun, H., Sun, H., Chu, D., Qin, S., Chen, J., Zhang, C., Hao, X., Shi, W., Liu, W., Gao, G. F., Digard, P., Lycett, S. and Bi, Y. 2023. Novel avian influenza virus (H5N1) clade 2.3.4.4b reassortants in migratory birds, China. *Emerg Infect Dis.* **29**: 1244–1249.
39. Lee, S., Cho, A. Y., Kim, T., Ahn, S., Song, J. H., Lee, H., Choi, Y. J., Otgontogtokh, N., Kwon, J. H., Song, C. S. and Lee, D. H. 2023. Novel highly pathogenic avian influenza A (H5N1) clade 2.3.4.4b virus in wild birds, South Korea. *Emerg Infect Dis.* **29**: 1475–1478.
40. Soda, K., Tomioka, Y., Usui, T., Ozaki, H., Ito, H., Nagai, Y., Yamamoto, N., Okamatsu, M., Isoda, N., Kajihara, M., Sakoda, Y., Takada, A. and Ito, T. 2023. Susceptibility of common dabbling and diving duck species to clade 2.3.2.1 H5N1 high pathogenicity avian influenza virus: An experimental infection study. *J Vet Med Sci.* 23–0122.
41. Hiono, T., Kobayashi, D., Kobayashi, A., Suzuki, T., Satake, Y., Harada, R., Matsuno, K., Sashika, M., Ban, H., Kobayashi, M., Takaya, F., Fujita, H., Isoda, N., Kimura, T. and Sakoda, Y. 2023. Virological, pathological, and glycovirological investigations of an Ezo red fox and a tanuki naturally infected with H5N1 high pathogenicity avian influenza viruses in Hokkaido, Japan. *Virology*. **578**: 35–44.
42. Ministry of Environment, Japan. 2023. Information about highly pathogenic avian influenza. https://www.env.go.jp/nature/dobutsu/bird_flu/index.html [accessed on: 14 March 2024].
43. Yamamoto, N., Sakoda, Y., Motoshima, M., Yoshino, F., Soda, K., Okamatsu, M. and Kida, H. 2011. Characterization of a non-pathogenic H5N1 influenza virus isolated from a migratory duck flying from Siberia in Hokkaido, Japan, in October 2009. *Virol J.* **8**: 65.
44. Hebert, P. D. N., Stoeckle, M. Y., Zemlak, T. S. and Francis, C. M. 2004. Identification of birds through DNA barcodes. *PLoS Biol.* **2**: e312.

45. Kida, H. and Yanagawa, R. 1979. Isolation and characterization of influenza A viruses from wild free-flying ducks in Hokkaido, Japan. *Zentralblatt Bakteriol Parasitenkd Infekt Hyg Erste Abt Orig Reihe Med Mikrobiol Parasitol.* **244**: 135–143.
46. Kakogawa, M., Onuma, M., Saito, K., Watanabe, Y., Goka, K. and Asakawa, M. 2020. Epidemiologic survey of avian influenza virus infection in shorebirds captured in Hokkaido, Japan. *J Wildl Dis.* **56**: 651.
47. Hoffmann, E., Stech, J., Guan, Y., Webster, R. G. and Perez, D. R. 2001. Universal primer set for the full-length amplification of all influenza A viruses. *Arch Virol.* **146**: 2275–2289.
48. Ip, H. S., Uhm, S., Killian, M. L. and Torchetti, M. K. 2023. An evaluation of avian influenza virus whole-genome sequencing approaches using nanopore technology. *Microorganisms*. **11**: 529.
49. Tamura, K. and Nei, M. 1993. Estimation of the number of nucleotide substitutions in the control region of mitochondrial DNA in humans and chimpanzees. *Mol Biol Evol.* 512–526.
50. Kumar, S., Stecher, G. and Tamura, K. 2016. MEGA7: Molecular Evolutionary Genetics Analysis version 7.0 for bigger datasets. *Mol Biol Evol.* **33**: 1870–1874.
51. Isoda, N., Twabela, A. T., Bazarragchaa, E., Ogasawara, K., Hayashi, H., Wang, Z. J., Kobayashi, D., Watanabe, Y., Saito, K., Kida, H. and Sakoda, Y. 2020. Re-invasion of H5N8 high pathogenicity avian influenza virus clade 2.3.4.4b in Hokkaido, Japan, 2020. *Viruses.* **12**: 1439.
52. Kanehira, K., Uchida, Y., Takemae, N., Hikono, H., Tsunekuni, R. and Saito, T. 2015. Characterization of an H5N8 influenza A virus isolated from chickens during an outbreak of severe avian influenza in Japan in April 2014. *Arch Virol.* **160**: 1629–1643.
53. Hiono, T., Okamatsu, M., Matsuno, K., Haga, A., Iwata, R., Nguyen, L. T., Suzuki, M., Kikutani, Y., Kida, H., Onuma, M. and Sakoda, Y. 2017. Characterization of H5N6 highly pathogenic avian influenza viruses isolated from wild and captive birds in the winter season of 2016-2017 in northern Japan: Characterization of H5N6 HPAIVs in Japan. *Microbiol Immunol.* **61**: 387–397.

54. Twabela, A. T., Okamatsu, M., Tshilenge, G. M., Mpiana, S., Masumu, J., Nguyen, L. T., Matsuno, K., Monne, I., Zecchin, B. and Sakoda, Y. 2020. Molecular, antigenic, and pathogenic characterization of H5N8 highly pathogenic avian influenza viruses isolated in the Democratic Republic of Congo in 2017. *Arch Virol*. **165**: 87–96.
55. Isoda, N., Sakoda, Y., Kishida, N., Soda, K., Sakabe, S., Sakamoto, R., Imamura, T., Sakaguchi, M., Sasaki, T., Kokumai, N., Ohgitani, T., Saijo, K., Sawata, A., Hagiwara, J., Lin, Z. and Kida, H. 2008. Potency of an inactivated avian influenza vaccine prepared from a non-pathogenic H5N1 reassortant virus generated between isolates from migratory ducks in Asia. *Arch Virol*. **153**: 1685–1692.
56. Smith, D. J., Lapedes, A. S., de Jong, J. C., Bestebroer, T. M., Rimmelzwaan, G. F., Osterhaus, A. D. M. E. and Fouchier, R. A. M. 2004. Mapping the antigenic and genetic evolution of influenza virus. *Science*. **305**: 371–376.
57. Suttie, A., Deng, Y. M., Greenhill, A. R., Dussart, P., Horwood, P. F. and Karlsson, E. A. 2019. Inventory of molecular markers affecting biological characteristics of avian influenza A viruses. *Virus Genes*. **55**: 739–768.
58. Baek, Y. G., Lee, Y. N., Lee, D. H., Shin, J., Lee, J. H., Chung, D. H., Lee, E. K., Heo, G. B., Sagong, M., Kye, S. J., Lee, K. N., Lee, M. H. and Lee, Y. J. 2021. Multiple reassortants of H5N8 clade 2.3.4.4b highly pathogenic avian influenza viruses detected in South Korea during the winter of 2020–2021. *Viruses*. **13**: 490.
59. Okuya, K., Mine, J., Tokorozaki, K., Kojima, I., Esaki, M., Miyazawa, K., Tsunekuni, R., Sakuma, S., Kumagai, A., Takadate, Y., Kikutani, Y., Matsui, T., Uchida, Y. and Ozawa, M. 2022. Genetically diverse highly pathogenic avian influenza A (H5N1/H5N8) viruses among wild waterfowl and domestic poultry, Japan, 2021. *Emerg Infect Dis.* **28**: 1451–1455.
60. Smith, A. M. and McCullers, J. A. 2013. Molecular signatures of virulence in the PB1-F2 proteins of H5N1 influenza viruses. *Virus Res.* **178**: 146–150.
61. Gao, W., Zu, Z., Liu, J., Song, J., Wang, X., Wang, C., Liu, L., Tong, Q., Wang, M., Sun, H., Sun, Y., Liu, J., Chang, K. C. and Pu, J. 2019. Prevailing I292V PB2 mutation in avian influenza H9N2 virus increases viral polymerase function and attenuates IFN-β induction in human cells. *J Gen Virol.* **100**: 1273–1281.

62. DesRochers, B. L., Chen, R. E., Gounder, A. P., Pinto, A. K., Bricker, T., Linton, C. N., Rogers, C. D., Williams, G. D., Webby, R. J. and Boon, A. C. M. 2016. Residues in the PB2 and PA genes contribute to the pathogenicity of avian H7N3 influenza A virus in DBA/2 mice. *Virology*. **494**: 89–99.
63. Gabriel, G., Dauber, B., Wolff, T., Planz, O., Klenk, H. D. and Stech, J. 2005. The viral polymerase mediates adaptation of an avian influenza virus to a mammalian host. *Proc Natl Acad Sci.* **102**: 18590–18595.
64. Gao, Y., Zhang, Y., Shinya, K., Deng, G., Jiang, Y., Li, Z., Guan, Y., Tian, G., Li, Y., Shi, J., Liu, L., Zeng, X., Bu, Z., Xia, X., Kawaoka, Y. and Chen, H. 2009. Identification of amino acids in HA and PB2 critical for the transmission of H5N1 avian influenza viruses in a mammalian host. *PLoS Pathog.* **5**: e1000709.
65. Hulse-Post, D. J., Franks, J., Boyd, K., Salomon, R., Hoffmann, E., Yen, H. L., Webby, R. J., Walker, D., Nguyen, T. D. and Webster, R. G. 2007. Molecular changes in the polymerase genes (PA and PB1) associated with high pathogenicity of H5N1 influenza virus in mallard ducks. *J Virol.* **81**: 8515–8524.
66. Tada, T., Suzuki, K., Sakurai, Y., Kubo, M., Okada, H., Itoh, T. and Tsukamoto, K. 2011. NP body domain and PB2 contribute to increased virulence of H5N1 highly pathogenic avian influenza viruses in chickens. *J Virol.* **85**: 1834–1846.
67. Dugan, V. G., Chen, R., Spiro, D. J., Sengamalay, N., Zaborsky, J., Ghedin, E., Nolting, J., Swayne, D. E., Runstadler, J. A., Happ, G. M., Senne, D. A., Wang, R., Slemons, R. D., Holmes, E. C. and Taubenberger, J. K. 2008. The evolutionary genetics and emergence of avian influenza viruses in wild birds. *PLoS Pathog.* **4**: e1000076.
68. Gobbo, F., Zanardello, C., Bottinelli, M., Budai, J., Bruno, F., de Nardi, R., Patregnani, T., Catania, S. and Terregino, C. 2022. Silent infection of highly pathogenic avian influenza virus (H5N1) clade 2.3.4.4b in a commercial chicken broiler flock in Italy. *Viruses*. **14**: 1600.
69. Perlas, A., Argilaguet, J., Bertran, K., Sánchez-González, R., Nofrarías, M., Valle, R., Ramis, A., Cortey, M. and Majó, N. 2021. Dual host and pathogen RNA-Seq analysis unravels chicken genes potentially involved in resistance to highly pathogenic avian influenza virus infection. *Front Immunol*. **12**: 800188.

70. Agüero, M., Monne, I., Sánchez, A., Zecchin, B., Fusaro, A., Ruano, M. J., Arrojo, M. del V., Fernández-Antonio, R., Souto, A. M., Tordable, P., Cañás, J., Bonfante, F., Giussani, E., Terregino, C. and Orejas, J. J. 2023. Highly pathogenic avian influenza A (H5N1) virus infection in farmed minks, Spain, October 2022. *Eurosurveillance*. **28**: 2300001.
71. de Vries, E., Guo, H., Dai, M., Rottier, P. J. M., van Kuppeveld, F. J. M. and de Haan, C. A. M. 2015. Rapid emergence of highly pathogenic avian influenza subtypes from a subtype H5N1 hemagglutinin variant. *Emerg Infect Dis.* **21**: 842–846.
72. Hew, L. Y., Isoda, N., Takaya, F., Ogasawara, K., Kobayashi, D., Huynh, L. T., Morita, T., Harada, R., Zinyakov, N. G., Andreychuk, D. B., Chvala, I. A., Irza, V. N., Watanabe, Y., Fujita, H., Saito, K., Hiono, T. and Sakoda, Y. 2024. Continuous introduction of H5 high pathogenicity avian influenza viruses in Hokkaido, Japan: Characterization of viruses isolated in winter 2022–2023 and early winter 2023–2024. *Transbound Emerg Dis.* **2024**: 1199876.
73. Sakuma, S., Uchida, Y., Kajita, M., Tanikawa, T., Mine, J., Tsunekuni, R. and Saito, T. 2021. First outbreak of an H5N8 highly pathogenic avian influenza virus on a chicken farm in Japan in 2020. *Viruses*. **13**: 489.
74. European Food Safety Authority, European Centre for Disease Prevention and Control, European Union Reference Laboratory for Avian Influenza, Fusaro, A., Gonzales, J. L., Kuiken, T., Mirinavičiūtė, G., Niqueux, É., Ståhl, K., Staubach, C., Svartström, O., Terregino, C., Willgert, K., Baldinelli, F., Delacourt, R., Georganas, A. and Kohnle, L. 2024. Avian influenza overview December 2023–March 2024. *EFSA J.* **22**.
75. Świętoń, E., Fusaro, A., Shittu, I., Niemczuk, K., Zecchin, B., Joannis, T., Bonfante, F., Śmietanka, K. and Terregino, C. 2020. Sub-saharan Africa and Eurasia ancestry of reassortant highly pathogenic avian influenza A(H5N8) virus, Europe, December 2019. *Emerg Infect Dis*. **26**: 1557–1561.
76. Zinyakov, N., Andriyasov, A., Zhestkov, P., Kozlov, A., Nikonova, Z., Ovchinnikova, E., Grekhneva, A., Shcherbakova, L., Andreychuk, D., Sprygin, A., Prokhvatilova, L. and Chvala, I. 2022. Analysis of avian influenza (H5N5) viruses isolated in the southwestern European part of the Russian Federation in 2020–2021. *Viruses*. **14**: 2725.

77. Hoffmann, T. W., Munier, S., Larcher, T., Soubieux, D., Ledevin, M., Esnault, E., Tourdes, A., Croville, G., Guérin, J. L., Quéré, P., Volmer, R., Naffakh, N. and Marc, D. 2012. Length variations in the NA stalk of an H7N1 influenza virus have opposite effects on viral excretion in chickens and ducks. *J Virol.* **86**: 584–588.
78. European Union Reference Laboratory For Avian Influenza. EURL avian flu data portal. https://eurlaidata.izsvenezie.it [accessed on: 6 August 2024].
79. Isoda, N., Hiono, T., Hew, Y. L., Takaya, F., Nguyen, B. L., Kobayashi, D., Fujino, K. and Sakoda, Y. 2025. Dynamics of high pathogenicity avian influenza virus infection with multiple introductions in a crow flock in an urban park in Hokkaido, Japan. *Comp Immunol Microbiol Infect Dis*. **121**: 102367.
80. Esaki, M., Okuya, K., Tokorozaki, K., Haraguchi, Y., Hasegawa, T. and Ozawa, M. 2025. Highly pathogenic avian influenza A (H5N1) outbreak in endangered cranes, Izumi plain, Japan, 2022–23. *Emerg Infect Dis.* **31**: 937–947.
81. Takadate, Y., Mine, J., Tsunekuni, R., Sakuma, S., Kumagai, A., Nishiura, H., Miyazawa, K. and Uchida, Y. 2024. Genetic diversity of H5N1 and H5N2 high pathogenicity avian influenza viruses isolated from poultry in Japan during the winter of 2022–2023. *Virus Res*. **347**: 199425.
82. Hew, Y. L., Hiono, T., Monne, I., Nabeshima, K., Sakuma, S., Kumagai, A., Okamura, S., Soda, K., Ito, H., Esaki, M., Okuya, K., Ozawa, M., Yabuta, T., Takakuwa, H., Nguyen, L. B., Isoda, N., Miyazawa, K., Onuma, M. and Sakoda, Y. 2024. Cocirculation of genetically distinct highly pathogenic avian influenza H5N5 and H5N1 viruses in crows, Hokkaido, Japan. *Emerg Infect Dis*. **30**: 1912–1917.
83. Seo, Y. R., Cho, A. Y., Kim, D. J., Si, Y. J., Jeong, H., Lee, S., Song, C. S. and Lee, D. H. 2025. Transmission dynamics of highly pathogenic avian influenza A (H5N1) and A (H5N6) viruses in wild birds, South Korea, 2023–2024. *Emerg Infect Dis*. **31**: 1561–1572.
84. Lee, D. H., Torchetti, M. K., Winker, K., Ip, H. S., Song, C. S. and Swayne, D. E. 2015. Intercontinental spread of asian-origin H5N8 to North America through Beringia by migratory birds. *J Virol*. **89**: 6521–6524.
85. Signore, A. V., Giacinti, J., Jones, M. E. B., Erdelyan, C. N. G., McLaughlin, A., Alkie, T. N., Cox, S., Lair, S., Jardine, C. M., Stevens, B., Bravo-Araya, M., Pople, N., Pybus, M. J., Hisanaga, T., Xu, W., Koziuk, J., Lung, O., Kruczkiewicz, P.,

Fisher, M., Wight, J., Rahman, I., Hargan, K. E., Lang, A. S., Hochman, O., Ojkic, D., Yason, C., British Columbia Wildlife AIV Surveillance Program, Bourque, L., Bollinger, T. K., Provencher, J. F., Ogilvie, S., Clark, A., MacPhee, R., Eaglesome, H., Gilbert, S., Saboraki, K., Davis, R., Jerao, A., Ginn, M., Soos, C. and Berhane, Y. 2025. Spatiotemporal reconstruction of the North American A (H5N1) outbreak reveals successive lineage replacements by descendant reassortants. *Sci Adv*. **11**: 2375–2548.

86. Guinat, C., Vergne, T., Kocher, A., Chakraborty, D., Paul, M. C., Ducatez, M. and Stadler, T. 2021. What can phylodynamics bring to animal health research? *Trends Ecol Evol.* **36**: 837–847.
87. Featherstone, L. A., Zhang, J. M., Vaughan, T. G. and Duchene, S. 2022. Epidemiological inference from pathogen genomes: A review of phylodynamic models and applications. *Virus Evol.* **8**: veac045.
88. Carnegie, L., Raghwani, J., Fournié, G. and Hill, S. C. 2023. Phylodynamic approaches to studying avian influenza virus. *Avian Pathol*. **52**: 289–308.
89. Perdue, M. L. 2008. Molecular determinants of pathogenicity for avian influenza viruses. pp. 23–41. *In*: *Avian Influenza*, 1st ed., (Swayne, D. E. eds.) Blackwell Publishing, Ames, Iowa, USA.
90. Katoh, K. and Standley, D. M. 2013. MAFFT multiple sequence alignment software version 7: Improvements in performance and usability. *Mol Biol Evol*. **30**: 772–780.
91. Larsson, A. 2014. AliView: a fast and lightweight alignment viewer and editor for large datasets. *Bioinformatics*. **30**: 3276–3278.
92. Minh, B. Q., Schmidt, H. A., Chernomor, O., Schrempf, D., Woodhams, M. D., Von Haeseler, A. and Lanfear, R. 2020. IQ-TREE 2: New models and efficient methods for phylogenetic inference in the genomic era. *Mol Biol Evol*. **37**: 1530–1534.
93. Shapiro, B., Rambaut, A. and Drummond, A. J. 2006. Choosing appropriate substitution models for the phylogenetic analysis of protein-coding sequences. *Mol Biol Evol*. **23**: 7–9.
94. Rambaut, A., Lam, T. T., Max Carvalho, L. and Pybus, O. G. 2016. Exploring the temporal structure of heterochronous sequences using TempEst (formerly Path-O-Gen). *Virus Evol*. **2**: vew007.

95. Yu, G. 2020. Using ggtree to visualize data on tree-like structures. *Curr Protoc Bioinforma.* **69**: e96.
96. Kühnert, D., Stadler, T., Vaughan, T. G. and Drummond, A. J. 2016. Phylodynamics with migration: A computational framework to quantify population structure from genomic data. *Mol Biol Evol.* **33**: 2102–2116.
97. Vaughan, T. G. and Stadler, T. 2025. Bayesian phylodynamic inference of multitype population trajectories using genomic data. *Mol Biol Evol.* **42**: msaf130.
98. Barido-Sottani, J., Vaughan, T. G. and Stadler, T. 2020. A Multitype Birth–Death Model for Bayesian inference of lineage-specific birth and death rates. *Syst Biol*. **69**: 973–986.
99. Zhukova, A., Hecht, F., Maday, Y. and Gascuel, O. 2023. Fast and accurate maximum-likelihood estimation of Multi-Type Birth–Death epidemiological models from phylogenetic trees. *Syst Biol*. **72**: 1387–1402.
100. Ayres, D. L., Darling, A., Zwickl, D. J., Beerli, P., Holder, M. T., Lewis, P. O., Huelsenbeck, J. P., Ronquist, F., Swofford, D. L., Cummings, M. P., Rambaut, A. and Suchard, M. A. 2012. BEAGLE: An application programming interface and high-performance computing library for statistical phylogenetics. *Syst Biol.* **61**: 170–173.
101. Drummond, A. J., Ho, S. Y. W., Phillips, M. J. and Rambaut, A. 2006. Relaxed phylogenetics and dating with confidence. *PLoS Biol.* **4**: e88.
102. Imperia, E., Bazzani, L., Scarpa, F., Borsetti, A., Petrosillo, N., Giovanetti, M. and Ciccozzi, M. 2023. Avian influenza: Could the H5N1 virus be a potential next threat? *Microbiol Res*. **14**: 635–645.
103. Jourdain, E., Gauthier-Clerc, M., Bicout, D. and Sabatier, P. 2007. Bird migration routes and risk for pathogen dispersion into western mediterranean wetlands. *Emerg Infect Dis.* **13**: 365–372.
104. Guinat, C., Tang, H., Yang, Q., Valenzuela Agüí, C., Vaughan, T. G., Scire, J., Yu, H., Wang, W., Chen, Z., Ducatez, M. F. and Stadler, T. 2023. Bayesian phylodynamics reveals the transmission dynamics of avian influenza A (H7N9) virus at the human–live bird market interface in China. *Proc Natl Acad Sci*. **120**: e2215610120.

105. Rambaut, A., Drummond, A. J., Xie, D., Baele, G. and Suchard, M. A. 2018. Posterior summarization in Bayesian phylogenetics using Tracer 1.7. *Syst Biol*. **67**: 901–904.

106. Suchard, M. A., Lemey, P., Baele, G., Ayres, D. L., Drummond, A. J. and Rambaut, A. 2018. Bayesian phylogenetic and phylodynamic data integration using BEAST 1.10. *Virus Evol.* **4**: vey016.

107. Si, Y. J., Kim, D. J., Lee, S. H., Seo, Y. R., Jeong, H., Lee, S. and Lee, D. H. 2025. New incursions of H5N1 clade 2.3.4.4b highly pathogenic avian influenza viruses in wild birds, South Korea, October 2024. *Front Vet Sci*. **11**: 1526118.

108. Seo, Y. R., Cho, A. Y., Si, Y. J., Lee, S. I., Kim, D. J., Jeong, H., Kwon, J. H., Song, C. S. and Lee, D. H. 2024. Evolution and spread of highly pathogenic avian influenza A (H5N1) clade 2.3.4.4b virus in wild birds, South Korea, 2022–2023. *Emerg Infect Dis*. **30**: 299–309.

109. Meng, W., Yang, Q., Vrancken, B., Chen, Z., Liu, D., Chen, L., Zhao, X., François, S., Ma, T., Gao, R., Ru, W., Li, Y., He, H., Zhang, G., Tian, H. and Lu, J. 2019. New evidence for the east–west spread of the highly pathogenic avian influenza H5N1 virus between Central Asian and East Asian-Australasian flyways in China. *Emerg Microbes Infect.* **8**: 823–826.

110. Ito, T., Okazaki, K., Kawaoka, Y., Takada, A., Webster, R. G. and Kida, H. 1995. Perpetuation of influenza A viruses in Alaskan waterfowl reservoirs. *Arch Virol*. **140**: 1163–1172.

111. Kang, Y. M., Heo, G. B., An, S. H., Lee, Y. N., Cha, R. M., Cho, H. K., Sagong, M., Kim, D. H., Lee, E. K., Kang, H. M., Lee, K. N. and Lee, Y. J. 2023. Introduction of multiple novel high pathogenicity avian influenza (H5N1) virus of clade 2.3.4.4b into South Korea in 2022. *Transbound Emerg Dis.* **2023**: 1–8.

112. Zeng, J., Du, F., Xiao, L., Sun, H., Lu, L., Lei, W., Zheng, J., Wang, L., Shu, S., Li, Y., Zhang, Q., Tang, K., Sun, Q., Zhang, C., Long, H., Qiu, Z., Zhai, K., Li, Z., Zhang, G., Sun, Y., Wang, D., Zhang, Z., Lycett, S. J., Gao, G. F., Shu, Y., Liu, J., Du, X. and Pu, J. 2024. Spatiotemporal genotype replacement of H5N8 avian influenza viruses contributed to H5N1 emergence in 2021/2022 panzootic. *J Virol*. **98**: e01401-23.

113. Ministry of Agriculture, Forestry and Fisheries, Japan. 2024. Livestock infectious disease surveillance monthly report. https://www.maff.go.jp/j/syouan/douei/katiku_yobo/livestock_surveillance/attach/pdf/r5-17.pdf [accessed on: 29 August 2025].
114. Hiono, T., Okamatsu, M., Yamamoto, N., Ogasawara, K., Endo, M., Kuribayashi, S., Shichinohe, S., Motohashi, Y., Chu, D. H., Suzuki, M., Ichikawa, T., Nishi, T., Abe, Y., Matsuno, K., Tanaka, K., Tanigawa, T., Kida, H. and Sakoda, Y. 2016. Experimental infection of highly and low pathogenic avian influenza viruses to chickens, ducks, tree sparrows, jungle crows, and black rats for the evaluation of their roles in virus transmission. *Vet Microbiol*. **182**: 108–115.
115. Fujimoto, Y., Ogasawara, K., Isoda, N., Hatai, H., Okuya, K., Watanabe, Y., Takada, A., Sakoda, Y., Saito, K. and Ozawa, M. 2022. Experimental and natural infections of white-tailed sea eagles (*Haliaeetus albicilla*) with high pathogenicity avian influenza virus of H5 subtype. *Front Microbiol.* **13**: 1007350.
116. Hirschinger, J., Höfle, U., Sánchez-Cano, A., Guinat, C., Croville, G., Barral, M., Donázar, J. A., Ladevèze, C. L. G., Walch, M., Alvarez, V., Gerrikagoitia, X., Du Plessis, L., Dellicour, S., Arrondo, E., Sánchez-Zapata, J. A., Cortés-Avizanda, A., Martín, S. M., Tornos, J., Perret, S., Boulinier, T., Orabi, P., van de Wiele, A., Guerin, J. L., Duriez, O. and Le Loc'h, G. 2025. Multidisciplinary tracking of highly pathogenic avian influenza A (H5N1) outbreak in griffon vultures, southern Europe, 2022. *Emerg Infect Dis*. **31**: 1589–1599.
117. Lv, X., Li, X., Sun, H., Li, Y., Peng, P., Qin, S., Wang, W., Li, Y., An, Q., Fu, T., Qu, F., Xu, Q., Qin, R., Zhao, Z., Wang, M., Wang, Y., Wang, Y., Zeng, X., Hou, Z., Lei, C., Chu, D., Li, Y. and Chai, H. 2022. Highly pathogenic avian influenza A (H5N8) clade 2.3.4.4b viruses in satellite-tracked wild ducks, Ningxia, China, 2020. *Emerg Infect Dis*. **28**: 1039–1042.
118. Esaki, M., Okuya, K., Tokorozaki, K., Haraguchi, Y., Ito, J. and Ozawa, M. 2025. Surveillance of avian influenza viruses in the Izumi plain reveals the role of wild ducks in the introduction of H5N1 HPAIVs during the 2023/24 winter season. *Comp Immunol Microbiol Infect Dis.* **123**: 102389.

119. de Maio, N., Wu, C. H., O'Reilly, K. M. and Wilson, D. 2015. New routes to phylogeography: A Bayesian structured coalescent approximation. *PLoS Genet*. **11**: e1005421.
120. Koch, G. and Elbers, A. R. W. 2006. Outdoor ranging of poultry: A major risk factor for the introduction and development of high-pathogenicity avian influenza. *NJAS Wagening J Life Sci*. **54**: 179–194.
121. Bossers, A., de Rooij, M. M., van Schothorst, I., Velkers, F. C. and Smit, L. A. 2024. Detection of airborne wild waterbird-derived DNA demonstrates potential for transmission of avian influenza virus via air inlets into poultry houses, the Netherlands, 2021 to 2022. *Eurosurveillance*. **29**: 2400350.
122. Ministry of Agriculture, Forestry and Fisheries of Japan. 2023. Avian influenza information. https://www.maff.go.jp/j/syouan/douei/tori/index.html [accessed on: 29 August 2025].
123. Sanekata, T., Fukuda, T., Miura, T., Morino, H., Lee, C., Maeda, K., Araki, K., Otake, T., Kawahata, T. and Shibata, T. 2010. Evaluation of the antiviral activity of chlorine dioxide and sodium hypochlorite against feline calicivirus, human influenza virus, measles virus, canine distemper virus, human herpesvirus, human adenovirus, canine adenovirus and canine parvovirus. *Biocontrol Sci*. **15**: 45–49.
124. Köhler, A. T., Rodloff, A. C., Labahn, M., Reinhardt, M., Truyen, U. and Speck, S. 2018. Efficacy of sodium hypochlorite against multidrug-resistant gram-negative bacteria. *J Hosp Infect.* **100**: e40–e46.
125. Ito, M., Alam, Md. S., Suzuki, M., Takahashi, S., Komura, M., Sangsriratakul, N., Shoham, D. and Takehara, K. 2018. Virucidal activity of a quaternary ammonium compound associated with calcium hydroxide on avian influenza virus, newcastle disease virus and infectious bursal disease virus. *J Vet Med Sci*. **80**: 574–577.
126. Caschera, A. G., McAuley, J., Kim, Y., Purcell, D., Rymenants, J. and Foucher, D. A. 2022. Evaluation of virucidal activity of residual quaternary ammonium-treated surfaces on SARS-CoV-2. *Am J Infect Control*. **50**: 325–329.
127. Da Cruz Nizer, W. S., Inkovskiy, V. and Overhage, J. 2020. Surviving reactive chlorine stress: Responses of gram-negative bacteria to hypochlorous acid. *Microorganisms*. **8**: 1220.

128. Han-Hsing Lin, J., Karabucak, B. and Lee, S. M. 2021. Effect of sodium hypochlorite on conventional and heat-treated nickel-titanium endodontic rotary instruments – An in vitro study. *J Dent Sci.* **16**: 738–743.
129. Kabir, Md. H., Miyaoka, Y., Hasan, Md. A., Yamaguchi, M., Shoham, D., Murakami, H. and Takehara, K. 2021. Synergistic effects of quaternary ammonium compounds and food additive grade calcium hydroxide on microbicidal activities at low temperatures. *J Vet Med Sci.* **83**: 1820–1825.
130. Tao, C., Tang, X., Gan, Y., Qin, Y., Yang, S. and Huang, F. 2024. Investigation of the disinfection efficiency of commercial hydrogen peroxide, chlorine dioxide, and chlorine disinfectant on different surfaces. *Am J Vet Res.* **85**: ajvr.24.03.0079.
131. Moran, T., Pace, J. and McDermott, E. E. 1953. Interaction of chlorine dioxide with flour: Certain chemical aspects. *Nature*. **171**: 103–106.
132. Yue, C., Yuya, H., Zhihuan, L., Zimo, W. and Jianying, F. 2024. Study on the disinfection effect of chlorine dioxide disinfectant ($ClO_2$) on dental unit waterlines and its in vitro safety evaluation. *BMC Oral Health*. **24**: 648.
133. Imoto, Y., Matsui, H., Ueda, C., Nakajima, E. and Hanaki, H. 2025. Inactivation effects of hypochlorous acid, chlorine dioxide, and ozone on airborne SARS-CoV-2 and influenza A virus. *Food Environ Virol.* **17**: 9.
134. Kadota, C., Miyaoka, Y., Kabir, M. H., Hakim, H., Hasan, M. A., Shoham, D., Murakami, H. and Takehara, K. 2023. Evaluation of chlorine dioxide in liquid state and in gaseous state as virucidal agent against avian influenza virus and infectious bronchitis virus. *J Vet Med Sci.* **85**: 1040–1046.
135. Morino, H., Fukuda, T., Miura, T. and Shibata, T. 2011. Effect of low-concentration chlorine dioxide gas against bacteria and viruses on a glass surface in wet environments: Inactivation of microbes by low-concentration $ClO_2$ gas. *Lett Appl Microbiol*. **53**: 628–634.
136. Wilson, S. C., Wu, C., Andriychuk, L. A., Martin, J. M., Brasel, T. L., Jumper, C. A. and Straus, D. C. 2005. Effect of chlorine dioxide gas on fungi and mycotoxins associated with sick building syndrome. *Appl Environ Microbiol*. **71**: 5399–5403.
137. Ogata, N. and Shibata, T. 2008. Protective effect of low-concentration chlorine dioxide gas against influenza A virus infection. *J Gen Virol.* **89**: 60–67.

138. Sun, Z., Qian, Y., Ogata, N., Cai, X., Han, W., Xie, Y., Morino, H., Sogawa, K., Shibata, T. and Qu, D. 2022. Effect of chlorine dioxide on avian influenza A (H7N9) virus. *Biosaf Health*. **4**: 53–57.

139. Ge, Y., Zhang, X., Shu, L. and Yang, X. 2021. Kinetics and mechanisms of virus inactivation by chlorine dioxide in water treatment: A review. *Bull Environ Contam Toxicol*. **106**: 560–567.

140. Ogata, N. 2012. Inactivation of influenza virus haemagglutinin by chlorine dioxide: oxidation of the conserved tryptophan 153 residue in the receptor-binding site. *J Gen Virol.* **93**: 2558–2563.

141. Reed, L. J. and Muench, H. 1938. A simple method of estimating fifty percent endpoints. *Am J Epidemiol.* **27**: 493–497.

142. Al-Dalawi, L., Yang, J., Blanchard, A. M., Clark, M., Chang, K. C., Iqbal, M. and Goulding, L. V. 2025. Research note: Use of in vitro and in ovo approaches to characterise avian influenza viruses and assess species specific responses to infection. *Poult Sci*. **104**: 105987.

143. Scoizec, A., Niqueux, E., Thomas, R., Daniel, P., Schmitz, A. and Le Bouquin, S. 2018. Airborne detection of H5N8 highly pathogenic avian influenza virus genome in poultry farms, France. *Front Vet Sci.* **5**: 15.

144. Dubuis, M. E., Racine, É., Vyskocil, J. M., Turgeon, N., Tremblay, C., Mukawera, E., Boivin, G., Grandvaux, N. and Duchaine, C. 2021. Ozone inactivation of airborne influenza and lack of resistance of respiratory syncytial virus to aerosolization and sampling processes. *PLoS One*. **16**: e0253022.

145. Occupational Safety and Health Administration (OSHA). 2024. Occupational health guideline for chlorine dioxide. https://www.osha.gov/chemicaldata/16 [accessed on: 25 September 2025].

146. Nagy, A., Černíková, L. and Sedlák, K. 2025. Genetic data and meteorological conditions suggesting windborne transmission of H5N1 high-pathogenicity avian influenza between commercial poultry outbreaks. *PLoS One*. **20**: e0319880.

147. Fukuma, S., Matsuo, T., Miura, T., Shimadera, H. and Kondo, A. 2025. The effect of temperature and humidity on the decomposition rate of chlorine dioxide. *Int J Eng Technol*. **17**: 7–11.

148. Park, S. H. and Kang, D. H. 2018. Effect of temperature on chlorine dioxide inactivation of Escherichia coli O157:H7, Salmonella typhimurium, and Listeria monocytogenes on spinach, tomatoes, stainless steel, and glass surfaces. *Int J Food Microbiol.* **275**: 39–45.